# Stage-Based Identification of Policy Effects*

Christian Alemán
NYU Abu Dhabi

Christopher Busch
LMU Munich
CESifo

Alexander Ludwig
Goethe University Frankfurt
ICIR, UAB and CEPR

Raül Santaeulàlia-Llopis
NYU Abu Dhabi
UAB, BSE and CEPR

March 22, 2023

**Abstract**

We develop a method that identifies the effects of nationwide policy—i.e., implemented across all regions at the same time. In our method, we put forward the idea of tracking outcome paths in terms of stages rather than time, where a stage of a regional outcome at time $t$ is defined as its location on the support of a reference outcome path. Through a normalization that maps the time-paths of regional outcomes onto a reference path—using only pre-policy data, we uncover cross-regional heterogeneity in the stage at which policy is implemented, even if policy is implemented at the same time in all regions. This stage variation serves to identify the policy effects: a stage-leading region provides the counterfactual path inside a window of stages in which non-leading regions are subject to the policy whereas the leading region is not. We assess the performance of our method with Monte-Carlo experiments, and illustrate it in several empirical applications. Furthermore, we show that our method is able to capture not only heterogeneous policy effects across stages but also the aggregate effects of policy. Additionally, we show how our method can be used for the assessment of non-nationwide policy.

**Keywords**: Stages, Identification, Policy, Evaluation
**JEL Classification**: C01, H00, E01, E22, E25

*We thank Alberto Abadie, Jaap Abbring, Francesco Agostinelli, Manuel Arellano, Brant Callaway, Jeffrey Campbell, Davide Cantoni, Xu Cheng, Hanming Fang, Hans-Peter Kohler, José-Víctor Ríos-Rull, Frank Schorfheide and participants at seminars and conferences for helpful comments and suggestions. Raül Santaeulàlia-Llopis acknowledges financial support from the AGAUR 2020PANDE00036 "Pandemies" Grant 2020-2022, from the Spanish Ministry of Economy and Competitiveness, through the Proyectos I+D+i 2019 Retos Investigacion PID2019-110684RB-I00 Grant, Europa Excelencia EUR2021-122011 and the Severo Ochoa Programme for Centres of Excellence in R&D (CEX2019-000915-S).
Alemán: christian.c.aleman@gmail.com; Busch: chris.busch.econ@gmail.com; Ludwig: mail@alexander-ludwig.com; Santaeulàlia-Llopis: loraulet@gmail.com

# 1 Introduction

**Motivation.** The empirical assessment of a policy requires a credible counterfactual. Standard empirical strategies critically rely on cross-regional heterogeneity in the time of policy implementation as source of identification—e.g., the existence of one untreated region or a staggered rollout.[1] Further, the credibility of the counterfactual requires the pre-policy paths of the outcome of interest to be similar across regions with differences not exceeding a constant gap over time—the so-called parallel trends assumption.[2] However, many relevant policy contexts violate these conditions. First, many policies are implemented nationwide, carried out in all regions at the same time, which eliminates the source of identification for standard empirical strategies. Second, the pre-policy outcome paths can be non-linear and differ across regions—e.g., in their starting date, speed, or magnitude—in a way that violates the parallel trends assumption. In panel (a) of Figure 1, we illustrate one such scenario. Our goal in this paper is to provide an identification strategy for such policy contexts.

**Idea.** Our idea is to track outcome paths in terms of stages rather than time. Specifically, we define a stage of a regional outcome at time $t$ as its location on the support of a reference outcome path. Panel (b) of Figure 1 illustrates this concept by showing a reference outcome path evolving through stages. At any given time, the outcome path of one region may be at a different stage compared to another region. For example, as shown in the figure, at time $t$ region $\mathcal{C}$ has progressed to a more advanced stage than region $\mathcal{T}$. This implies that cross-regional heterogeneity in stages may be present at the time of policy implementation, $t_p$. The core of our method is tracing out and exploiting this heterogeneity in stages for the identification of policy effects, hence, the label, Stage-Based Identification (SBI).

**The Method.** Our method is comprised of two steps: normalization and identification. First, we normalize the pre-policy outcome time paths of non-reference regions to that of a reference region. This entails normalizing the coordinates of outcome time paths to transform time into stages (i.e., normalized time) and the outcome level into a normalized level.[3] To conduct these transformations, we use low degree polynomials with a set of associated coefficients—the normalization coefficients. These coefficients are determined as the ones that minimize the distance

[1] See, among others, Angrist and Krueger (1999), Blundell and Macurdy (1999) and Imbens and Rubin (2015). See also the more recent discussions in Athey and Imbens (2017) and Card (2022).

[2] The assumption of parallel trends is relaxed in Abadie (2005). Indeed, there is a growing and exciting body of research work regarding more flexible forms of parallel trend assumptions (e.g. Callaway and Sant'Anna, 2021; Rambachan and Roth, 2021). As we discuss later, our methodology mainly differs from previous work in that it does not require heterogeneity in the time of policy implementation for the identification of policy effects.

[3] This normalization of coordinates relates to earlier work in Iorio and Santaeulàlia-Llopis (2010, 2016).

Figure 1: A Stage-Based Identification of the Effects of Nationwide Policy: An Illustration

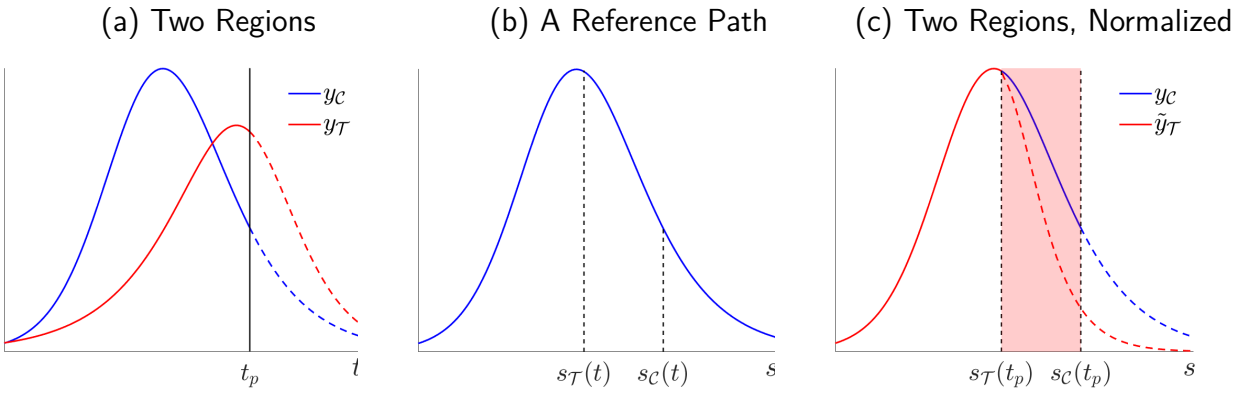


*Notes:* Panel (a) shows the time paths of an outcome variable for two regions, $\mathcal{C}$ and $\mathcal{T}$; policy is implemented in both regions at the same time $t_p$; dashed sections indicate post-policy paths. Panel (b) shows a reference path, where at some $t$, region $\mathcal{C}$ is at a more advanced stage thatn region $\mathcal{T}$. Panel (c) shows the result of mapping $y_{\mathcal{T}}$ onto $y_{\mathcal{C}}$, resulting in the normalized path $\widetilde{y}_{\mathcal{T}}$; the pink shaded area indicates the identification window.

between the pre-policy outcome path of the reference region and the normalized pre-policy outcome path of the non-reference region. As a result, the pre-policy regional paths are identical—up to a minimization error—in the stage domain before the stage at which policy is implemented first across regions; see panel (c) of Figure 1 in which we use the outcome time path of region $\mathcal{C}$ as reference and normalize the path of region $\mathcal{T}$ to the reference.[4]

Second, our identification is based on the cross-regional heterogeneity in the stages at which the policy is implemented across regions, which we uncover through our normalization using pre-policy data. For example, in the illustration, policy is implemented at an earlier stage in region $\mathcal{T}$ than in region $\mathcal{C}$. Then, applying the normalization coefficients—resulting from pre-policy data—on post-policy data opens a window of stages in which a stage-leading region (in the example, region $\mathcal{C}$) is not subject to policy whereas the other region (in the example, region $\mathcal{T}$) is subject to policy, see pink shaded area in panel (c) of Figure 1. Our identification assumption is that the normalization coefficients that minimize the distance between the pre-policy outcome paths across regions in the stage domain are unaffected by policy. That is, we assume that our normalization would make the post-policy paths line up as well in the absence of policy. Thus, under our identification assumption, the stage-leading region serves as control region for the other region, which is considered treatment.[5] The difference between the control region and treatment region inside the identification window captures the effects of policy.

[4]We show examples in which the normalization coefficients can be solved analytically. Our closed-form solutions show that the normalization coefficients reshape the structural parameters that determine the outcome path of the non-reference region into those of the reference region before policy is implemented; see Section 2.3.

[5]Note that since the stage at which each region receives the policy is a result of our normalization, SBI does not require an ex-ante assignment of control or treatment across regions—this assignment is determined endogenously by the normalization coefficients in our approach, see Section 2.2.

**Method Performance.** We apply SBI to model-generated data in order to assess whether the identified policy effects recover the true policy effects. We focus on three nationwide policies that resemble our empirical applications: a stay-home policy against a pandemic using a model where economic activity shapes and is shaped by the pandemic; the approval of oral contraceptives in a model with women fertility and education choices; and the removal of an institutional barrier to economic growth in a model of structural transformation. Within the model framework, we know the true counterfactual path that would occur if policy were absent throughout. Using the data that would be available to a policy evaluator, we find that SBI can successfully identify the true effects of nationwide policy generated by the model.

We further assess whether and when our normalization procedure comes to its limits and plausible identification is not feasible using SBI. Precisely, we perform a Monte Carlo study that numerically characterizes the bounds within which SBI is able to recover the true (model-generated) effects of policy. We consider one benchmark region which we pair up with a large set of regions (drawing from a large set of structural parameters) one-by-one. Applying SBI to these pairs, we find that the error by which SBI captures the true policy effects systematically increases when moving farther away from the benchmark region in the space of the normalization coefficients. Under the interpretation that the normalization reshapes the structural parameters that determine the outcome paths, SBI requires—for successful identification of policy effects—the structural parameters to not be too dissimilar across regions before policy implementation.

In addition, we assess how SBI fares in contexts where there are potential confounding factors such as time-varying latent heterogeneity, confounding policy and endogenous policy. Using model-generated data, we find that SBI is able to identify the true policy effects in these contexts as long as the confounding factors keep the regional outcome paths sufficiently close in the space of the normalization coefficients. We further establish in a set of Placebo diagnoses that SBI successfully estimates a zero policy effect when there is none. We also show how to conduct inference on our identified policy effects with data that incorporates a stochastic component.

**Three Applications.** We apply SBI to study the effects of nationwide policy in three empirical applications. First, we assess the effectiveness of the stay-home policy implemented nationwide in response to the first wave of the Covid-19 pandemic in Spain. SBI assigns Madrid as the stage-leading (control) region at the time of policy implementation. We find that the stay-home policy significantly reduces the amount of deaths by 24.7% in the rest of Spain inside an identification window of seven days. In other words, had the stay-home policy not been implemented, there would have been 1,734 more deaths over the course of one week. Second, we assess the effects of the Food and Drugs Administration (FDA) approval of oral contraceptives (the pill) in the

United States (U.S.) in 1960. We find that the pill reduced the crude fertility rate (number of births per 10,000) by 8.36%; where the stage-leading region is West Virginia and the effects are measured for the rest of the U.S. We also find that the pill increased the proportion of college women by 24.9% during the decade that followed the FDA approval; where the stage-leading region is Washington DC and the effects are measured for the rest of the U.S. Third, we study the effects of the German reunification in 1990 on income per capita in West Germany where SBI assigns Hessen as the stage-leading region. Using the path of GDP per capita of Hessen as no-policy counterfactual, we find that the German Reunification significantly reduces income per capita of the rest of West Germany by 3.29% in a window of approximately seven years.

**Heterogeneous Effects.** To assess how the policy effects potentially differ by stage, we map the outcome paths of the non-leading regions one-by-one onto the path of the leading region. Focusing on the Covid-19 application, we find that the policy effects systematically vary across stages. The earlier (in stages) the policy is implemented, the larger are the effects: the amount of prevented deaths is 65% in Murcia where the policy is implemented two weeks earlier in the stage domain than Madrid and 12% in the Basque Country where policy arrives two days earlier in the stage domain than Madrid. Both the size of the identification window (policy implemented at earlier stages has a larger window) and the interim policy effects (i.e. effects under the same horizon inside the identification window) contribute to generate the heterogeneous effects by stage. We reach similar insights using a set of artificial regions from the power set of regions.

**Aggregate Effects.** By requiring heterogeneity in the time of policy implementation for identification, standard empirical strategies cannot assess the aggregate effects of policy—because the control region needs to be untreated at the time other regions are treated (i.e. contemporaneously in the time domain). Instead, our methodology is based on heterogeneity across stages at the time of policy implementation which allows for the aggregate (i.e. the complete set of all regions) to be treated. Precisely, the outcome path of the aggregate is typically at an earlier stage than the stage-leading region at the time of policy implementation. We use this variation in stages between the aggregate and the stage-leading region in order to assess the aggregate effects of policy. For example, applying SBI to assess the stay-home policy against Covid-19 in Spain, we find that the stay-home policy significantly reduced the amount of deaths for aggregate Spain by 20.37% in an identification window of 5.5 days.

**Related literature.** Our method is directly related to the standard empirical strategies designed for settings that resemble natural experiments. These strategies rely on a difference-in-differences methodology in order to generate the counterfactual path (or potential outcome as in Imbens and Rubin, 2015) that serves as control for a treated region—i.e., the region subject to policy. We

emphasize two main differences of SBI. First, a critical common factor in previous strategies is that the source of identification relies on the heterogeneity in the time of policy implementation across regions either with the existence of one untreated region (e.g., Card, 1990; Card and Krueger, 2000) or a staggered policy adoption (e.g., Athey and Imbens, 2021; Borusyak et al., 2021).[6] This is not the case in our method. Precisely, our main point of departure with respect to previous work is that SBI is able to deliver identification of policy effects for contexts in which the cross-regional heterogeneity in the time of policy implementation is absent. In this paper, we provide a new identification that uncovers cross-regional heterogeneity in the stage of the outcome of interest. Then, we use this cross-regional heterogeneity in stages at the time of policy implementation to identify the effects of policy, including nationwide policy.

Second, a relevant concern is that there might be cross-regional differences in the pre-policy determinants of the outcome of interest that also determine the outcome paths after policy. In standard empirical strategies, the policy effects are only credibly identified after controlling for these determinants, an idea that is typically conveyed through the parallel trends assumption (e.g. Bertrand et al., 2004, among many others).[7] Our approach to this question is rather different and does not rely on a parallel trends assumption for identification. Instead, we normalize pre-policy paths in a stage domain in a way that aims to minimize the cross-regional differences in the pre-policy determinants of outcomes, whether observable or not. Our identification assumption is that, absent policy, the normalization coefficients—obtained using pre-policy data only—would also map the post-policy path of the non-reference region onto the post-policy reference path. Thus, we apply the pre-policy normalization coefficients onto post-policy data in order to find a counterfactual path and identify the policy effects.

Our work also relates to other policy evaluation approaches like synthetic control methods (SCM) (Abadie and Gardeazabal, 2003; Abadie et al., 2010). The SCM approach essentially constructs a counterfactual time path based on a carefully weighted average across untreated (control) regions.[8] Two main differences stand out. First, analogous to other empirical strategies, SCM requires the existence of a set of untreated regions to construct the synthetic control group for identification. In contrast, SBI relies on cross-regional heterogeneity in the stage—not time—at which the policy is implemented. For this reason, we can apply SBI to a nationwide policy occurring at the same time across all regions, unlike with SCM—or other methods for that matter.

[6] See also the recent discussion in Goodman-Bacon (2021).

[7] In this context, there is a growing discussion on how to identify effects when parallel trends do not exactly hold. Abadie (2005) conditions the parallel trends to a set of observables using propensity scores (Heckman et al., 1998). This idea is extended to staggered rollout policy in Callaway and Sant'Anna (2021). Recently, Rambachan and Roth (2021) discuss how much the trends before policy implementation can differ from the trends after policy while still being able to identify causal effects.

[8] Doudchenko and Imbens (2017) use a joint framework for difference-in-differences and SCMs.

Second, our method does not require the use of observable determinants of cross-regional outcome differences in order to generate the counterfactual. Instead, the counterfactual in our method is constructed using solely the time paths of the outcome of interest. Also, similar to SBI, the changes-in-changes method in Athey and Imbens (2006) features a mapping outcomes across regions. Their focus lies on capturing heterogeneity of the policy effect over the cross-sectional distribution of an individual level outcome. To this end, they map pre-policy cumulative cross-sectional distributions across regions and use this to construct the counterfactual distribution in the treated region.[9] Instead of cross-sectional distributions, we map pre-policy time paths of region-level outcomes. At the same time, the main difference described above remains, namely that the identification in changes-in-changes is also based on regional heterogeneity in the time of policy implementation, whereas SBI does not require that heterogeneity.

Finally, alternative definitions of stages are some times used in economics and other disciplines. For example, in the analysis of structural transformation (e.g., Galor and Weil, 2000; Herrendorf et al., 2014; Cervellati and Sunde, 2015) or, similarly, in the analysis of the demographic transition (e.g., Greenwood et al., 2005), the level of income per capita typically summarizes the "stage" of development for an outcome of interest (e.g. agricultural share of output, urbanization rates, population growth rates, etc.) in cross-country comparisons. In contrast, rather than replacing time for an observable such as income per capita, SBI provides a normalization of the time path of the outcome of interest (possibly income per capita itself: see our evaluation of the effect of the German reunification on income per capita in West Germany). This also implies that the level of the outcome of interest (e.g., income per capita) is not a sufficient statistic to define the stage of a region in our approach. This same argument is discussed in the earlier work of Iorio and Santaeulàlia-Llopis (2010, 2016) that also conducts a normalization mapping country-specific time paths of HIV prevalence onto a reference path in order to define stages of the epidemic. We depart from that work in that we use our normalization to a reference path as base for identifying the effects of policies that aim to alter the path of the outcome of interest. For this reason, our normalization coefficients are obtained by strictly using pre-policy outcome paths.

The rest of the paper is structured as follows. We discuss our identification strategy in Section 2. We assess the performance of our method using model-generated data for several policy contexts in Section 3. Our empirical applications are in Section 4. We discuss heterogeneous effects, aggregate policy effects and non-nationwide policy in Section 5. Section 6 concludes.

[9] Their analysis is closely linked to Altonji and Blank (1999), who consider a decomposition of relative wage changes across groups into changes of the distribution of skills and the payoff for those skills.

## 2 A Stage-Based Method to Identify Policy Effects

To contextualize our contribution, we first briefly discuss how standard empirical strategies identify policy effects.[10] Consider a scenario in which, absent any policy intervention, the time path of an outcome $y_r(t)$ is identical across two regions $r \in \{\mathcal{C}, \mathcal{T}\}$.[11] Now assume that a policy is implemented only in region $\mathcal{T}$ at some date $t_p$ which affects the outcome path in that region thereafter. Illustratively, we plot an outcome path of a treated region $y_{\mathcal{T}}(t)$ before policy implementation (solid red) and after policy implementation (dashed red) in panel (a) of Figure 2. We also show an outcome path for a region where the policy is not implemented, $y_{\mathcal{C}}(t)$ (solid blue). This scenario is ideal for the estimation of policy effects because the pre-policy outcome paths are identical across regions warranting the use of region $\mathcal{C}$ as control for region $\mathcal{T}$. That is, the outcome path $y_{\mathcal{C}}(t)$ provides a useful no-policy counterfactual to assess the effects of policy on $y_{\mathcal{T}}(t)$ after $t_p$. The effects of policy are captured by the difference between $y_{\mathcal{C}}(t)$ and $y_{\mathcal{T}}(t)$ in the interval $(t_p, \infty)$. We can further add the implementation of the same policy to region $\mathcal{C}$ at some later date $t_p + \Delta$ with $\Delta > 0$; see panel (b) of Figure 2. Under this staggered rollout of the policy, the effects of policy on region $\mathcal{T}$ are identified using region $\mathcal{C}$ as counterfactual within the interval $(t_p, t_p + \Delta]$. In that interval, region $\mathcal{T}$ is subject to the policy whereas region $\mathcal{C}$ is not.

The standard identification strategies of policy effects just described fundamentally rely on two principles. First, the behavior of the outcome path before policy implementation must be credibly similar (the so-called parallel trends) across regions. Second, there must be variation in the time of policy implementation across regions which serves as source of identification. However, many policy contexts violate these conditions: First, the regional paths of the outcome variable before policy is implemented often differ across regions. In particular, outcome paths can differ by starting date, evolve at different speed and have different magnitude. Second, a large set of policies are implemented nationwide—i.e., carried out to *all regions* at the *same time*, which eliminates the source of identification used in standard strategies. We illustrate these two challenges in panel (a) of Figure 3 where a nationwide policy is implemented in a context where the outcome path in region $\mathcal{C}$ starts earlier, evolves at a faster speed and reaches a larger magnitude than in region $\mathcal{T}$.

Our strategy addresses these challenges in two steps. First, a normalization of regional outcome paths, and second, an identification based on the normalized paths.

[10] See comprehensive dicussions in, for example, Imbens and Rubin (2015) and Card (2022).

[11] We use *regions* in the description of the method due to the applications presented below. *Region* can be used interchangeably with *group* or *unit* throughout.

Figure 2: Ideal Policy Scenarios with Two Regions: Standard Identification Strategies

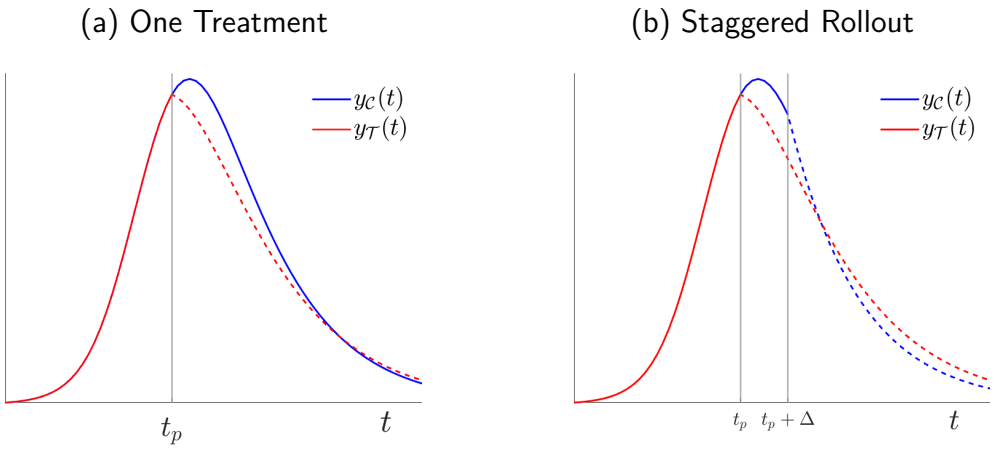


*Notes:* Denote with $y_{\mathcal{C}}(t)$ and $y_{\mathcal{T}}(t)$ the outcome paths of, respectively, region $\mathcal{C}$ and $\mathcal{T}$. Solid lines depict paths before policy implementation and dashed lines after policy. The identified policy effects are $\frac{\int_{\to t_p}^{h}(y_{\mathcal{C}}(t)-y_{\mathcal{T}}(t))dt}{\int_{\to t_p}^{h} y_{\mathcal{T}}(t)dt}$ with $h = \infty$ in the one-treatment case and $h = t_p + \Delta$ in the staggered rollout.

## 2.1 Normalization Procedure

Again, consider two regional outcome paths $y_r(t)$ with $r \in \{\mathcal{C}, \mathcal{T}\}$. We define the stage of a non-reference region as its location on the support of a reference path, which is the outcome path of a reference region. For this reference region, the stage is defined as time. For the non-reference region, the stage is the result of a normalization that maps its outcome time path onto the reference time path using only pre-policy data and uncovers stage variation at the time of policy implementation. We now describe our normalization—of the time and level of an outcome of interest—and provide a formal definition of stages afterwards.

The normalization starts with postulating the existence of the composite function,

$$\widetilde{y}_r(s) = (f_r \circ y_r \circ t_r)(s) = f_r(y_r(t_r(s))), \tag{1}$$

where $t_r(s) : S \to T$ is a stage-to-time transformation mapping stages $s \in S = \mathbb{R}$ into time $t \in T = \mathbb{R}$; $y_r(t) : T \to Y$ maps time into outcomes $y \in Y = \mathbb{R}$; and $f_r(y) : Y \to \widetilde{Y}$ maps outcomes into normalized outcomes $\widetilde{y}_r \in \widetilde{Y} = \mathbb{R}$. Thus, the composite function $\widetilde{y}_r(s) : S \to \widetilde{Y}$ defined in (1) maps stages $s$—i.e. normalized time—into normalized outcomes $\widetilde{y}$ for region $r$.

Without loss of generality, we treat the outcome path of region $\mathcal{T}$ as the reference path and that of region $\mathcal{C}$ as the non-reference path.[12] For the reference region, we set $s$ to be a fixed point of $t_{\mathcal{T}}(.)$ for all $s$ (i.e. $t = t_{\mathcal{T}}(s) = s$) and $y$ to be a fixed point of $f_{\mathcal{T}}(.)$ for all $y$ (i.e. $\widetilde{y} = f_{\mathcal{T}}(y) = y$) which implies that $\widetilde{y}_{\mathcal{T}}(s) = y_{\mathcal{T}}(s) = y_{\mathcal{T}}(t)$ always. Instead, for the non-reference region, we approximate $t_{\mathcal{C}}(.)$ and $f_{\mathcal{C}}(.)$ with $t_{\mathcal{C}}(.) \approx t(.;\boldsymbol{\psi}) = \sum_{k=0}^{K} \psi_k B_k^t(.)$ and $f_{\mathcal{C}}(.) \approx f(.;\boldsymbol{\omega}) = \sum_{m=0}^{M} \omega_m B_m^f(.)$, respectively. $\{B^f(.), B^t(.)\} \in \mathcal{B}^2$ are known basis functions in the space of continuous and differentiable functions. We denote the set of $M + K + 2$ unknown normalization coefficients by $\boldsymbol{\phi} = \{\boldsymbol{\psi}, \boldsymbol{\omega}\}$. This gives the composite function $\widetilde{y}_{\mathcal{C}}(s;\boldsymbol{\phi}) = (f_{\mathcal{C}}(.;\boldsymbol{\omega}) \circ y_{\mathcal{C}} \circ t_{\mathcal{C}}(.;\boldsymbol{\psi}))(s) = f_{\mathcal{C}}(y_{\mathcal{C}}(t_{\mathcal{C}}(s;\boldsymbol{\psi}));\boldsymbol{\omega})$ by which we approximate $\widetilde{y}_{\mathcal{C}}(s)$:

$$\widetilde{y}_{\mathcal{C}}(s) \approx \widetilde{y}_{\mathcal{C}}(s;\boldsymbol{\phi}) = \sum_{m=0}^{M} \omega_m B_m^f \left( \left( y_{\mathcal{C}} \left( \sum_{k=0}^{K} \psi_k B_k^t(s) \right) \right) \right). \tag{2}$$

Then, conversely to the stage-to-time transformation, the stages in each region are defined as,

$$s = s_r(t;\boldsymbol{\psi}) = \begin{cases} t & \text{if } r = \mathcal{T} \\ t_{\mathcal{C}}^{-1}(s;\boldsymbol{\psi}) & \text{if } r = \mathcal{C}, \end{cases} \tag{3}$$

where for the reference region (here, $r = \mathcal{T}$), the stage at time $t$ is the time itself (i.e. $s_{\mathcal{T}}(t;\boldsymbol{\psi}^*) = t = s$), whereas for the non-reference region (here, $r = \mathcal{C}$) the stage is the time in which region $\mathcal{C}$ is at the same stage than region $r = \mathcal{T}$ at time $t$ (i.e. $s_{\mathcal{C}}(t;\boldsymbol{\psi}^*) = t_{\mathcal{C}}^{-1}(s_{\mathcal{T}}(t;\boldsymbol{\psi}^*);\boldsymbol{\psi}^*) = t_{\mathcal{C}}^{-1}(s;\boldsymbol{\psi}^*)$).

We choose monomials as benchmark for the basis functions $B^f(.)$ and $B^t(.)$ in (2). Then, the approximated normalized path of the non-reference region is,

$$\widetilde{y}_{\mathcal{C}}(s;\boldsymbol{\phi}) = \sum_{m=0}^{M} \omega_m \left( y_{\mathcal{C}} \left( \sum_{k=0}^{K} \psi_k s^k \right) \right)^m. \tag{4}$$

A nice feature of the monomial basis is that it delivers a straightforward interpretation of the coefficients behind the stage-to-time transformation, $t_{\mathcal{C}}(s;\boldsymbol{\psi}) = \sum_{k=0}^{K} \psi_k s^k$. The parameter $\psi_0$ shifts the entire outcome path of region $\mathcal{C}$ forward (with $\psi_0 > 0$) or backwards (with $\psi_0 < 0$) in time, adjusting for different start dates. The parameter $\psi_1$ adjusts the speed in a constant way across periods. If $\psi_1 < 1$, then the outcome time-path of region $\mathcal{C}$ (in time) expands, whereas with $\psi_1 > 1$ it contracts. That is, if $\psi_1 < 1$, then region $\mathcal{C}$ is permanently faster (in time) than region $\mathcal{T}$—in one time-period region $\mathcal{C}$ advances by more than one stage, and vice versa for $\psi_1 > 1$. Further, allowing for the stage-to-time transformation to be quadratic (i.e. $\psi_2 \neq 0$) captures the notion that the relative speed across the regions can change over time: for example, the outcome path of region $\mathcal{C}$ might initially be slower than region $\mathcal{T}$, then catch up, and eventually move

[12] The choice of the reference region is innocuous, see our discussion in Section 2.2.

Figure 3: Stage-Based Identification of Policy Effects: A Nationwide Policy

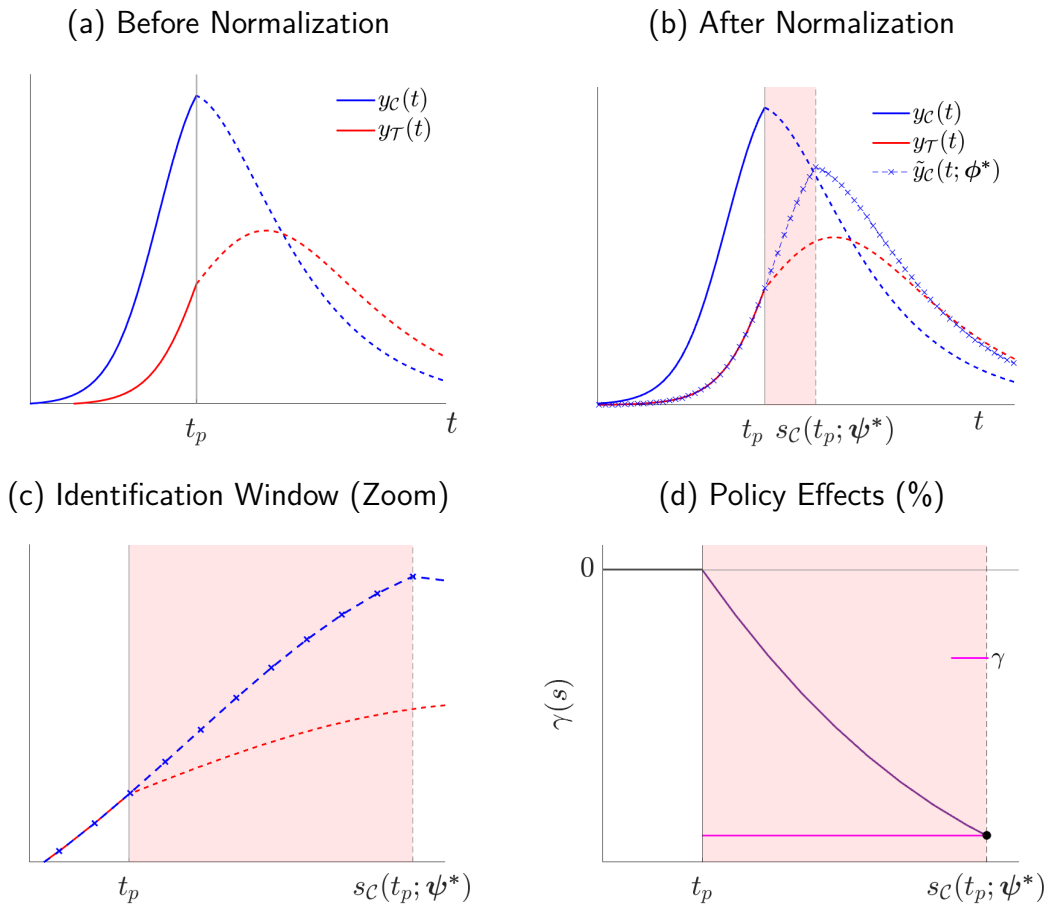


*Notes:* In panel (d), we report the policy effects $\gamma$ together with the interim cumulative effects of policy, $\gamma(s)$, as defined in Section 2.2.

faster. Throughout our analysis and applications, we typically set $K = 1$ and $M = 1$ in (4) and, hence, the normalized path of the non-reference region is $\widetilde{y}_{\mathcal{C}}(s;\boldsymbol{\phi}) = \omega_0 + \omega_1 y_{\mathcal{C}}(\psi_0 + \psi_1 s)$.

Given observed time paths for all regions, i.e., $y_r(t)$ for $r \in \{\mathcal{C}, \mathcal{T}\}$, we determine the unknown coefficients $\boldsymbol{\phi} = \{\boldsymbol{\psi}, \boldsymbol{\omega}\}$ by minimizing the difference between the normalized path of the non-reference region, $\widetilde{y}_{\mathcal{C}}(s;\boldsymbol{\phi})$, and the outcome path of the reference region, $y_{\mathcal{T}}(s)$, that is:

$$\min_{\{\boldsymbol{\phi}\}} \|\widetilde{y}_{\mathcal{C}}(s;\boldsymbol{\phi}) - y_{\mathcal{T}}(s)\|_{\mathbb{C}(s)}\,, \tag{5}$$

where $\|\cdot\|$ is the squared Euclidean distance defined on the interval of stages,

$$\mathbb{C}(s) = \left[s_{\overline{r}}(t_0;\boldsymbol{\psi}), s_{\underline{r}}(t_p;\boldsymbol{\psi})\right] \tag{6}$$

where $s_{\overline{r}}(t_0;\boldsymbol{\psi}) = \max\{s_r(t_0;\boldsymbol{\psi})\}$ and $s_{\underline{r}}(t_p;\boldsymbol{\psi}) = \min\{s_r(t_p;\boldsymbol{\psi})\}$ for $r \in \{\mathcal{C},\mathcal{T}\}$. That is, the interval $\mathbb{C}(s)$ ensures that the minimization (5) only uses the outcome paths up to the stage $s$ in which the policy is implemented first across regions, i.e. $s_{\underline{r}}(t_p;\boldsymbol{\psi})$. Note that the interval $\mathbb{C}(s)$ is determined endogenously during the minimization procedure. Now, we can define the stages of an outcome $y_r(t)$.

**Definition 1.** *The stage of an outcome $y_r(t)$ of region $r$ at time $t$ is $s_r(t;\boldsymbol{\psi}^*)$ where $\boldsymbol{\phi}^* \supset \boldsymbol{\psi}^*$ is the solution to the minimization of (5) subject to (4) and (6).*

In this way, the stages formally emerge as the result of our normalization procedure that maps the outcome path of a non-reference region onto the outcome path of the reference region before policy is implemented. To gain some intuition, we exemplify our method using a nationwide policy that affects the outcome paths of two regions, $y_{\mathcal{C}}(t)$ and $y_{\mathcal{T}}(t)$, in Figure 3. Before policy implementation at time $t_p$, the outcome path of region $\mathcal{C}$ (solid red) differs from region $\mathcal{T}$ (solid blue) in that it starts earlier, grows faster and is larger; see panel (a), which also shows the outcome paths after policy implementation for the two regions (dashed lines).

The normalization procedure—i.e., the minimization of (5) subject to (4) and (6)—achieves two goals. First, it generates a normalized outcome path for the non-reference region in the stage domain, $\widetilde{y}_{\mathcal{C}}(s;\boldsymbol{\phi}^*)$ (cross-dashed blue), that maps—up to minimization error—onto the outcome path of the reference region before the earliest stage in which policy is implemented across regions, $s_{\underline{r}}(t_p;\boldsymbol{\psi}^*)$; see panel (b) of Figure 3.[13] Second, since $s_{\underline{r}}(t_p;\boldsymbol{\psi}^*)$ is endogenous to $\boldsymbol{\psi}^*$, the normalization uncovers heterogeneity in the stage of policy implementation across regions.[14] For example, in our illustration, policy is implemented earlier—in stages—in region $\mathcal{T}$ than in region $\mathcal{C}$, i.e. $s_{\underline{r}}(t_p;\boldsymbol{\psi}) = s_{\mathcal{T}}(t_p;\boldsymbol{\psi}) < s_{\mathcal{C}}(t_p;\boldsymbol{\psi}) = s_{-\underline{r}}(t_p;\boldsymbol{\psi}^*)$ with $\underline{r} = \mathcal{T}$. Also, since we picked $\mathcal{T}$ to be the reference region, we obtain $s_{\underline{r}}(t_p;\boldsymbol{\psi}) = t_p$.

We further decompose the effects of each of the normalization coefficients $\{\phi_i\} \in \boldsymbol{\phi}^*$ on the path of the non-reference region in Figure 4. Since these coefficients are jointly determined in our minimization, we provide a non-orthogonal decomposition where we sequentially add the effects of each parameter. Note that in our illustration $y_{\mathcal{C}}(t_0) = y_{\mathcal{T}}(t_0) = 0$ and $\lim_{t\to\infty} y_{\mathcal{C}}(t) = \lim_{t\to\infty} y_{\mathcal{T}}(t) = 0$ and thus we focus on the role of the proportional level shifter $\omega_1$ together with the stage-to-time transformation parameters $\psi_0$ and $\psi_1$—setting the constant level shifter to zero, $\omega_0 = 0$. In panel (a), we show that the coefficient $\omega_1^* < 1$ proportionally shifts down

[13] Note that outcome variables are typically observed on discrete dates. This is the case in all our applications. In these instances, since the mapping can generate dates $t_{\mathcal{C}}(s;\boldsymbol{\psi}^*)$ that are non-integer values—i.e., non-discrete dates—we interpolate between $y_{\mathcal{C}}(fl(t_{\mathcal{C}}(s;\boldsymbol{\psi}^*);\boldsymbol{\omega}^*)$ and $y_{\mathcal{C}}(cl(t_{\mathcal{C}}(s;\boldsymbol{\psi}^*);\boldsymbol{\omega}^*)$, where $fl(\cdot)$ and $cl(\cdot)$ denote the integer floor or integer ceiling, respectively.

[14] More generally, with more than two regions, $-\underline{r}$ refers to the complement set of $\underline{r}$, i.e. $-\underline{r} = \underline{r}^C$

Figure 4: Decomposition by Normalization Coefficient

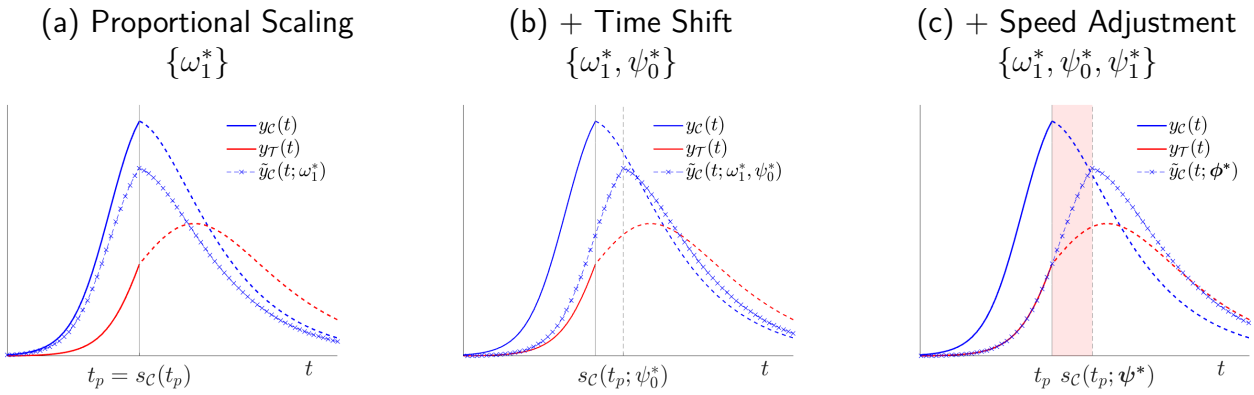


Notes: We sequentially add the normalization parameters $\{\boldsymbol{\phi}\}$ to the non-reference path $y_{\mathcal{C}}(t)$ one-by-one.

the entire outcome path of the non-reference region $\mathcal{C}$ throughout its support. In panel (b), the additional time shifter, $\psi_0^* > 0$, moves the outcome path to the right delaying the outcome's take off. In panel (c), adding the speed adjustment, $\psi_1^* < 1$, decreases the pace of the normalized outcome.[15,16]

## 2.2 Identifying the Policy Effects

In order to identify the policy effects, we exploit the fact that our normalization uncovers heterogeneity of the stage at the time of policy implementation, i.e. $s_{\underline{r}}(t_p;\boldsymbol{\psi}^*) < s_{-\underline{r}}(t_p;\boldsymbol{\psi}^*)$. In particular, we use the fact that inside a window (interval) of stages,

$$\mathbb{W}(s;\boldsymbol{\psi}^*) = \left[s_{\underline{r}}(t_p;\boldsymbol{\psi}^*), s_{-\underline{r}}(t_p;\boldsymbol{\psi}^*)\right], \tag{7}$$

region $\underline{r}$, i.e., the region where the policy is implemented first in stages, is subject to policy whereas region $-\underline{r}$ is not. In this context, we propose the following identification strategy:

**Identification Assumption 1.** *The normalization parameters $\boldsymbol{\phi}^*$ that solve the minimization of (5) subject to (4) and (6) are unaffected by policy.*

[15] We show further illustrations in which additional normalization coefficients provide further help in Appendix A. For example, in cases in which the policy arrives after the outcome path reaches its peak and there is asymmetric behavior in the outcome path—i.e. the growth rate at which the outcome reaches the peak is not the growth rate at which it moves away from the peak—that differs across regions, the normalization coefficient $\psi_2$ in the quadratic term of $t_{\mathcal{C}}$ captures the differences in asymmetric behavior across regions.

[16] Note that in the realm of standard empirical strategies one can partly address the time shift, $\psi_0$. This requires a choice by the researcher to fix the region-specific start dates of the outcome path of interest. For example, for the analysis of a Covid-19 containment policy this has been suggested in an event study design by Liu et al. (2021) and Glogowsky et al. (2021). In contrast, our method endogenously finds the appropriate time shifter ($\psi_0$) together with a potential speed adjustment ($\psi_1$), potential asymmetric behavior ($\psi_2$), etc.

That is, our identification assumes that, absent policy in region $\underline{r}$, the normalized path of the non-reference region obtained using $\phi^*$ and evaluated on stages $s > s_{\underline{r}}(t_p; \boldsymbol{\psi}^*)$ would yield a path identical to that of the reference region for all $s \in \mathbb{W}(s; \boldsymbol{\psi}^*)$.

Here, note that there is no ex-ante assignment to treatment or control for either reference or non-reference regions. Instead, the assignment of regions to treatment or control is determined endogenously (with $\boldsymbol{\psi}^*$) by the fact that policy arrives to the regions at different stages. We refer to the region that is at a more advanced (later) stage at the policy date as the stage-leading region. This region is then endogenously assigned to be the control region.[17] In the illustration, the stage-leading (control) region is $-\underline{r} = \mathcal{C}$, which is untreated inside $\mathbb{W}(s; \boldsymbol{\psi}^*) = [t_p, s_{\mathcal{C}}(t_p; \boldsymbol{\psi}^*)]$ and, hence, serves as no-policy counterfactual for the stage-lagging (treated) region $\underline{r} = \mathcal{T}$ inside that window; see panel (b) in Figure 4. The opposite roles (of reference and non-reference regions) would emerge if we picked $\underline{r} = \mathcal{C}$.[18]

**Policy effect.** Following our illustration, where the control region is $-\underline{r} = \mathcal{C}$ and the treated region is $\underline{r} = \mathcal{T}$, we measure the policy effect for the treated region as,

$$\gamma = \frac{\int_{\mathbb{W}(s;\boldsymbol{\psi}^*)} \left(y_{\mathcal{T}}(s) - \widetilde{y}_{\mathcal{C}}(s; \boldsymbol{\phi}^*)\right) ds}{\int_{\mathbb{W}(s;\boldsymbol{\psi}^*)} \widetilde{y}_{\mathcal{C}}(s; \boldsymbol{\phi}^*) ds}, \tag{8}$$

which measures the cumulative effect of policy relative to the scenario without policy in the treated region inside $\mathbb{W}(s; \boldsymbol{\psi}^*)$; see panel (c), Figure 3. The numerator is the area between the actual outcome path subject to policy of the treated region, i.e. $y_{\mathcal{T}}(s)$ (dashed red), and the no-policy counterfactual path for the treated region, i.e. $\widetilde{y}_{\mathcal{C}}(s; \boldsymbol{\phi}^*)$ (cross-dashed blue). The denominator captures the entire area below the no-policy counterfactual path for the treated region. In panel (d) of Figure 3, we zoom in on the identification window to show the policy effect $\gamma$ together with the interim cumulative effects, $\gamma(s)$. Precisely, $\forall s \in \mathbb{W}(s; \boldsymbol{\psi}^*)$, we define $\gamma(s) = \frac{\int_{s_{\underline{r}}(t_p;\boldsymbol{\psi}^*)}^{s} \left(y_{\mathcal{T}}(\mathfrak{s}) - \widetilde{y}_{\mathcal{C}}(\mathfrak{s};\boldsymbol{\phi}^*)\right) d\mathfrak{s}}{\int_{s_{\underline{r}}(t_p;\boldsymbol{\psi}^*)}^{s} \widetilde{y}_{\mathcal{C}}(\mathfrak{s};\boldsymbol{\phi}^*) d\mathfrak{s}}$ for $\mathfrak{s} \in [s_{\underline{r}}(t_p; \boldsymbol{\psi}^*), s]$ where if $s = s_{-\underline{r}}(t_p; \boldsymbol{\psi}^*)$, then $\gamma(s) = \gamma$.

So far, we have used region $\mathcal{T}$ as reference. Since—as the normalization reveals—, $y_{\underline{r}}(s) = y_{\mathcal{T}}(s)$ is the treated path for all $s \in \mathbb{W}(s; \boldsymbol{\psi}^*) = [t_p, s_{\mathcal{C}}(t_p; \boldsymbol{\psi}^*)]$, the policy effect (8) measures the impact of policy on region $\mathcal{T}$ using as no-policy counterfactual the normalized path of region $\mathcal{C}$. Instead, reversing the reference region to $\mathcal{C}$—i.e., mapping the outcome path $y_{\mathcal{T}}(t)$ onto $y_{\mathcal{C}}(t)$ using pre-policy data and, consequently, redefining the stages for region $\mathcal{C}$ as $\boldsymbol{s} = \boldsymbol{t}_{\mathcal{C}}(\boldsymbol{s}) = t$

[17] We rule out the case of $s_{\underline{r}}(t_p; \boldsymbol{\psi}^*) = s_{-\underline{r}}(t_p; \boldsymbol{\psi}^*)$, where the identification window is empty and thus no identification is possible. Note that this is the case where the pre-policy time paths of the reference and non-reference regions are identical before normalization.

[18] We assess our identification assumption in the context of an analytical examples with exact identification in Section 2.3 and also through a placebo test with model-generated data without exact identification in Section 3.3.1.

Figure 5: Policy Effects with Alternative Reference Region

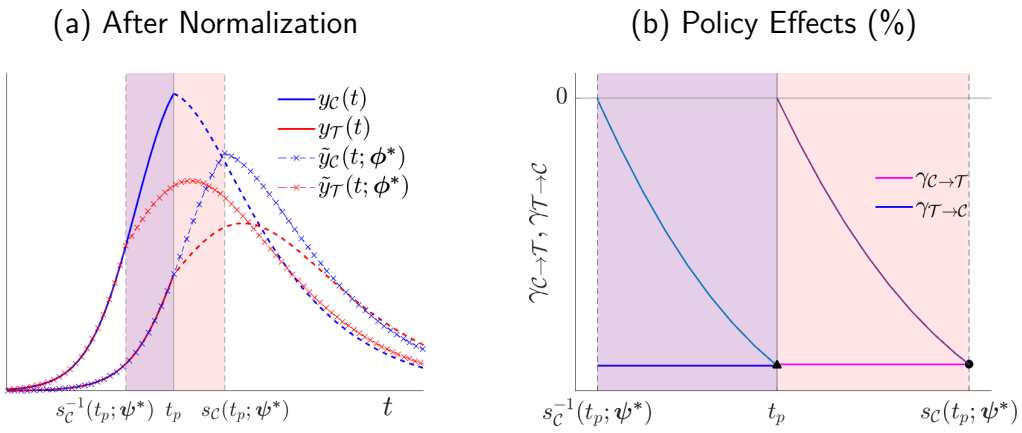


*Notes:* In panel (b), we report the policy effects $\gamma$ together with the interim cumulative effects of policy, $\gamma(s)$, as defined in Section 2.2.

together with $\tilde{\boldsymbol{y}}_{\mathcal{C}}(\boldsymbol{s}) = y_{\mathcal{C}}(t = \boldsymbol{s})$ (and analogously for region $\mathcal{T}$ using (2) and (3))—implies that the normalized path of $\mathcal{T}$, $\tilde{\boldsymbol{y}}_{\mathcal{T}}(\boldsymbol{s})$, is the treated path for all $\boldsymbol{s} \in \mathbb{W}(\boldsymbol{s};\boldsymbol{\psi}^*) = [\boldsymbol{s}_{\mathcal{T}}(t_p;\boldsymbol{\psi}^*), t_p]$, where $\boldsymbol{\psi}^*$ $(\neq \boldsymbol{\psi}^*)$ is the coefficient vector that is obtained when choosing $\mathcal{C}$ as reference region. The associated policy effect measures the impact that the policy would have had on region $\mathcal{C}$ had it been treated at an earlier stage $\boldsymbol{s}_{\mathcal{T}}(t_p;\boldsymbol{\psi}^*)$, where we now compare the observed path of region $\mathcal{C}$ (which is untreated) to the normalized path $\tilde{\boldsymbol{y}}_{\mathcal{T}}(\boldsymbol{s},\boldsymbol{\psi}^*)$ (which is treated). Further, note that the two mappings are explicitly linked because $s_{\mathcal{C}}^{-1}(\mathfrak{t};\boldsymbol{\psi}^*) = \boldsymbol{s}_{\mathcal{T}}(\mathfrak{t};\boldsymbol{\psi}^*)$ for any $\mathfrak{t} \in T$ (e.g. $\mathfrak{t} = t_p$)—that is, the mapping $\mathcal{T}$ to $\mathcal{C}$ undoes the mapping $\mathcal{C}$ to $\mathcal{T}$, and vice versa.[19]

Going back to our example, we show the relationship between mappings in panel (a) of Figure 5 where using region $\mathcal{T}$ as reference implies that the normalization yields the identification window $\mathbb{W}(s;\boldsymbol{\psi}^*) = [t_p, s_{\mathcal{C}}(t_p;\boldsymbol{\psi}^*)]$ (pink shaded area) whereas, when using region $\mathcal{C}$ as reference, the normalization yields the identification window $\mathbb{W}(\boldsymbol{s};\boldsymbol{\psi}^*) = [s_{\mathcal{T}}(t_p;\boldsymbol{\psi}^*), t_p]$, which corresponds to $\left[s_{\mathcal{C}}^{-1}(t_p;\boldsymbol{\psi}^*), t_p\right]$ (purple shaded area). In panel (b) of Figure 5, we show the policy effects for both mappings. In the context of our illustrative example, the policy effects are identical across mappings because there are no level differences across regions, i.e., $\omega_0 = 0$. More generally, in instances where the reference region determines the units of the policy effect (i.e. $\omega_0 \neq 0$), a slight modification of the policy effects defined in (8) that explicitly takes into account the

[19] To see this, note that for any $\mathfrak{t} \in T$ (e.g. $\mathfrak{t} = t_p$), the stage function in the mapping $\mathcal{C}$ to $\mathcal{T}$, $s_{\mathcal{C}}(t;\boldsymbol{\psi}^*) = s = \mathfrak{t}$, injects $t$ into $\mathfrak{t}$ whereas in the mapping $\mathcal{T}$ to $\mathcal{C}$ the function $\boldsymbol{s}_{\mathcal{T}}(\mathfrak{t};\boldsymbol{\psi}^*) = \boldsymbol{s} = t$ injects $\mathfrak{t}$ into $t$.

reference units makes irrelevant the choice of the reference region.[20] Nevertheless, our preferred measure of policy effects is (8) in which, as discussed above, the effects are interpreted differently across mappings.

### 2.3 Exact Identification of Policy Effects: Some Analytical Examples

We now discuss a setting in which we can explicitly express the normalization of the non-reference region in terms of the structural parameters of the data generating process. Note that this serves to illustrate the method, and to provide some guidance for interpretation of the normalization step. Indeed, if the data generating process were actually known, there would be no need to apply SBI; or any other identification method for that matter. Our method operates under the proposition that if there exists a composite function (1) such that

$$\widetilde{y}_{\mathcal{C}}(s) = y_{\mathcal{T}}(s), \tag{10}$$

then our normalization procedure—the minimization of (5) subject to (2) and (6)—recovers the coefficients $\boldsymbol{\phi} = \{\boldsymbol{\psi}, \boldsymbol{\omega}\}$ up to a minimization error by approximating the functions $t_{\mathcal{C}}(.) \approx t_{\mathcal{C}}(.;\boldsymbol{\psi})$, $f_{\mathcal{C}}(.) \approx f_{\mathcal{C}}(.;\boldsymbol{\omega})$ and, hence, $\widetilde{y}_{\mathcal{C}}(.) \approx \widetilde{y}_{\mathcal{C}}(.;\boldsymbol{\phi})$ for all $s \in \mathbb{C}(s)$. Thus, under our identification assumption, we can identify the policy effects for all $s \in \mathbb{W}(s;\boldsymbol{\psi}^*)$.

In this context, here, we are interested in cases where (10) holds and (2) holds with equality and, hence, analytical solutions for the normalization coefficients $\boldsymbol{\phi}$ potentially exist for all $s \in \mathbb{C}(s)$. In that pursuit, consider a scenario in which the outcome path of a region $r$ is,

$$y_r(t) = \left(1 - \gamma_{r,t}\mathbf{1}_{t \geq t_p}\right) g(t;\Theta_r), \qquad \text{for } t \in \{0, \ldots, t_p, \ldots, T\} \tag{11}$$

where $\Theta_r$ is a set of region-specific structural parameters that determine the behavior of the outcome path in that region and $\gamma_{r,t}$ captures the effect of policy that emerges after its nationwide implementation at $t_p$ in regions $r = \{\mathcal{C}, \mathcal{T}\}$.

To identify the effects of the implemented policy, we apply SBI. We pick a region (e.g. $\mathcal{T}$) for the reference outcome path, $y_{\mathcal{T}}(t)$, and postulate a composite function (1) for the outcome

[20] Precisely, for a reference unit $y(\bar{s})$, the adjusted policy effects are:

$$\gamma\left(y(\bar{s})\right) = \frac{\int_{\mathbb{W}(s;\boldsymbol{\psi}^*)} \left(y_{\mathcal{T}}(s) - \widetilde{y}_{\mathcal{C}}(s;\boldsymbol{\phi}^*)\right) ds}{\int_{\mathbb{W}(s;\boldsymbol{\psi}^*)} \left(\widetilde{y}_{\mathcal{C}}(s;\boldsymbol{\phi}^*) - y(\bar{s})\right) ds}. \tag{9}$$

E.g., if $y(\bar{s}) = y_r(s_{\underline{r}}(t_p;\boldsymbol{\psi}^*))$—where $y_{\mathcal{C}}(s_{\underline{r}}(t_p;\boldsymbol{\psi}^*)) = y_{\mathcal{T}}(t_p)$, then the adjusted policy effects (9) are measured with respect to the outcome of the reference region at the time of policy implementation. Note that although these adjusted policy effects are identical across mappings, now they depend on the choice of units, $y(\bar{s})$.

path of the non-reference region, $\widetilde{y}_{\mathcal{C}}(s;\boldsymbol{\phi})$. Here, we are interested in cases where (10) holds and (2) holds with equality because then $\widetilde{y}_{\mathcal{C}}(s;\boldsymbol{\phi})$ and $y_{\mathcal{T}}(s)$ share exactly the same functional form before policy is implemented first in the stage domain, i.e., for all $s \in \mathbb{C}(s)$ and, hence, we can recover—by the method of undetermined coefficients—the set of normalization coefficients by solving for $\phi$ in,

$$\Theta_{\mathcal{T}} = \widetilde{\Theta}_{\mathcal{C}}\left(\boldsymbol{\phi};\Theta_{\mathcal{C}}\right) \qquad \forall s \in \mathbb{C}(s), \tag{12}$$

which is a (potentially nonlinear) system with $n$ equations—where $n$ is the number of structural parameters—and with $p$ unknowns—where $p = M + K + 2$ is the number of normalization coefficients in $\boldsymbol{\phi}$.[21] An interpretation of system (12)—and, hence, of our normalization procedure—is that the normalization coefficients $\boldsymbol{\phi}$ reshape the structural parameters of the non-reference, $\Theta_{\mathcal{C}}$, region into those of the reference region, i.e. $\Theta_{\mathcal{T}} = \widetilde{\Theta}_{\mathcal{C}}$ before policy implementation.

**Theorem 1** *If there exists a composite function* (1) *such that* (10) *holds and* (2) *holds with equality for the regional outcome paths,* $y_r(t)$*, in* (11)*—i.e., if there exists a solution* $\boldsymbol{\phi}^*$ *for the system* (12)*—then stage-based identification (SBI) exactly and uniquely identifies the true policy effects for all* $s \in \mathbb{W}(s;\boldsymbol{\psi}^*)$*.*

*Proof.* If the system (12) holds—i.e., there is an exact solution for $\boldsymbol{\phi}^*$—then the normalized outcome path of the non-reference region, $\widetilde{y}_{\mathcal{C}}(s;\boldsymbol{\phi}^*)$, is exactly identical to the reference path, $y_{\mathcal{T}}(s)$ for all $s \in \mathbb{C}(s) = [s_{\overline{r}}(t_0,\boldsymbol{\psi}^*), s_{\underline{r}}(t;\boldsymbol{\psi}^*)]$. Since the outcome paths follow (11)—i.e., policy affects the path $y_r(t \geq t_p)$ but not the shape of $g(t;\Theta_r)$, then $\boldsymbol{\phi}^*$ is also a solution for the complement stage domain, i.e., for all $s \notin \mathbb{C}(s)$, in particular for $\mathbb{W}(s;\boldsymbol{\psi}^*) = [s_{\underline{r}}(t_p;\boldsymbol{\psi}^*), s_{-\underline{r}}(t_p;\boldsymbol{\psi}^*)]$. This implies that $\widetilde{y}_{\mathcal{C}}(s;\boldsymbol{\phi}^*)$ is exactly identical to $g(s;\Theta_T)$, that is, the true no-policy counterfactual of the reference region for all $s \in \mathbb{W}(s)$. Hence, SBI exactly and uniquely identifies the true policy effects, $\gamma(s)$, for all $s \in \mathbb{W}(s;\boldsymbol{\psi}^*)$. □

**Remark 1.** Note that uniqueness of the normalization coefficients $\boldsymbol{\phi}^*$ is not necessary to recover unique policy effects.[22] To see this, note that although the presence of multiple solutions of $\boldsymbol{\phi}$ implies that there are multiple shapes for $f(.;\boldsymbol{\omega})$ and $t(.;\boldsymbol{\psi})$ that satisfy (10), the implied solution $\widetilde{y}_{\mathcal{C}}(s;\boldsymbol{\phi})$ for (10) is unique and, hence, so is the identified policy effect, $\gamma(s)$. At the same time,

[21] That is, here, the minimization step in the normalization (in Section 2.1) is the solution to the system (12) emerging from the undetermined coefficients approach.

[22] Note that if (10) holds, (2) holds with equality and the inverse function $\boldsymbol{\phi} = \widetilde{\Theta}_{\mathcal{C}}^{-1}\left(\Theta_{\mathcal{T}};\Theta_{\mathcal{C}}\right)$ exists, then there exists a unique solution $\boldsymbol{\phi}^*$ for the system (12). This sufficiency for existence and uniqueness of $\boldsymbol{\phi}^*$ coincides with the Rouché–Frobenius Theorem in the cases where the system (12) is linear.

Figure 6: Stage-Based Identification of Policy Effects: Three Examples with Exact Identification

(a) Logistic Function (b) Trigonometric Function (b) Cubic Polynomial

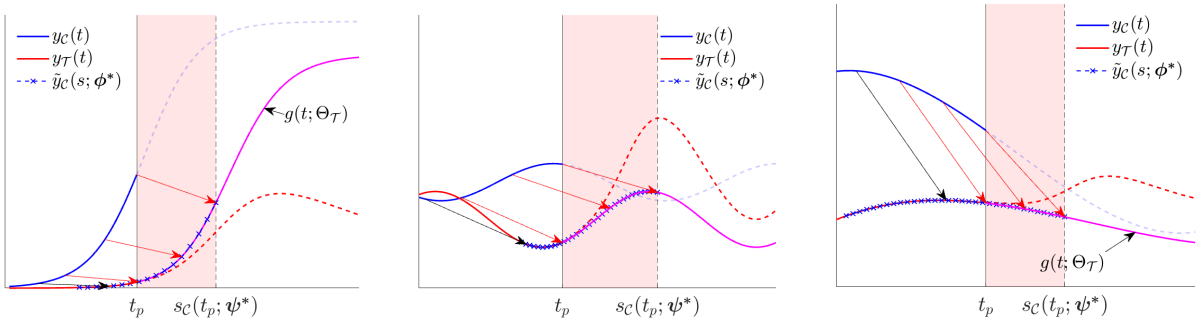


*Notes:* These panels show the SBI effects in examples with closed-form solutions for $\phi^*$ when the data generating process is assumed to be known. In each panel, we assume that the outcome time path $g(t;\Theta_r)$ in (11) follows: (a) the logistic function in (13); (b) a trigonometric function $\theta_{0,r}+\theta_{1,r}sin(\theta_{2,r}+\theta_{3,r}t)$; and (c) a cubic polynomial $\sum_{j=0}^{3}\theta_{j,r}t^j$, respectively. The analytical derivations are in Appendix B.

the overall policy effect, $\gamma$, is determined by the interim policy effects, $\gamma(s)$, and the size of the identification window, $W(s;\psi^*)$, which can differ by $\phi^*$; see our discussion in Appendix B.2.2.[23]

We now discuss some functional forms for the outcome paths, $y_r(t)$, for which SBI yields analytical solutions for $\phi$ using the approach just described. We start with logistic functions. Assume that the regional outcome paths $y_r(t)$ are determined by (11) and that, absent policy, these paths are determined by,

$$g(t;\Theta_r)=\frac{\theta_{1,r}-\theta_{0,r}}{1+\exp\left(-\theta_3 t+\theta_{2,r}\right)}+\theta_{0,r} \tag{13}$$

where $\Theta_r=\{\theta_{0,r},\theta_{1,r},\theta_{2,r},\theta_{3,r}\}$ is a set of region-specific structural parameters that determine the behavior of the outcome paths for regions $r=\{\mathcal{C},\mathcal{T}\}$. We show an illustration of these paths for region $\mathcal{C}$ and $\mathcal{T}$ in panel (a) of Figure 6.[24] To identify the policy effects, we apply SBI picking a region (e.g. $\mathcal{T}$) for the reference path and postulating a composite for the non-reference region, $\tilde{y}_{\mathcal{C}}(s;\phi)=\omega_1 y_{\mathcal{C}}(\psi_0+\psi_1 s)+\omega_0$. Then, we solve for the normalization coefficients

[23] If policy is applied non-nationwide (see Section 5.3), then the overall policy effect $\gamma$ is also identical across potential multiple solutions of $\phi^*$ because the identification window is open, i.e. $\mathbb{W}(s;\psi^*)=[s_{\underline{\mathcal{T}}}(t_p;\psi^*),\infty)$.

[24] We assume that the outcome path for region $\mathcal{C}$ takes off earlier, so that $-\frac{\theta_{2,\mathcal{C}}}{\theta_{3,\mathcal{C}}}<-\frac{\theta_{2,\mathcal{T}}}{\theta_{3,\mathcal{T}}}$, grows faster with $\theta_{3,\mathcal{C}}>\theta_{3,\mathcal{T}}$, starts at level $\theta_{0,\mathcal{C}}=\theta_{0,\mathcal{T}}=0$ (left asymptote) and shows a larger magnitude with $\theta_{1,\mathcal{C}}>\theta_{1,\mathcal{T}}$ (right asymptote) than the outcome path in region $\mathcal{T}$.

$\boldsymbol{\phi} = \{\psi_0, \psi_1, \omega_0, \omega_1\}$ in (10) holding (2) with equality for all $s \in \mathbb{C}(s)$, that is,

$$\widetilde{y}_{\mathcal{C}}(s;\boldsymbol{\phi}) = \omega_1 y_{\mathcal{C}}(\psi_0 + \psi_1 s) + \omega_0 = \frac{\overbrace{\omega_1\left(\theta_{1,\mathcal{C}} - \theta_{0,\mathcal{C}}\right)}^{\theta_{1,\mathcal{T}} - \theta_{0,\mathcal{T}}}}{1 + \exp(-\underbrace{\theta_{3,\mathcal{C}}\psi_1}_{\theta_{3,\mathcal{T}}} s + \underbrace{(\theta_{2,\mathcal{C}} - \theta_{3,\mathcal{C}}\psi_0))}_{\theta_{2,\mathcal{T}}}} + \underbrace{\omega_1\theta_{0,\mathcal{C}} + \omega_0}_{\theta_{0,\mathcal{T}}} = y_{\mathcal{T}}(s)$$

and, thus, by the method of undetermined coefficients we find $\boldsymbol{\phi} = \{\psi_0, \psi_1, \omega_0, \omega_1\}$ solving,

$$\underbrace{\begin{bmatrix} \theta_{0,\mathcal{T}} \\ \theta_{1,\mathcal{T}} \\ \theta_{2,\mathcal{T}} \\ \theta_{3,\mathcal{T}} \end{bmatrix}}_{\Theta_{\mathcal{T}}} = \underbrace{\begin{bmatrix} \omega_1\theta_{0,\mathcal{C}} + \omega_0 \\ \omega_1\theta_{1,\mathcal{C}} + \omega_0 \\ \theta_{2,\mathcal{C}} - \psi_0\theta_{3,\mathcal{C}} \\ \psi_1\theta_{3,\mathcal{C}} \end{bmatrix}}_{\widetilde{\Theta}_{\mathcal{C}}(\boldsymbol{\phi},\Theta_{\mathcal{C}})} \qquad \forall s \in \mathbb{C}(s), \tag{14}$$

which is a linear system of four equations and four unknown normalization coefficients $\boldsymbol{\phi}^* = \{\psi_0^*, \psi_1^*, \omega_0^*, \omega_1^*\}$. It is straightforward to see that the inverse $\boldsymbol{\phi} = \widetilde{\Theta}_{\mathcal{C}}^{-1}(\Theta_{\mathcal{T}}; \Theta_{\mathcal{C}})$ exists and, hence, there exists a unique analytical solution for $\boldsymbol{\phi}^*$,

$$\omega_1^* = \frac{\theta_{0,\mathcal{T}} - \theta_{1,\mathcal{T}}}{\theta_{0,\mathcal{C}} - \theta_{0,\mathcal{C}}}, \qquad \omega_0^* = \theta_{0,\mathcal{T}} - \theta_{0,\mathcal{C}}\left(\frac{\theta_{0,\mathcal{T}} - \theta_{1,\mathcal{T}}}{\theta_{0,\mathcal{C}} - \theta_{0,\mathcal{C}}}\right)$$
$$\psi_1^* = \frac{\theta_{3,\mathcal{T}}}{\theta_{3,\mathcal{C}}}, \qquad \psi_0^* = \frac{\theta_{2,\mathcal{C}} - \theta_{2,\mathcal{T}}}{\theta_{3,\mathcal{C}}}.$$

The normalization uncovers cross-regional stage heterogeneity at the time of policy implementation: in our illustration, the non-reference region is at a more advanced stage than the reference region at $t_p$, i.e. $s_{\underline{r}}(t_p; \boldsymbol{\psi}^*) = t_p$. This opens a window in the stage domain in which region $\mathcal{T}$ is subject to policy whereas region $\mathcal{C}$ is not, i.e., $\mathbb{W}(s; \boldsymbol{\psi}^*) = \left[t_p, s_{\mathcal{C}}(t_p, \boldsymbol{\psi}^*) = \frac{\theta_{2\mathcal{T}} - \theta_{2\mathcal{C}}}{\theta_{3\mathcal{T}}} + \frac{\theta_{3,\mathcal{C}}}{\theta_{3,\mathcal{T}}} t_p\right]$. Then, under our identification assumption, the normalized outcome path of the non-reference region, $\widetilde{y}_{\mathcal{C}}(s; \boldsymbol{\phi}^*)$, serves as no-policy counterfactual for the reference region for all $s \in \mathbb{W}(s; \boldsymbol{\psi}^*)$. Indeed, since the outcome paths follow (11), $\boldsymbol{\phi}^*$ is also an analytical solution for the complement stage domain, i.e., for all $s \notin \mathbb{C}(s)$. That is, for all $s \in \mathbb{W}(s; \boldsymbol{\psi}^*)$, the normalized outcome path of the non-reference region, i.e. $\widetilde{y}_{\mathcal{C}}(s; \boldsymbol{\phi}^*)$, is identical to the reference path in the no-policy scenario, i.e. $g(t; \Theta_{\mathcal{T}})$ (solid magenta line); see panel (a), Figure 6. Thus, the identified policy effect is unique and identical to the true policy effect.

We repeat this analysis for outcome paths that follow trigonometric functions, polynomial functions and generalized logistic functions. In panel (b) of Figure 6, we show the results of applying SBI for the case where $g(t; \Theta_r) = \theta_{1,t} \sin(\theta_{3,r} t + \theta_{2,t}) + \theta_{0,t}$. In panel (c) of Figure 6,

we show the results of applying SBI for the case where $g(t;\Theta_r) = \sum_{i=0}^{I} \theta_i t^{i=1}$ with $I = 3$. We further show the case for time paths that follow a generalized logistic function in Appendix B.3. In all these cases, we find a unique closed-form solution for $\phi^*$ (see our derivations in Appendix B) and the identified policy effect is unique and identical to the true policy effect.

# 3 Method Performance

More generally, we are interested in assessing policy in contexts where the data generating process is unknown. Here, we first implement SBI on model-generated data (without using any knowledge about the theoretical model) and compare the identified effects with the true effects; Section 3.1. Second, we conduct a Monte Carlo analysis that provides bounds to the performance of our method; Section 3.2. There, we further assess how our method fares with time-varying heterogeneity, confounding policy, and endogenous policy. Third, we conduct inference; Section 3.3.

## 3.1 Does SBI Identify the True Policy Effects?

To address this question, we use three alternative policy contexts: a public health policy against a pandemic using a model where economic activity in the form of hours worked shapes and is shaped by a pandemic; the effects of the approval of the pill in a model of women career and fertility choices; and an economic growth policy using a model of structural transformation.

### 3.1.1 Public Health Policy Against a Pandemic

Here, we pose an economic model in the context of an epidemic where labor supply generates infections (and deaths). Then, we assess whether SBI recovers the model-generated effects of a nationwide lockdown that restricts labor supply after some period $t_p$.

At the beginning of each period $t \in \{0, 1, \ldots\}$, total population $N_t$ is composed of a stock of susceptible population $S_t$, infected individuals $I_t$ and recovered individuals $R_t$, with $N_t = S_t + I_t + R_t$ and the normalization $N_0 = 1$. An epidemic starts with an initial number of infected $I_1 > 0$ in period $t = 1$. For pre-pandemic periods $t < 1$, the population is constant with $N_0 = S_0$ and $I_0 = R_0 = 0$. The probability that a susceptible individual meets an infected individual is given by $\beta \frac{I_t}{N_t}$, for $\beta \in (0, 1)$.[25] We assume that conditional on meeting there exists an objective probability $\lambda_{\mathcal{O}}(h_t)$ of getting infected which depends on economic activity here reflected by the average hours worked $h_t$. Further, with probability $\mu$ infected individuals in a given period $t$ recover or die from the disease where the conditional probability of death in turn

[25] Parameter $\beta$ captures features like density, health or pollution (among others) which can differ across regions.

is denoted by $\zeta$. New infections transit to death in the same period $t$, i.e. $h_t$ has an immediate effect on the survival rate between $t$ and $t+1$.[26]

In this context, we consider the problem of a social planner that is constrained in that she has imperfect knowledge about the infection process. In particular, the planner's beliefs of the infection probability are $\lambda_{\mathcal{P}}(h_t)$, which may differ from the objective probability. Specifically, let $\lambda_b(h_t) = \xi_b h_t^{\alpha}$, $\xi_b > 0$ and $\alpha \in (0,1)$, for beliefs $b \in \{\mathcal{O}, \mathcal{P}\}$, where $\mathcal{O}$ stands for objective and $\mathcal{P}$ for perceived. Thus, if $\xi_{\mathcal{P}} < \xi_{\mathcal{O}}$ then the constrained planner underestimates the actual effects of average hours worked $h_t$ on infections and vice versa if $\xi_{\mathcal{P}} > \xi_{\mathcal{O}}$.

At every period $t$, before making plans for all future periods $z \geq t$, the planner receives an unanticipated knowledge shock that reveals the actual state of the economy $G_{\mathcal{O},t}$ for $G = (S, I, R, D)$, which potentially differs from the perceived state $G_{\mathcal{P},t}$. We assume that the planner updates the perceived survival probability accordingly and before choosing labor supply. Precisely, letting $X_{G,b,t} = G_{b,t+1} - G_{b,t}$, the planner's perceived survival probability is revised at the beginning of every period $t$ to $\phi_{\mathcal{P}}(h_t) = 1 - \frac{X_{D,\mathcal{P},t}}{\tilde{N}_{b,t}}$ with $\tilde{N}_{b,t} = N_{\mathcal{O},t}$ for $t = z$ and $\tilde{N}_{b,t} = N_{\mathcal{P},t}$ if $t > z$.[27] Note that although the knowledge shock allows the planner to update the state of the economy at the beginning of every period $t$, however, since these shocks are unanticipated, the planner is unable to correct future forecast errors, i.e. $G_{\mathcal{O},z} - G_{\mathcal{P},z}\,|t$ for periods $z > t$.[28]

After updating the perceived survival probability, the planner maximizes the present-discounted stream of per period utilities for all periods $z \geq t$ with discount factor $\delta$ times the perceived unconditional probability to survive from any period $t$ to the future, $\prod_{j=t+1}^{z} \phi_{\mathcal{P}}(h_{j-1})$. Importantly, since the perceived survival probability is revised at the beginning of every period $t$, the nature of the discounting process changes each period $t$ and, hence, the planner needs to re-optimize—at each period $t$—the decision plans for all periods $z \geq t$. The per period utility, $u(c_z, h_z; \chi)$ is assumed strictly concave in consumption $c_z \geq 0$ and leisure $1 - h_z \in [0,1]$ for a value of life parameter $\chi$. Collecting elements, at each period $t$ the constrained social planner solves,

$$\max_{\{c_z \geq 0, h_z \in [0,1]\}_{z=t}^{\infty}} \sum_{z=t}^{\infty} \delta^{z-t} \prod_{j=t+1}^{z} \phi_{\mathcal{P}}(h_{j-1}) u(c_z, h_z; \chi), \tag{15}$$

subject to an aggregate resource constraint $N_{\mathcal{P},z} c_z = w h_z N_{\mathcal{P},z}$ where $w$ is the implicit price (marginal product) of labor using technology $Y_z = a h_z N_{\mathcal{P},z}$.

[26] This innocuous assumption eases the exposition of the trade-off between economic activity and public health.

[27] Note that without subjective beliefs, the population evolves essentially as in, for example, Atkeson (2020).

[28] The forecast errors $\varepsilon_{G,z} = (G_{\mathcal{O},z} - G_{\mathcal{P},z}\,|t)$ can be reduced asymptotically with learning (Adam et al., 2017). For example, there could be learning about the odds of infection as in Aleman et al. (2022).

Figure 7: Stage-Based Identification of Model-Generated Policy Effects: A Nationwide Public Health Policy Against a Pandemic

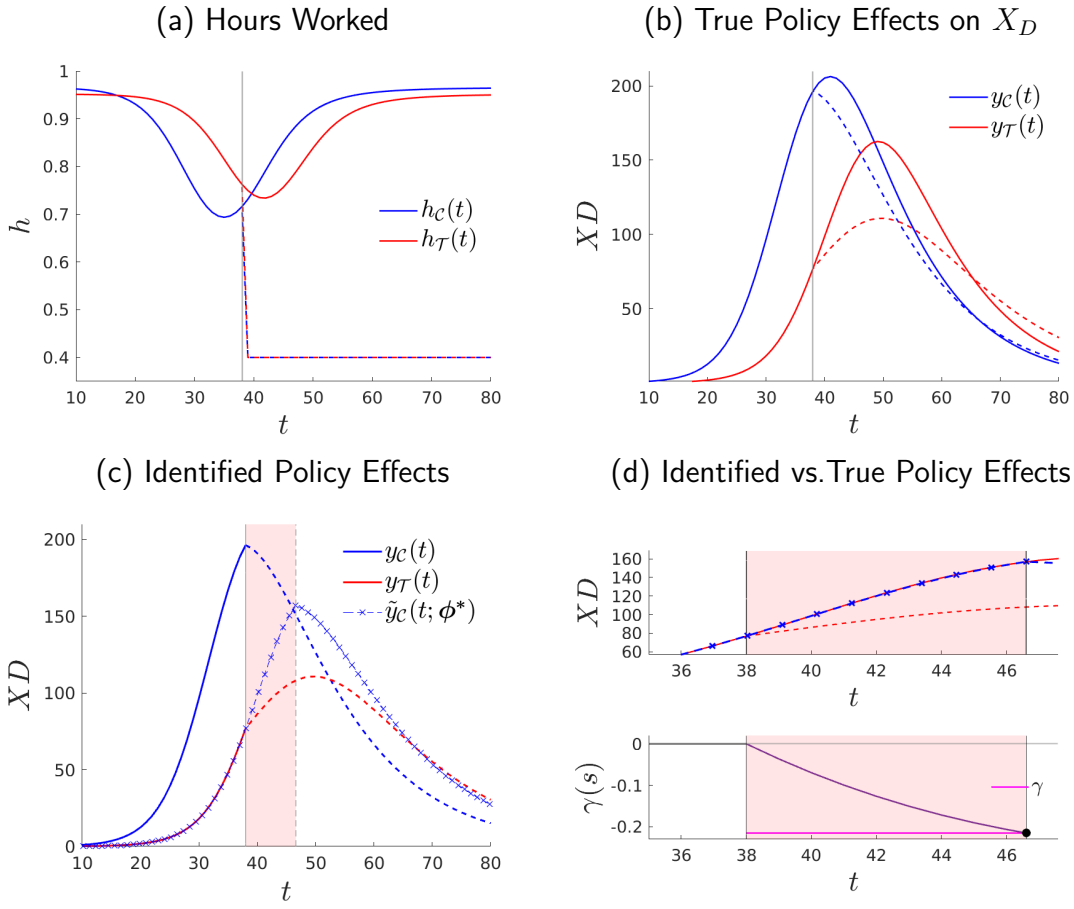


*Notes:* We assume that $u(c_z, h_z) = \ln(c_z) - \kappa \frac{h_z^{1+\frac{1}{\nu}}}{1+\frac{1}{\nu}} + \chi$ for value of life parameter $\chi$. Some parameters differ across regions: $\Theta_{\mathcal{C}} = \{\beta = 0.509, \zeta = 0.0010, \kappa = 1.05, \xi = 0.20, I_0 = 1\}$ and $\Theta_{\mathcal{T}} = \{\beta = 0.501, \zeta = 0.0008, \kappa = 1.07, \xi = 0.19, I_0 = 6\}$. The rest of the model parameters are identical across regions, $\{\delta = 0.95, \chi = 560400, z = 64, \beta = 0.501, \alpha = 0.65\}$. The parameters associated to the policy are $\bar{h} = 0.4, t_p = 38, t_f = 250$.

Then, given $t$, the amount of economic activity $h_z$ is determined by the following condition,

$$\underbrace{\frac{\partial u(c_z, h_z; \chi)}{\partial c_z} w}_{\substack{\text{Marginal Benefit of Working:} \\ \text{Consumption Gain}}} - \underbrace{\frac{\partial u(c_z, h_z; \chi)}{\partial h_z}}_{\substack{\text{Marginal Cost of Working:} \\ \text{Loss of Leisure}}} = \underbrace{\delta \frac{\partial \phi_{\mathcal{P}}(h_z)}{\partial h_z} u(c_{z+1}, h_{z+1}; \chi)}_{\substack{\text{Marginal Cost of Working:} \\ \text{Loss of Lives}}} \qquad \forall z \geq t, \tag{16}$$

stating that the marginal benefit of working (more consumption) equates its marginal costs consisting of an intratemporal component (disutility from working) and an intertemporal component

(loss of lives). Since the Euler equation (16) is a first-order difference equation in $h_z$, we can easily solve for the optimal labor path during the epidemic using standard techniques.[29]

**True (model-generated) policy effects.** We solve the model for two regions that differ in the underlying parameter values for $\Theta = \{\delta, \chi, a, \beta, \mu, \zeta, \kappa, \nu, \{\xi_i\}_{i\in\{\mathcal{O},\mathcal{P}\}}, \alpha, I_1\}$. In particular, we assume that the planner in region $\mathcal{C}$ underestimates the effect that economic activity has on infections by less than the planner in region $\mathcal{T}$. Consequently, hours are reduced earlier and also by a larger amount in region $\mathcal{C}$ than region $\mathcal{T}$ in response to the epidemic. The equilibrium response of hours without policy intervention for region $\mathcal{C}$ (solid blue) and region $\mathcal{T}$ (solid red) are shown in panel (a) of Figure 7. The earlier and stronger response in terms of hours of region $\mathcal{C}$ affects our outcome of interest, i.e., the epidemic path of deaths, by reducing the peak of deaths and flattening the curve in region $\mathcal{C}$ relative to region $\mathcal{T}$; see panel (b) in Figure 7. We also assume that region $\mathcal{C}$ has higher odds of encountering infected individuals at work (i.e., higher $\beta$) which advances and increases the peak of deaths for region $\mathcal{C}$ relative to region $\mathcal{T}$. Further, we assume that region $\mathcal{C}$ has a lower disutility of work $\kappa$ which implies a larger pre- and post-pandemic level of hours worked for region $\mathcal{C}$ than region $\mathcal{T}$.

In this scenario, we now introduce a nationwide public health policy that imposes an upper bound on hours worked, $h < \overline{h} = 0.5$, from $t_p = 38$ to $t_f = 250$. Since, without policy, households in both regions would work more hours than $\overline{h}$, the policy is binding in both $\mathcal{C}$ and $\mathcal{T}$—see the respective dashed lines that emerge after $t_p$ in panel (a) of Figure 7. The lower economic activity imposed by the policy has consequences for the flow of deaths. With policy, the flow of deaths peaks earlier and by a lower magnitude in both $\mathcal{C}$ and $\mathcal{T}$—see the respective dashed lines that emerge after $t_p$ in panel (b) of Figure 7. The difference between the flow of deaths with policy (dashed lines) and the flow of deaths without policy (solid lines) after $t_p$ captures the true effects of policy generated from the model. However, the counterfactual paths of the flow of deaths without policy after policy implementation (i.e. the solid lines after $t_p$) are not available outside of the model. That is, from the perspective of an evaluator that wants to assess the policy effects, the data available for policy evaluation consists of the path without policy (solid lines) for all periods up to $t_p$ along with the path with policy (dashed lines) for all periods after $t_p$. We now apply SBI on this data.

**Stage-Based identified policy effects.** The policy effects identified in this manner are shown in panel (c) of Figure 7. In particular, we map the path of the flow of deaths in region $\mathcal{C}$ (solid blue line) onto the path of region $\mathcal{T}$ (solid red line) using *only* pre-policy data; as described in Section 2. The result of SBI is a candidate no-policy counterfactual $\widetilde{y}_{\mathcal{C}}(s;\boldsymbol{\phi}^*)$ (blue line with cross

[29] We provide the algorithms that we use to solve this (and the other models) of this paper in Appendix C.

markers) for region $\mathcal{T}$ in the identification window $\mathbb{W}(s;\boldsymbol{\psi}^*) = [t_p, s_{\mathcal{C}}(t_p;\boldsymbol{\psi}^*)]$ (shaded pink area). In order to assess whether the identified policy effects recover the true policy effects generated by the model, we zoom in on the identification window in panel (d) of Figure 7 and compare our candidate counterfactual $\widetilde{y}_{\mathcal{C}}(s;\boldsymbol{\phi}^*)$ with the true counterfactual (solid red line). The main result is that the identified policy effects are not significantly different from the true effects. The identified total number of lives saved is $\int_{\mathbb{W}(s;\boldsymbol{\psi}^*)} (\widetilde{y}_{\mathcal{C}}(s,\boldsymbol{\phi}^*) - y_{\mathcal{T}}(s))\, ds = 248.545$ in a window of $s_{\mathcal{C}}(t_p;\boldsymbol{\psi}^*) - t_p = 8.601$ days, whereas the true policy effects are 250.728 lives saved. Therefore, the policy prevented $\gamma = -21.496\%$ of the total deaths that would have occurred had the policy not been implemented, whereas the true effect is $\gamma_{\text{true}} = -21.644\%$. This implies that the margin of error is $\varepsilon(\gamma) = \left|\left(\frac{\gamma}{\gamma_{\text{true}}} - 1\right) \times 100\right| = 0.683\%$.

### 3.1.2 Oral Contraceptives and Women's Choices

We now pose a model in which the introduction of oral contraceptives (the pill) has effects on women's human capital, sexual and fertility choices. The pill provides access to a technology that reduces unwanted pregnancies at the time (age) where human capital decisions are taken. We use this framework to assess whether SBI recovers the model-generated effects of the pill.

We assume that each cohort $t$ of women derives utility from their choices on consumption $c \geq 0$, children $n \geq 0$ and sexual intercourse $x \geq 0$ and experiences disutility from pill usage $o$—e.g. a social norm. In addition, a woman chooses human capital investment paying $q$ (tuition fees or job training) per unit of human capital. Earnings feature two components, a wage level $w$, and an endogenous human capital wage premium $z_t e(h)$ with the two components technology level $z_t$ and a complementarity factor $e(h) \in [0,1]$[30] with $e_h(h) > 0, e_{hh}(h) < 0$ so that earnings per unit of time are $w(1 + z_t e(h))$. We model skill-biased technical change (SBTC) with a cohort-$t$ specific growth factor $\gamma_t$ so that $z_t = z_0 \prod_{\tau=1}^{\tau=t}(1+\lambda_\tau)$, where $z_0 > 0$ and $\lambda_t > 0$. We further assume that raising children bears a time cost of $\tau(n) \in [0,1]$ with $\tau_n(n) > 0, \tau_{nn}(n) < 0$ so that earnings are $(1 - \tau(n))w(1 + z_t e(h))$. Sexual intercourse increases the probability of pregnancy $\phi(x) \in [0,1]$ where $\phi_x(x) > 0, \phi_{xx}(x) < 0$ and we assume that successful pregnancies result in children. If women have access to the pill—which we model through policy dummy $\mathbf{1}_{t_p}$ that is equal to zero if a cohort $t$ does not have access to the pill, and equal to one otherwise—, then the probability of pregnancy is adjusted downward by the pill effectiveness in preventing pregnancy, $g(o) \in [0,1]$. We assume that larger use of the pill—e.g., better adherence to follow protocol—increases the effectiveness of the pill. That is, $g_o(o) > 0$ with $g_{oo}(o) < 0$.[31]

[30] The mapping of the outcome variable from $h$ to $e(h)$ is innocuous. In particular, since we model $e(h)$ as a rate we can interpret it as the fraction of educated women (e.g. college degree completion) in the population.

[31] Lawful access to the pill does not suffice to determine use which is also likely affected by social norms Goldin and Katz (2002). Further, the pill can—at the same time—shape social norms (Fernández-Villaverde et al., 2014).

Collecting elements, a woman solves

$$\max_{\{h,o,x\}} c + \kappa n + \zeta x - \iota o \tag{17}$$

subject to the budget constraint (18) and the children production technology (19):

$$c + qh = (1 - \tau(n))w(1 + z_t e(h)), \tag{18}$$

$$n = \phi(x)[1 - \mathbf{1}_{t_p} g(o)] \tag{19}$$

Plugging (18) and (19) into (17), the first order condition (FOC) of $h$ is,

$$FOC(h): \quad \underbrace{q}_{\text{Marginal Cost of Human Capital}} = \underbrace{(1 - \tau(n))w z_t e_h(h)}_{\text{Marginal Benefit of Human Capital}}, \tag{20}$$

where the price of human capital equates the marginal benefit consisting of a wage premium net of the costs of children. Since $q$ is constant, the marginal benefit trades off $n$ and $h$, i.e. a technology that reduces $n$ enhances human capital. The FOC for sexual intercourse $x$ is:

$$FOC(x): \quad \underbrace{\tau_n(n)\phi_x(x)(1 - \mathbf{1}_{t_p} g(o))w(1 + z_t e(h))}_{\text{Marginal Cost of Intercourse}} = \underbrace{\zeta + \kappa_t \phi_x(x)(1 - \mathbf{1}_{t_p} g(o))}_{\text{Marginal Benefit of Intercourse}}, \tag{21}$$

where the marginal benefit considers the additional utility from sex and children. The marginal cost reflects the cost of children in terms of human capital. The FOC for pill use $o$ is:

$$FOC(o): \quad \underbrace{\tau_n(n)\phi(x)\mathbf{1}_{t_p} g(o) w(1 + z_t e(h))}_{\text{Marginal Benefit of Pill}} = \underbrace{\kappa_t \phi(x)\mathbf{1}_{t_p} g_o(o) + \iota}_{\text{Marginal Cost of Pill}} \tag{22}$$

where the marginal cost of the pill is a reduction of utility derived from children and the marginal benefit of the pill is a reduction in the price of human capital.

**True (model-generated) policy effects.** In Figure 8, we show the equilibrium path for women's schooling choices in panel (a) and fertility choices in panel (b). We show the model-generated paths in a scenario without the pill (solid lines) and in a scenario in which the government grants women legal access to the pill technology (dashed lines). We do this separately for region $\mathcal{C}$ (blue) and region $\mathcal{T}$ (red). Regions differ in the model parameters $\Theta = \{\kappa, \xi, q, w, z, \{\lambda_t\}_{t=1}^T, \theta_x, \theta_h, \theta_o\}$. In particular, we allow for the returns to human capital to be larger and grow faster in region $\mathcal{C}$ than in region $\mathcal{T}$ which explains the higher human capital in region $\mathcal{C}$ than in region $\mathcal{T}$. This also explains the lower fertility in region $\mathcal{C}$ than in region $\mathcal{T}$. Further, we exogenously shape the SBTC parameter $\gamma$ such that the endogenous human capital

Figure 8: Stage-Based Identification of Model-Generated Policy Effects: Introduction of the Pill

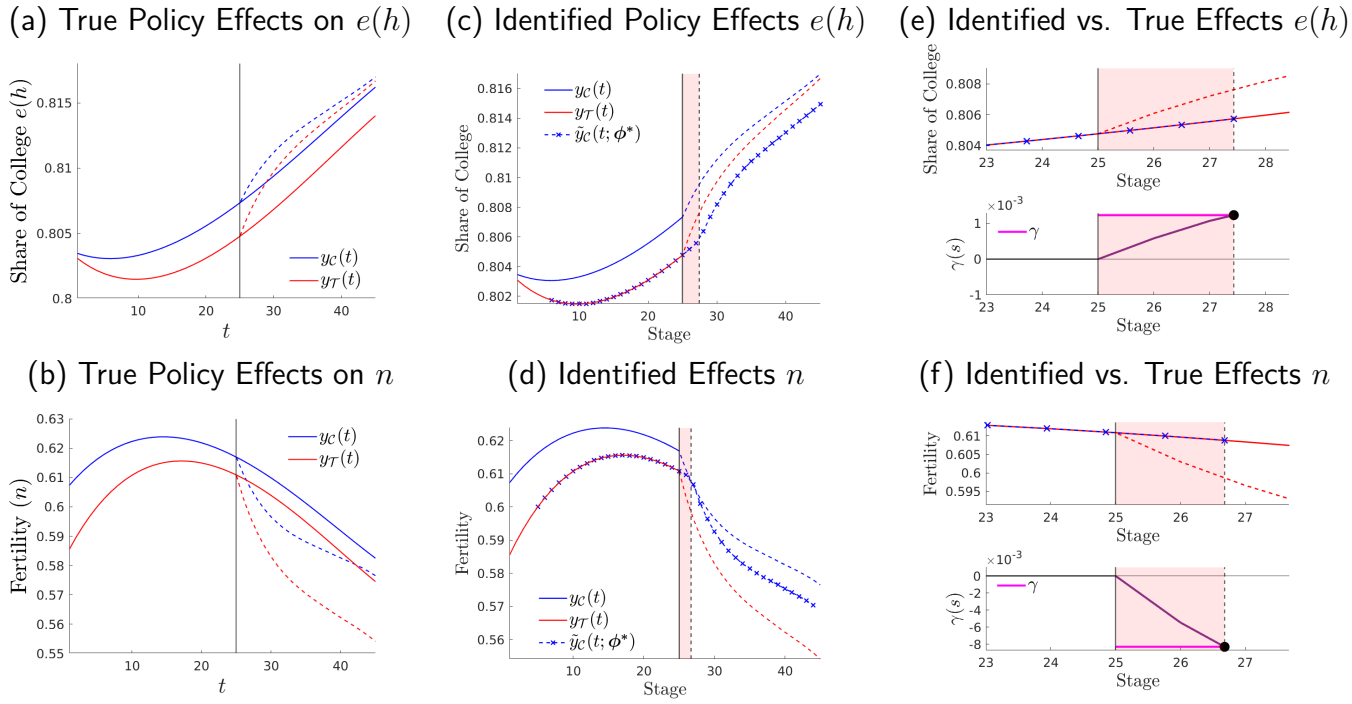


*Notes:* We plot outcomes for region $\mathcal{C}$ (red) and $\mathcal{T}$ (blue) without policy (solid lines) and with policy (dashed lines). The policy is the introduction of the pill for all periods $t_p \geq 25$. The parameter values that we choose for region $\mathcal{C}$ are $\Theta_{\mathcal{C}} = \{\xi = 8, q = 3.2, w = 64, z_0 = 1, \lambda = 0.1\%, \theta_x = 0.5, \theta_h = 0.4, \theta_o = 0.43, \iota_{t,\mathcal{C}}, \kappa_{t,\mathcal{C}}\}$ and for region $\mathcal{T}$ are $\Theta_{\mathcal{T}} = \{\xi = 8, q = 3.3, w = 63, z_0 = 1, \lambda = 0.1\%, \theta_x = 0.5, \theta_h = 0.4, \theta_o = 0.43, \iota_{t,\mathcal{T}}, \kappa_{t,\mathcal{T}}\}$.

path is S-shaped for both regions. We also choose an exogenous path for the relative utility derived from children, $\kappa$, in order for endogenous fertility to display a boom and bust.

Here, we assess the efffects of legalizing the pill permanently with $\mathbf{1}_{t_p} = 1$ for all cohorts of women $t_p \geq 25$. The policy endogenously reduces births $(n)$ in both regions (dashed lines panel (b), Figure 8).[32] By reducing fertility, the pill reduces the cost of acquiring human capital which increases the share of women entering college $(e(h))$ (dashed lines in panel (a), Figure 8).

**Stage-Based Identified policy effects.** We apply SBI using region $\mathcal{T}$ as reference, hence, mapping the outcome path of region $\mathcal{C}$ (solid blue) onto that of region $\mathcal{T}$ (solid red) using only pre-policy data as in Section 2. Again, SBI delivers a candidate counterfactual $\widetilde{y}_{\mathcal{C}}(s;\boldsymbol{\phi}^*)$ (blue line with cross markers) for an identification window $\mathbb{W}(s;\boldsymbol{\psi}^*) = [t_p, s_{\mathcal{C}}(t_p;\boldsymbol{\psi}^*)]$ (shaded pink area); see panels (c) and (d) of Figure 8 for human capital and children, respectively. We zoom in the comparison between the identified and the true effects in panel (e) and (f) of Figure 8 for

[32] The reduction in fertility follows an increase in the use of the new technology. The pill sustains a higher amount of sex with a lower amount of children and, hence, higher human capital.

human capital and children, respectively. We find that the SBI policy effects capture well the true effects. The identified effect on human capital is an increase in the proportion of women going to college $e(h)$ by $\gamma = 0.122\%$, whereas the true policy effects are $\gamma_{\text{true}} = 0.123\%$. The identified effect on fertility is a reduction by $\gamma = 0.830\%$, whereas the true effect is $\gamma_{\text{true}} = 0.828\%$. The error $\varepsilon(\gamma)$ of the identified policy effects relative to the true policy effects is 0.182% for human capital and of 0.232% for fertility.

### 3.1.3 Growth Policy and Structural Transformation

We pose a structural transformation model assuming the presence of inefficient institutions in one economic sector (e.g. agriculture). Then, we assess whether SBI captures the model-generated effects on per capita income of a nationwide policy reform that reduces this inefficiency.

There are two sectors in the model denoted by $i \in \{a, m\}$, for agriculture and manufacturing, respectively. A representative firm per sector faces competitive markets. The agricultural firm produces output $y_a$ at relative price $p_a$ (manufacturing is the numeraire good) employing labor $n_a$ at wage rate $w_a$ and land $\ell$. We assume inefficient institutions in agriculture captured by a parameter $\tau$ that taxes revenue. Agricultural firms thus solve the problem,

$$\max_{n_{at}} \pi_t(\ell) = (1-\tau)p_{at}y_{at} - w_{at}n_{at} \quad \text{s.t} \quad y_{at} = z_{at}n_{at}^{\phi}\ell^{1-\phi},$$

where $\phi$ is the labor share in agriculture. Since land is fixed, the agricultural technology exhibits decreasing returns to scale.[33] Manufacturing firms produce output $y_{mt}$ with labor $n_{mt}$—hired at wage $w_{mt}$—and capital $k_t$—rented at rate $r_t$—and solve the problem,

$$\max_{n_{mt},k_{t+1}} \quad y_{mt} - w_{mt}n_{mt} - r_t k_t \quad \text{s.t} \quad y_{mt} = z_{mt}n_{mt}^{\alpha}k_t^{1-\alpha},$$

where $\alpha$ is the labor share in manufacturing. Further, we assume that total factor productivity (TFP) differs by sector according to $z_{it} = z_{i,0}(1+\lambda_i)^t$ for $i = \{a, m\}$ with $\gamma_a < \gamma_m$.

An infinitely-lived representative agent discounts the future at factor $\beta \in (0, 1)$ and chooses sectoral allocations of consumption $\{c_{at}, c_{mt}\}_{t=0}^{\infty}$, labor $\{n_{at}, n_{mt}\}_{t=0}^{\infty}$, and next period capital $\{k_{t+1}\}_{t=0}^{\infty}$. The per period utility function from agricultural goods, $u(c_{at} - \bar{c}_a)$, features a non-homotheticity through a subsistence level, $\bar{c}_a$. Utility from manufacturing goods, $v(c_m)$, is additively separable. Both $u(\cdot)$ and $v(\cdot)$ are strictly concave. The household is endowed with one unit of time in each period, i.e. $n_{at} + n_{mt} = 1 \ \forall t$, that is allocated to either agriculture or

[33] The structural change—from a decreasing returns to scale technology (Malthus) to a constant returns to scale (Solow) is studied in Hansen and Prescott (2002) in the context of a one-good economy. Below, we also introduce non-homothetic preferences as an additional mechanism for structural change (e.g. Gollin et al., 2002).

manufacturing and receives wage rates $\{w_{at}, w_{mt}\}$. The household receives the rents $\pi(\ell)$ from inelastically supplying (renting) land to agricultural firms. Thus, the household maximizes,

$$\max_{\{c_{at},c_{mt},n_{at},n_{mt},k_{t+1}\}_{t=0}^{\infty}} \sum_{t=0}^{\infty} \beta^t \left(u(c_{at} - \bar{c}_a) + \kappa v(c_{mt})\right) \tag{23}$$

where $\kappa > 0$ is a relative utility parameter, subject to the budget constraint

$$p_{at}c_{at} + c_{mt} + k_{t+1} = \sum_{i\in\{a,m\}} w_{it}n_{it} + r_t k_t + (1-\delta)k_t + \pi_t(\ell). \tag{24}$$

There are three first order conditions for the household problem.[34] First, an intratemporal condition governing the substitution across consumption goods:

$$FOC(c_{at}): \qquad u_{c_{at}}(c_{at})\frac{1}{p_{at}} = \kappa v_{c_{mt}}(c_{mt}) \tag{25}$$

Second, an intertemporal Euler condition for $k_{t+1}$ governing the trade off between one additional unit of consumption today versus tomorrow's consumption,

$$FOC(k_{t+1}): \qquad u_{c_a}(c_{at})\frac{1}{p_{at}} = \beta u_{c_a}(c_{at+1})\frac{1}{p_{at+1}}\left(1 + r_{t+1} - \delta\right), \tag{26}$$

and note that we can rewrite this intertemporal condition in terms of $c_m$ using (25). Third, an intratemporal condition for $n_a$ equates wages across sectors,

$$FOC(n_{at}): \qquad u_{c_a}(c_{at})(w_{at} - w_{mt}) = 0 \tag{27}$$

These allocations need to satisfy the marginal product conditions arising from the firms' problems in competitive markets, that is, $w_{at} = \phi\frac{p_{at}y_{at}}{n_{at}}$, $w_{mt} = \alpha\frac{y_{mt}}{n_{mt}}$ and $r_t = (1-\alpha)\frac{y_{mt}}{k_t}$.

**True (model-generated) policy effects.** We consider two regions that potentially differ in model parameters $\Theta = \{\beta, \bar{c}_a, \kappa, \delta, z_{a,0}, \lambda_a, z_{m,0}, \lambda_m, \phi, \alpha, \tau\}$. In particular, we allow for the total factor productivity in the manufacturing sector to be larger in region $\mathcal{C}$ than in region $\mathcal{T}$. The larger productivity of manufacturing in region $\mathcal{C}$ generates a larger amount of investment, lower agricultural share of labor and, ultimately, higher income per capita in region $\mathcal{C}$ than in region $\mathcal{T}$ at any point in time; see panel (a) in Figure 9.The model is able to generate an agricultural share that declines over time whereas, at the same time, capital and income per capita increase asymptotically reaching a balanced growth path with a trifling agricultural share. In this context,

[34] Note that we can isolate $c_m$ from (24) and plug it into (23) plus use $n_{mt} = 1 - n_{at}$. This implies that we can maximize the objective function in terms of the sequences of three unknowns $\{c_{at}, n_{at}, k_{t+1}\}_{t=0}^{\infty}$.

Figure 9: Stage-Based Identification of Model-Generated Policy Effects: Growth Policy

(a) True Policy Effects (b) Identified Policy Effects (c) Identified vs. True Effects

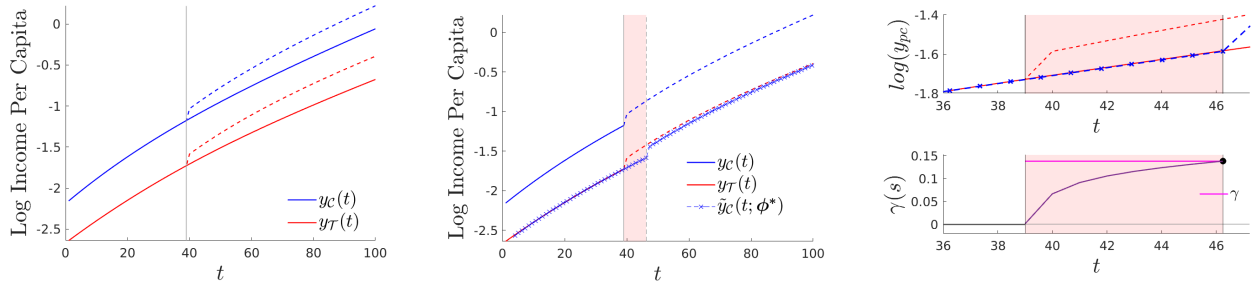


*Notes:* For region $\mathcal{T}$, we choose, $n_{a,0} = 0.45, z_{a,0} = 0.15, z_{m,0} = 0.17, \gamma_a = 0.007, \gamma_m = 0.0073$. For region $\mathcal{C}$, we choose, $n_{a,0} = 0.65, z_{a,0} = 0.145, z_{m,0} = 0.145, \lambda_a = 0.007, \lambda_m = 0.0072$. Common parameters between both regions are $\beta = 0.98, \alpha = 0.6, \phi = 0.8, \kappa = 2, \delta = 0.02$. Further, we assume that the felicity functions are logs, that is, $u(c_a - \bar{c}_a) = \ln(c_a - \bar{c}_a)$ and $v(c_m) = \ln c_m$.

we introduce an unexpected nationwide growth policy that removes the institutional constraint $\tau$ in the agricultural sector in both regions; setting $\tau = 0$ after $t_p$ in both regions. Removing the constraint in the agricultural sector accelerates investment (and capital) and the decline in agricultural sector. The reallocation to the non-agricultural sector increases income per capita in the eocnomy, see (dashed lines) in panel (a) of Figure 9.

**Stage-Based Identified policy effects.** The policy evaluator is not provided with the true counterfactual path without policy (solid lines for the periods after $t_p$). Under these same data constraints, we implement SBI mapping the outcome path in region $\mathcal{C}$ (solid blue line) onto the outcome path in region $\mathcal{T}$ (solid red line) using only pre-policy data. We plot the resulting counterfactual candidate $\widetilde{y}_{\mathcal{C}}(s;\boldsymbol{\phi}^*)$ (blue line with cross markers) for the identification window between $t_p$ and $s_C(t_p;\boldsymbol{\psi}^*)$ (shaded pink area); see panel (b), Figure 9. We zoom in on the identified counterfactual $\widetilde{y}_{\mathcal{C}}(s;\boldsymbol{\phi}^*)$ and the true effects of policy in panel (c) of Figure 9. According to SBI, the growth policy increases income per capita by $\gamma = 13.781\%$ in the identification window whereas the true policy effect is $\gamma_{\text{true}} = 13.537\%$. That is, the identified policy effects catch the true policy effects with an error of $\varepsilon(\gamma) = 1.797\%$.

### 3.2 Bounds to Method Performance

The performance analysis in Section 3.1 shows that our identification strategy can recover the true policy effects. However, it is intuitive to assume that our strategy faces some boundaries. Here, we numerically characterize the bounds within which our method is able to recover the true effects of policy with a Monte Carlo experiment in Section 3.2.1. We further assess how our method

fares in the presence of time-varying latent heterogeneity; confounding policy interventions; and endogenous policy in Section 3.2.2.

### 3.2.1 A Monte Carlo Analysis

We focus this analysis on the benchmark economic model with an endogenous pandemic described in Section 3.1.1. Specifically, we hold fixed the parameters of the non-reference region $\mathcal{C}$ and randomize a subset—$(\beta, \zeta, \kappa, t_o)$—of the structural parameters in that region in order to generate a large number of reference outcome paths $y_{\mathcal{T}}(m)$ for regions $m \in \mathcal{M} = \{1, ..., m, ..., M\}$.[35] In panel (a) of Figure 10, we show the epidemic path of our benchmark regions $\mathcal{C}$ and $\mathcal{T}$ as described in Section 3.1.1, together with one of the simulated reference regions that starts later, grows slower and reaches a lower magnitude than the benchmark reference region, $y_{\mathcal{T}}(t)$, and, therefore, is further away from the non-reference region, $y_{\mathcal{C}}(t)$.[36]

In this context, in order to assess the ability of SBI to identify the true policy effect we study the policy error across all simulations. For each simulation $m$, we apply SBI mapping the non-reference region, $y_{\mathcal{C}}(t)$, onto the simulated reference path, $y_{\mathcal{T}(m)}(t)$. This implies that we find a set of normalization coefficients $\boldsymbol{\phi}^*(m) = \{\boldsymbol{\psi}_0^*(m), \boldsymbol{\psi}_1^*(m), \boldsymbol{\omega}_1^*(m)\}$ per simulation $m \in \mathcal{M}$. Then, for each simulation, we measure the policy error as the (absolute) value of the policy effect identified by SBI relative to the (model-generated) policy effect; i.e. $\varepsilon(\gamma)(m) = \left|\left(\frac{\gamma(m)}{\gamma_{\text{true}}(m)} - 1\right) \times 100\right|$. In panel (b) of Figure 10, we plot the policy errors of each of our simulations $\boldsymbol{\phi}^*(m)$ that belong to the vector space $\Phi^q = \Psi_0^q \times \Psi_1^q \times \Omega_1^q = \{\psi_0(m) > 0.0\} \times \{\psi_1(m) > 1.0\} \times \{\omega_1(m) < 1.0\} \subset \Phi = \mathbb{R}^3$. We restrict the plot to the vector space $\{\psi_0(m) \in (0.000, 10.000)\} \times \{\psi_1(m) \in (1.000, 1.500)\} \times \{\omega_1(m) \in (0.350, 1.000)\} \subset \Phi^q$, which suffices to capture the policy error associated with the benchmark reference region $y_{\mathcal{T}}(t)$.[37]

Our main result is that the success of our method in identifying the true policy effects is bounded. To see this, first, note that the centroid in the vector space $\Phi$, i.e. $\boldsymbol{\phi}_{\mathbf{c}}^* = (0.000, 1.000, 1.000)$, implies that the outcome path of the simulated reference region, $y_{\mathcal{T}(m)}(t)$, and that of the non-reference region, $y_{\mathcal{C}}(t)$, are identical.[38] Second, note that if the outcome path of a simulated reference region, $y_{\mathcal{T}(m)}(t)$, and the outcome path of the non-reference region, $y_{\mathcal{C}}(t)$, are similar—in that our identification strategy delivers a set of normalization coefficients that is

[35] We assume that the randomized parameters—$\beta, \zeta, \kappa$ and $t_o$—are uniformly and independently distributed. Then, we draw a total of $M = 381,000$ simulations (quadruplets).

[36] Note that there can be cases where the simulated reference region flips control versus treatment assignment.

[37] Our insights do not change with alternative choices of the vector space.

[38] Indeed, exactly at the centroid the policy effects are not identified because $y_{\mathcal{C}}(t) = y_{\mathcal{T}(m)}(t)$ and there is no heterogeneity in stages at the time of policy implementation.

Figure 10: Bounds to Method Performance: A Monte Carlo Analysis

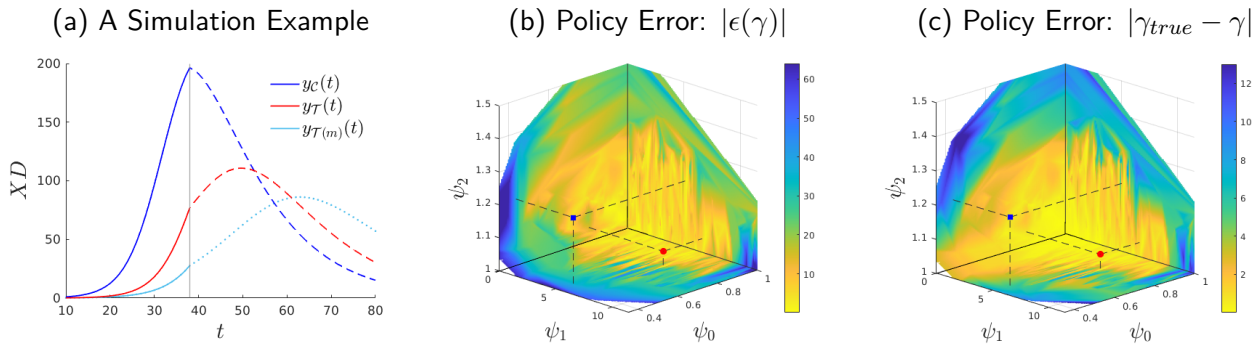


*Notes:* When constructing the set $\{y_{\mathcal{T}(m)}(t)\}_m$, we assume that $\{\beta, \zeta, \kappa, t_0\}$ are uniformily and independnetly distributed. The simulations are drawn from the intervals $\left[\beta^{lb}, \beta^{ub}\right] \times \left[\zeta^{lb}, \zeta^{ub}\right] \times \left[\kappa^{lb}, \kappa^{ub}\right] \times \left[t_o^{lb}, t_o^{ub}\right] = [0.5, 0.9] \times [0.001, 0.008] \times [1.05, 1.89] \times [-10, 10]$ where the superindices $lb$ and $ub$ denote, respectively, the lower and upper bounds of each parameter space. We pick the bounds of the uniform distribution in a manner that our simulations generate sufficiently different outcome paths of the reference region in order to assess the performance of our method. We constructed a total of $M = 381{,}000$ simulations though not all the simulations fall in the vector space $\boldsymbol{\psi}^*$ in panel (b). Precisely, the hyperplane $(\psi_0, \omega_1)$ has 3,698 simulations, the hyperplane $(\psi_1, \omega_1)$ has 17,504 simulations and the hyperplane $(\psi_0, \psi_1)$ has 3,698 simulations. Panels (b) and (c) show values from an evenly spaced $200 \times 200$ grid on each hyperplane. We approximate the values on the grid through linear interpolation of the simulated data.

in a neighborhood of the centroid $\mathcal{N}(\boldsymbol{\phi}_{\mathbf{c}}^*) \subset \Phi^q$—then the policy error is small; see panel (b) of Figure 10. To see this, note that policy errors with values of $\varepsilon(\gamma) \leq 5\%$ emerge in a bounded neighborhood (approximately) $\mathcal{N}(\boldsymbol{\phi}_{\mathbf{c}}^*) = \{0.000, 6.776\} \times \{1.000, 1.210\} \times \{0.764, 1.000\}$ which we depict (yellow area) around the centroid. Here, note that our benchmark reference outcome path $y_{\mathcal{T}}(t)$ falls in that neighborbood with a set of normalization coefficients $\boldsymbol{\phi}^* = \{6.592, 1.041, 0.803\}$ and a policy error $\varepsilon(\gamma) = 0.68\%$ (red marker). Third, moving away from the centroid increases the policy error. For example, the simulated reference outcome path $y_{\mathcal{T}(m)}(t)$ in panel (a) of Figure 10 implies a set of normalization coefficients $\boldsymbol{\phi}^*(m) = \{5.083, 1.200, 0.436\}$ that falls outside of the neighborhood $\mathcal{N}(\boldsymbol{\phi}_{\mathbf{c}}^*)$ and delivers a larger policy error of 36.04%. We further reconduct our exercise using an alternative measure of the policy error defined as $|\gamma - \gamma_{\text{true}}|$ in panel (c) of Figure 10 reaching similar insights. Thus, as long as the regional outcome paths are similar enough, the method can successfully identify the policy effect.

### 3.2.2 Confounding Factors

We assess how the presence of time-varying latent heterogeneity, confounding policy and endogenous policy affects the ability of SBI to recover the true effects of policy. Here, we would like

Figure 11: Stage-Based Identification of Policy Effects: Time-Varying Latent Heterogeneity

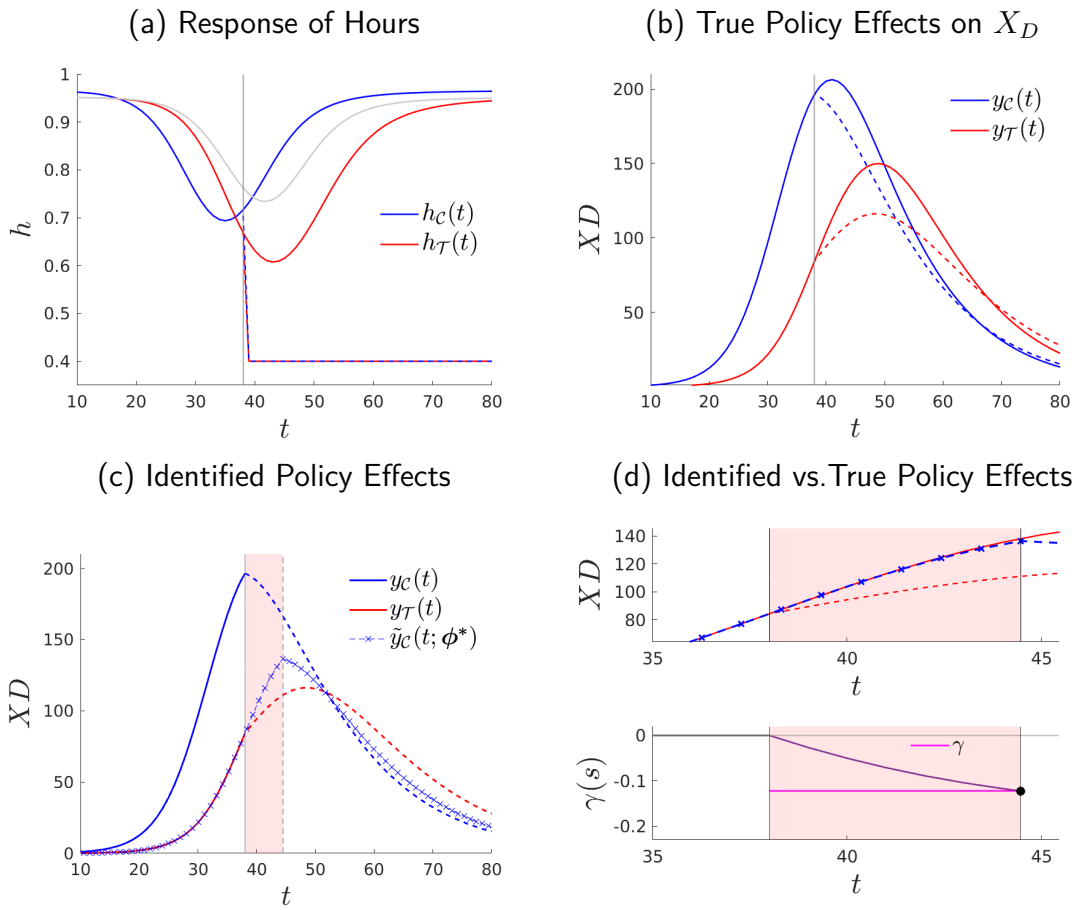


*Notes:* Where $\bar{h} = 0.4, t_p = 38, t_f = 250$, $\gamma = -12.242\%, \epsilon(\gamma) = -3.318\%$.

to emphasize that the goal of our method is not to answer what would have been the effect of the policy under evaluation had the time-varying latent heterogeneity, confounding policy or endogenous policy (or other confounding factors for that matter) not been present. That is, we do not pursue the identification of a "pure" policy effect that nets out (controls for) the presence of confounding factors.[39]

Instead, we acknowledge that the effect of the same policy can naturally be different when it is applied in a different context—e.g., due to the presence of different confounding factors. SBI is designed to measure these conditional policy effects. Thus, we are interested in assessing how

[39]Therefore, from the perspective of SBI, the presence of confounding factors does not change neither the aim of the normalization step, which is to reduce the cross-regional differences in the pre-policy determinants—including potentially unobserved structural parameters—of the path of the outcome of interest, nor the identification step that assumes the normalization parameters are unaffected by the policy that is evaluated.

well SBI can recover the true policy effects that emerge given different confounding factors. To do so, we use as benchmark the econ-epi model described in Section 3.1.1 in which there were no confounding factors. Then, we introduce confounding factors (one by one) into the model in order to show how the true policy effects, which now explicitly depend on the specific set of confounding factors that are present, change and assess whether SBI can recover these true policy effects.

**Time-Varying Latent Heterogeneity** Using the econ-epi model in Section 3.1.1, we formalize the time-varying latent heterogeneity across two regions as an underlying time-varying structural parameter present in one region but not the other. In particular, we consider a scenario in which one region, $\mathcal{T}$, learns about the process of infection before policy implementation. That is, we allow for the beliefs on the infection process, $\xi_{\mathcal{P}}$, to exogenously and gradually move closer to the actual $\xi$ in region $\mathcal{T}$ but not in region $\mathcal{C}$; see Figure 31 in the Appendix D. This path of beliefs induces pre-policy behavioral change relative to the scenario with a fixed $\xi_{\mathcal{P}}$. In region $\mathcal{T}$, there is now a larger behavioral response (reduction of hours) to the pandemic, see panel (a) in Figure 11, which also plots the path under fixed beliefs in gray. Note that in our illustration the pre-policy behavioral change is rather large, in the sense that now the drop in hours worked before policy implementation in region $\mathcal{T}$ becomes larger than that in region $\mathcal{C}$. We show the implied true policy effects on the flow of deaths in panel (b), the identified policy effects in panel (c) and a comparison between true and identified effects in panel (d) of Figure 11. The main finding is that our method can recover the true policy effects under time-varying unobserved heterogeneity. The estimated percentage of lives saved is $\gamma = 12.242\%$ which is close to the true effects, $\gamma_{\text{true}} = 12.663\%$. Hence, SBI can recover the policy effects in contexts where there is time-varying latent heterogeneity. However, analogously to our discussion in Section 3.2.1, the robustness of our method to time-varying heterogeneity is bounded by how far the time-varying component drives the outcome paths across regions away from each other.

**Confounding (Exogenous) Policy** We now consider a scenario in which an additional confounding policy is introduced in region $\mathcal{T}$ right before the actual nationwide stay-home policy under evaluation is implemented in period $t_p$. In particular, we assume the existence of an unanticipated policy that imposes an additional (and weaker) constraint on hours worked, $\bar{h} = 0.71$, one period before the nationwide stay-home policy is put in place; see panel (a) of Figure 13. Then, we apply SBI to assess the nationwide stay-home policy introduced at $t_p$, while purposefully ignoring the presence of the additional policy introduced before $t_p$ in region $\mathcal{T}$. Our method identifies the effects of policy to be a 14.708% of lives saved in the identification window which is close to the true effects in that window, 15.588%. This implies a policy error of 5.644%. We further

Figure 12: Stage-Based Identification of Policy Effects: With Confounding Policy in $\mathcal{T}$

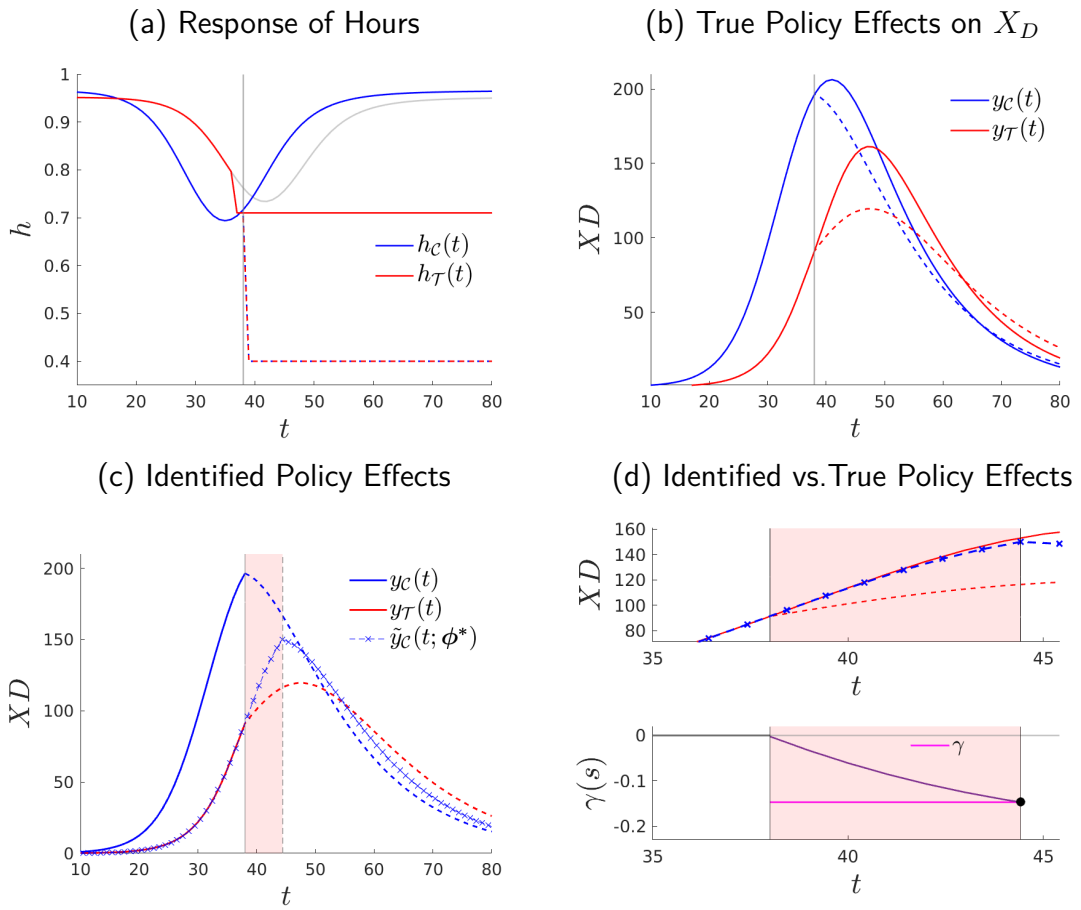


*Notes:* Where $\bar{h}_1 = 0.71$ at $t = 37$ in $\mathcal{T}$, this policy is unobserved, $\bar{h}_2 = 0.4$ (lockdown) at $t_p = 38, t_f = 250$, $\gamma = -14.708\%, \epsilon(\gamma) = -5.644\%$.

re-conduct the exercise imposing less strict confounding policies in region $\mathcal{T}$ one period before $t_p$ with similar insights. That is, SBI can recover the true policy effects in a context where there exists a confounding policy. At the same time, analogously to our discussion in Section 3.2.1, it is straightforward to show that the error by which SBI captures the true policy effect increases if the effect of the additional confounding policy makes the cross-regional outcome paths sufficiently dissimilar before $t_p$. That is, how much our identification strategy recovers of the true policy effects in a context where confounding policy is present is bounded by the strength of the confounding policy in making the cross-regional outcome paths differ from each other.[40]

[40]We do not find additional insights when the confounding policy arrives first to region $\mathcal{C}$; see Appendix D.

**Endogenous Policy** Consider now a scenario in which the date at which the policy is implemented across all regions, $t_p$, is endogenously determined by the stock of deaths of solely one region (here: region $\mathcal{T}$). Precisely, the nationwide policy (a lockdown that restricts hours worked to $\bar{h} = 0.40$ in all regions) is implemented when the stock of deaths in region $\mathcal{T}$, $D_{\mathcal{T},t}$, surpasses a threshold $\bar{D}$. We assume that only the agents in region $\mathcal{T}$ are aware of this constraint and chooses $h$ accordingly. The agents in region $\mathcal{C}$ remain unaware, therefore they do not adjust hours and the policy arrives unexpectedly to their eyes. Further, note that the date at which the policy arrives remains the same across regions. Taking into account the endogenous policy, hours in region $\mathcal{T}$ (solid red line) react more strongly than in their corresponding response in the benchmark case where policy was exogenous (gray line) (see panel (a), Figure 13). Precisely, using the same parameterization as in our benchmark econ-epi model in Section 3.1.1, the endogenous policy takes place one day later ($t_p = 39$) than in the benchmark model ($t_p = 38$). This larger reaction translates into less deaths for region $\mathcal{T}$ than their counterpart in the benchmark model (panel (b), Figure 13). We apply SBI to this scenario (panel (c), Figure 13). Our proposed no policy counterfactual, when mapping region $\mathcal{C}$ on to region $\mathcal{T}$, delivers the path of deaths had the policy not been implemented endogenously and letting the agents in $\mathcal{T}$ choose $h_t$ freely for $t \leq t_p$. Accordingly, we compute the corresponding no policy counterfactual path $y_{\mathcal{T},t}$ $t \leq t_p$ (solid red line after $t_p$). We find the effects of policy to be a 8.332% of lives saved in the identification window which are, due to the behavior response to endogenous policy, lower than those attained with the benchmark model where the policy was exogenous. The identified policy effects are close to the true effects in that window, 11.268% (panel (d), Figure 13). This implies a policy error of 21.616%.

## 3.3 Inference

We conduct inference in two ways. First, we conduct a placebo diagnosis in order to assess how our method evaluates inexistent policy effects. Second, we assess our method when the outcome path of interest is subject to a stochastic component.

### 3.3.1 Placebo Diagnosis

Here, we assess whether SBI identifies policy effects when the policy effects are non-existent. In such scenario, a successful diagnosis is one in which our method identifies the effects of policy to be nil, as they truly are. To conduct this assessment, we apply our method to model-generated data from models that are not subject to policy. We use as benchmark the econ-epi model from Section 3.1.1 with the relevant difference that we do not impose a policy at time $t_p$. Under such scenario, the paths for the flow of deaths in region $\mathcal{C}$ (solid blue) and region $\mathcal{T}$ (solid red) are as

Figure 13: Stage-Based Identification of Policy Effects: With Endogenous Policy in $\mathcal{T}$

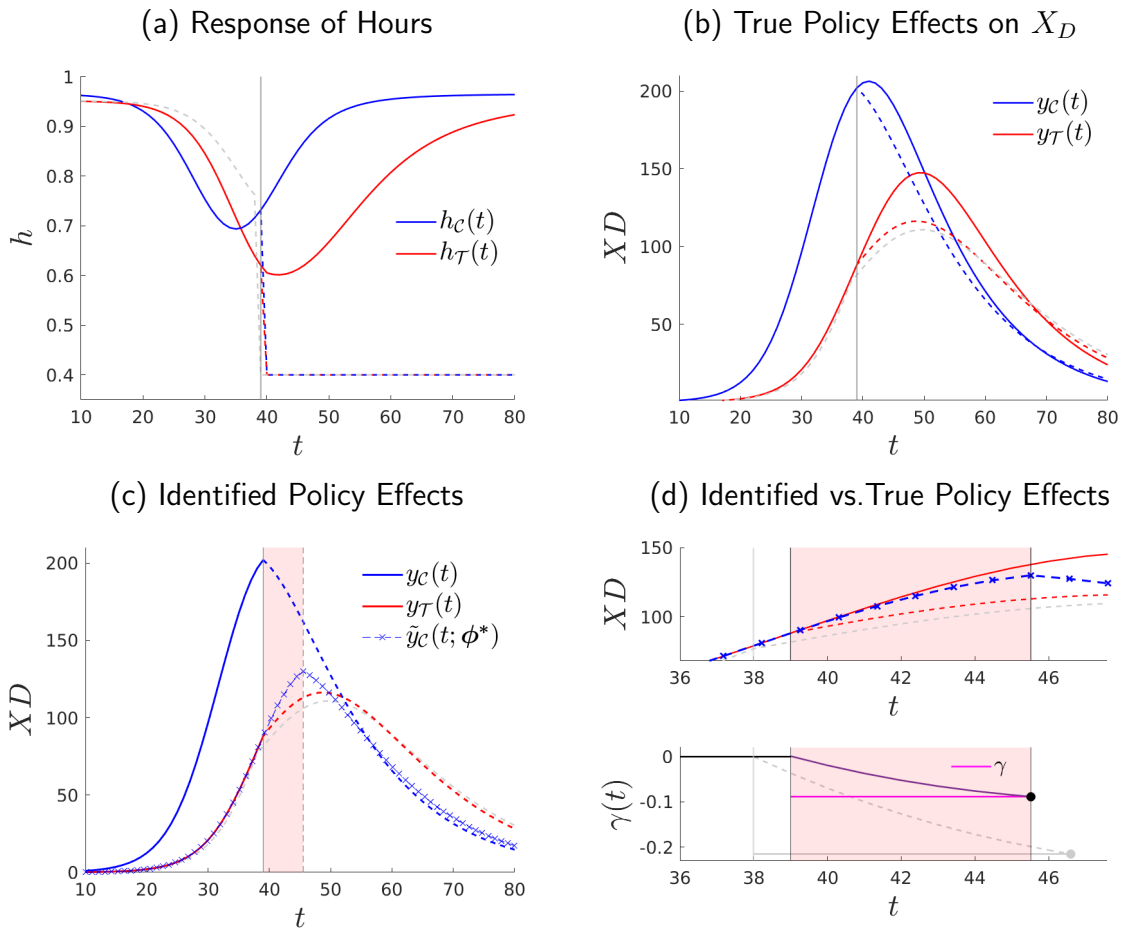


*Notes:* We assume $\bar{h} = 0.40$ and $\bar{D} = 460$ are identical to the corresponding policy restriction on hours worked and the stock of deaths attained at the time policy implementation ($t_p = 38$) in the benchmark model with exogenous policy. We find that the policy is endogenously implemented at $t = 39$. $\gamma = -8.332\%$ and $\epsilon(\gamma) = -21.616\%$.

depicted in panel (a) of Figure 14. For reference, we also plot the path for deaths that would have occurred (dashed light gray) had the policy been implemented at $t_p$ as we did in Section 3.1.1.

We now apply SBI as if there was a policy at some period $t_p$—when there is actually none. Given that the normalization uses only pre-policy data, we obtain the same identification window over stages as if there was an actual policy. We show the outcome paths for the two regions, $y_{\mathcal{T}}(t)$ and $y_{\mathcal{C}}(t)$, along with the obtained normalized path $\widetilde{y}_{\mathcal{C}}(s, \boldsymbol{\phi}^*)$ in panel (b) of Figure 14; panel (c) zooms in on the identification window. Note that the normalized outcome path $\widetilde{y}_{\mathcal{C}}(s, \boldsymbol{\phi}^*)$ is practically identical to the outcome path $y_{\mathcal{T}}(t)$ on the identification interval: the identified counterfactual matches the actual outcome path—which here is also the outcome path without policy. That is, SBI correctly identifies that in this scenario without policy the policy effects

Figure 14: Stage-Based Identification of Policy Effects: A Placebo Test

(a) True Policy Effects (b) Identified Policy Effects (b) Identified vs.True Effects

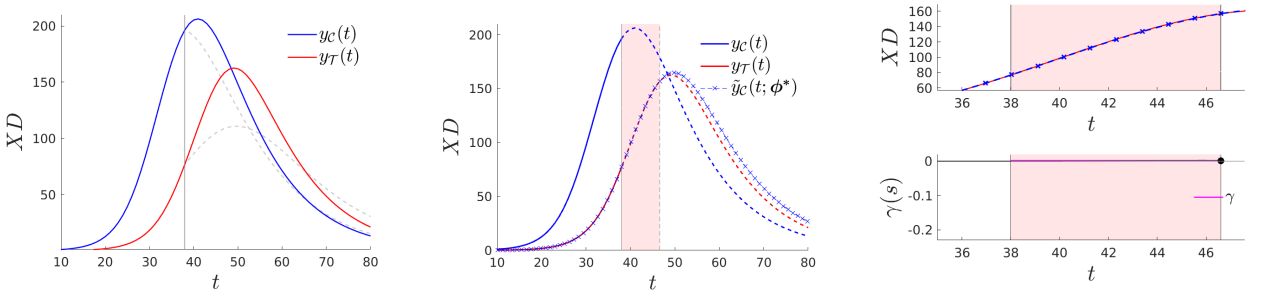


*Notes:* Where $\bar{h} = 0.4, t_p = 38, t_f = 250$, $\gamma = 0.188\%$.

are non-existent—or quantitatively negligible, $\gamma = 0.188\%$. We find similar insights after re-conducting this exercise for different values of $t_p$.

### 3.3.2 Stochastic Component

In empirical applications, the outcome path of interest often is subject to fluctuations due to the presence of a stochastic component, which can capture measurement error.[41] When facing such noisy data, we add a smoothing—or trend-extraction—step that precedes the normalization step of the SBI method. The goal of this smoothing step is to purge the observed pre-policy outcome paths of the stochastic fluctuations—of higher frequency than the object of interest—defined as deviations from some estimand. We then apply the normalization step of the SBI method on the smoothed pre-policy data. Furthermore, given that the available data does not exactly capture the true path, it is important to conduct statistical inference, for which we propose a bootstrap procedure that builds on the stochastic component around an extracted fitted value.

Consider first the presence of classical measurement error, and let the outcome paths be

$$\widehat{y}_r(t) = y_r(t) + u_r(t) \quad \text{with} \quad u_r(t) \sim N(0, \sigma^2_{u,r}), \tag{28}$$

for each region $r = \{\mathcal{C}, \mathcal{T}\}$, where $\widehat{y}_r(t)$ is the outcome path observable to the policy evaluator, $y_r(t)$ is the unobservable true outcome path and the innovations $u_r(t)$ capture measurement error that follows a Normal distribution with zero mean and variance $\sigma^2_r$. In the case where the stochastic component is autocorrelated, we replace the innovations in specification (28) with $u_r(t) = \rho u_r(t-1) + v_r(t)$ where $v_r(t) \sim N(0, \sigma^2_{v,r})$. In panel (a.1) of Figure 15, we show

[41] Alternatively, the stochastic fluctuations might be genuine but yet of higher frequency than the outcome path of interest—e.g., autocorrolated business cycles when the object of interest is the growth path. Also in this scenario it is important to extract the lower-frequency component, in order to then use SBI on it.

Figure 15: Stage-Based Identification of Model-Generated Policy Effects: Inference

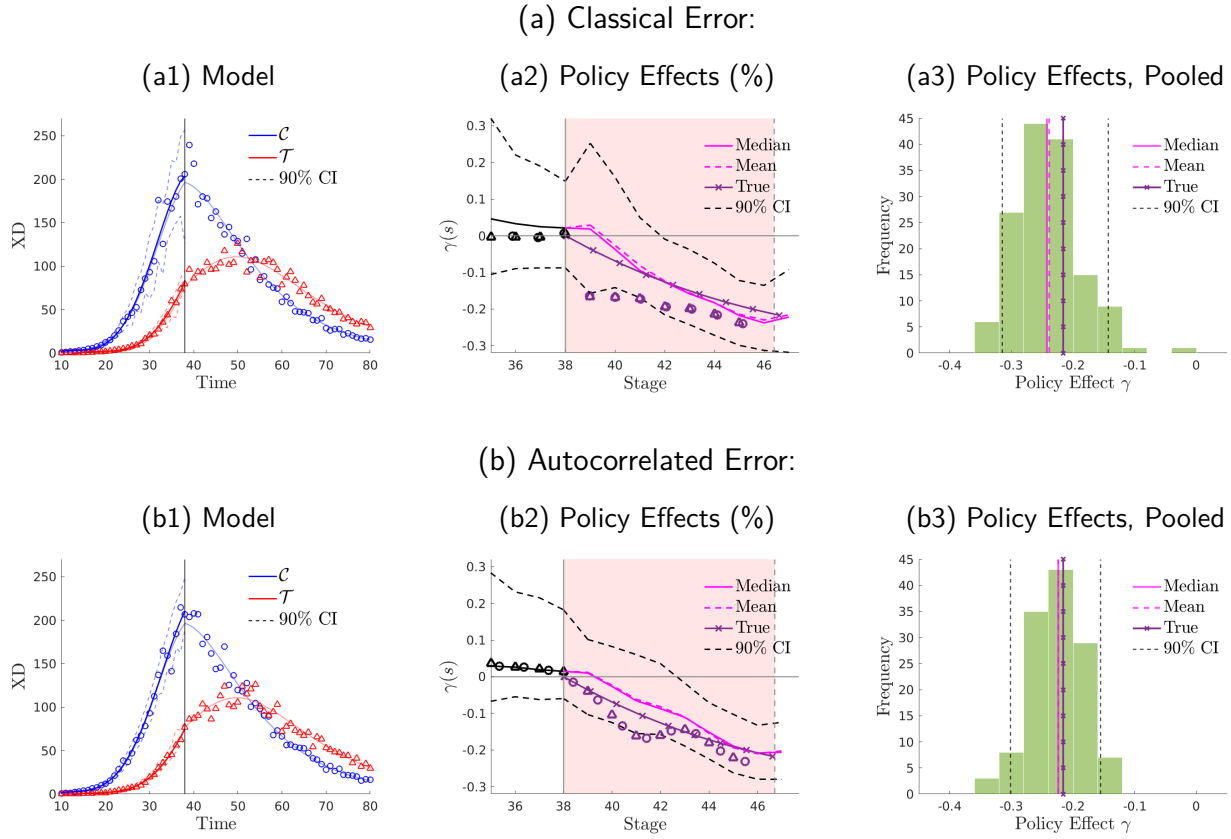


*Notes:* We use the benchmark parameterization of Section 3.1.1. The top panels (a) add classical error in our model with $\{\sigma^2_{\mathcal{C}}, \sigma^2_{\mathcal{T}}\} = \{0.008, 0.008\}$. The bottom panels (b) add autocorrelated error with $\{\rho_{\mathcal{C}}, \rho_{\mathcal{T}}\} = \{0.13, 0.13\}$ and $\{\sigma^2_{\mathcal{C}}, \sigma^2_{\mathcal{T}}\} = \{0.008, 0.008\}$.

the (unobserved) true outcome paths $y_r(t)$ for the two regions as light blue and light red lines, together with the observed outcome paths $\widehat{y}_r(t)$ for one simulation of the errors in (28), which are indicated by the circle and triangle markers. Further, in what follows we denote by $\widehat{\widehat{y}}_r(t < t_p)$ the estimand of $y_r(t < t_p)$. To obtain this estimand, we fit Chebyshev polynomials to the observed data $\widehat{y}_r(t < t_p)$ and, hence, also recover the time-series of regional errors $u_r(t < t_p)$ as the deviations from the fitted values. Then, for each region, we construct $B = 1,000$ bootstrap draws, $\widehat{y}_{r,b}(t)$ with $b \in B$. For each bootstrap draw, we randomly draw a sequence of errors from the region-specific set of errors with replacement, which we add to the fitted values of the pre-policy path, $\widehat{\widehat{y}}_r(t < t_p)$. In panel (a1) of Figure 15, we show the median (solid lines) and 90% confidence intervals (dashed lines) of the bootstrap pre-policy paths $\widehat{y}_{r,b}(t < t_p)$.

Now, we apply SBI to each bootstrap sample using the recovered estimands $\widehat{\widehat{y}}_{r,b}(t < t_p)$ to perform the normalization, i.e., the mapping of the non-referece region $\mathcal{C}$ onto the reference region $\mathcal{T}$. Then, on the obtained identification window, we use the data of region $\mathcal{T}$ and the

normalized path for region $\mathcal{C}$ to measure the effect of policy effect for each bootstrap draw, $\gamma_b$. Importantly, the heterogeneity in $\gamma_b$ across bootstrap draws arises from both, differences in the policy effect per stage during the identification window, and differences in the size of the identification window itself, stemming from the bootstrap-draw-specific stage of policy implementation in the non-reference region, $s_{\mathcal{C}}(t_p; \boldsymbol{\psi}_b^*)$. We thus split the reporting into two steps. First, we report confidence bands over the window of the observed original data, for which we focus on those bootstrap simulations that deliver roughly the same window length. Second, we report overall confidence bands of the policy effect, based on all bootstrap draws. In panel (a2) of Figure 15 we plot again the true cumulative policy effects $\gamma_b(s)$ from Figure 7. We then add to the figure the mean, median, and the 5th and 95th percentiles of the bootstrap draws that give a window of about the same length—we select those bootstrap draws that fall into plus/minus 10% of the length of the average bootstrap draw. Two results emerge. First, the normalization generates outcome paths that are not significantly different before policy implementation; see the non-shaded area in panel (a2). Second, the identified policy effects—using data with measurement error—are not significantly different from the true (model-generated) policy effects without measurement error (purple line with crossed markers): the identified mean policy effect (dashed magenta line) is 22.58%—within a 90 percent confidence interval of [11.71,31.58]—which is not significantly different from the true (model-generated) policy effect without measurement error, i.e., 21.50%. The median policy effect (solid magenta line) is of similar size, 23.1%. However, unsurprisingly, the significance of the identified policy effect can be affected by the size of the measurement error. Further, we find that the identified mean policy effect is similar (23.89%) when we do not restrict our analysis to bootstrap draws of the same window size; see panel (a3) of Figure 15, which shows the distribution of the overall policy effects across all bootstrap draws. Naturally, the distribution is somewhat wider than within the restricted bootstrap subsample—however, the 90% confidence band is only mildly larger. We also conduct robustness of our methodology using a wider set of smoothers and find similar insights—our alternative smoothers include B-splines, cubic splines, moving averages and the Hodrick-Prescott filter.[42]

We re-conduct our analysis assuming that the stochastic component is autocorrelated, see panel (b1) of Figure 15. In this case, to keep the empirical autocorrelation structure of the error terms—including potentially temporal differences in the cross-sectional variance—we use a block bootstrap procedure that increses the sampling weight of preceding error terms in a pre-

[42] An altogether alternative way to conduct inference with the recovered estimates for the error terms $u_r(t)$ is to estimate the sample variance of the errors, i.e. $\widehat{\sigma}_r$. Then, under a normality assumption on the error term in (28), we simulate $Q = 1,000$ paths of errors (instead of drawing from the empirical distribution). The results under this different inference are in Appendix E. Overall, we find similar insights with an identified mean policy effect of 21.12% [14.41,28.23] that is not significantly different from the true (model-generated) policy effect.

specified window (Carlstein, 1986).[43] With autocorrelated measurement error, we also find that our identification strategy is able to recover policy effects that are not significantly different from the true (model-generated) policy effects, see panel (b2) and (b3) of Figure 15.

Finally, in order to assess the role of the smoother on the identification of the true policy effects, we perform SBI directly on the observed data $\widehat{y}_r(t < t_p)$—i.e., the markers in panel (a1) of Figure 15. That is, we conduct the normalization by mapping directly the outcome path $\widehat{y}_{\mathcal{C}}(t)$ onto $\widehat{y}_{\mathcal{T}}(t)$ without the smoothing step.[44] There is a unique identified policy effect (purple markers) that we show in panel (a2) of Figure 15. The policy effect identified using the observed data $\widehat{y}_r(t)$ also replicates the true policy effect, which suggests that the smoothing step (which is necessary to conduct inference in the way described here) does not substantially affect the identified policy effect itself.

# 4 Applications

We use SBI to identify the policy effects in a set of empirical applications associated with nationwide policies. First, we assess the effects of stay-home policies on the flow of Covid-19 deaths in Spain in Section 4.1.[45] Second, we assess the effects of the approval of oral contraceptivies on fertility rates and women's college education in the United States in Section 4.2. Third, we study the effects of the German reunification on income per capita Section 4.3.[46]

## 4.1 The Spanish *Confinamiento* Against Covid-19

In response to the Covid-19 pandemic, on March 14, 2020, the Spanish government announced a nationwide stay-at-home policy—enacted the following day—which locked down all non-essential workers in all regions of Spain. Indicative of its strictness, the public debate referred to the policy as confinement. The strictest measures were lifted on May 2 when the first wave of the epidemic flattened out. Here, we apply SBI to assess the effects of this policy intervention on the course of the pandemic. As outcome of interest, we focus on the daily flow of deaths attributed to Covid-19.[47] We use two Spanish regions to assess the nationwide policy: Madrid and an artificially

[43] We select a block window of size 5

[44] To measure the distance between the normalized data of the non-reference region and the actual data of the reference region, we apply linear interpolation.

[45] The Covid-19 has generated lots of empirical work assessing public health policies against the pandemic; see, for example, Fang et al. (2020) for a careful study of the early mobility restrictions in China and Liu et al. (2021) for the provision of density forecasts with Bayesian techniques for a panel of countries and regions.

[46] We discuss data sources and data construction used for each of our applications in Appendix F.

[47] Although daily deaths are potentially imperfectly measured, we regard these data as less prone to measurement error than infections data, especially during the onset of the pandemic, when testing was largely unavailable.

created region Rest of Spain (RoSPA) which is composed of all Spanish regions without Madrid. We label Madrid as region $\mathcal{C}$ and RoSPA as region $\mathcal{T}$.[48]

We show the daily flow of Covid-19 deaths (per million inhabitants) for Madrid (blue circles) and the RoSPA (red triangles) in panel (a) of Figure 16; Instituto de Salud Carlos III. In order to mitigate potential measurement error on the reported deaths, we smooth the pre-policy data using as benchmark Chebyshev polynomials separately by region as described in Section 3.3.[49] Note that we add a lag parameter to the policy date, reflecting that a policy that aims at reducing infections will show an effect on the flow of deaths with a delay. We choose a lag of 12 days, which implies that the policy is (effectively) implemented on March 27; The resulting smoothed daily flow of deaths for Madrid (solid blue) and RoSPA (solid red) are also in panel (a) of Figure 16.

There are clear differences in the path of the flow of deaths between Madrid and the RoSPA. First, one death (per million inhabitants) is reached in March 08 for Madrid and March 14 for the RoSPA. Second, by March 14 the daily flow of deaths in Madrid is 9.3 deaths (per million inhabitants) whereas this figure is 1.2 for the RoSPA. Furthermore, at the (effective) time of policy implementation, the flow of deaths is reaching a peak in Madrid at 50 deaths (per million inhabitants), whereas the peak in the RoSPA is smaller at 16 deaths (per million inhabitants) and occurs about a week after that in Madrid. That is, the flow of deaths starts at an earlier date, it raises more rapidly and reaches a larger peak in Madrid than in the RoSPA.

**Normalization.** We now apply SBI following the normalization described in Section 2. Picking the RoSPA as reference region $\mathcal{T}$, we map the flow of deaths of the region Madrid ($y_{\mathcal{C}}(t)$, solid blue circles) onto the flow of deaths of RoSPA ($y_{\mathcal{T}}(t)$, solid red circles) using *only* pre-policy data. The normalization step delivers a normalized path for Madrid $\widetilde{y}_{\mathcal{C}}(s;\boldsymbol{\phi}^*)$ that is not different—up to a minimization error—from that of RoSPA, $y_{\mathcal{T}}(t)$; see panel (b) of Figure 16. We find $\psi_0$ =-0.14 [-0.24,-0.04], $\psi_1$ =1.21 [1.16,1.24] and $\omega_1$ =0.47 [0.39,0.53] which, respectively, delays the start, slows down the growth and lowers the peak of daily deaths in Madrid. A result of our normalization is that Madrid leads the epidemic in Spain. Precisely, the policy is implemented in Madrid at a later stage than in RoSPA, i.e. $s_{\mathcal{T}}(t_p;\boldsymbol{\psi}^*) = t_p < s_{\mathcal{C}}(t_p;\boldsymbol{\psi}^*)$. Hence, the normalization unveils a window in stages $\mathbb{W}(s;\boldsymbol{\psi}^*) = [t_p, s_{\mathcal{C}}(t_p;\boldsymbol{\psi}^*)]$ (shaded pink area) running from March 27 to April 03 in which the stage-leading region, Madrid, is not yet subject to policy

[48] Note that SBI can be conducted for all pairs of regions; see Section 5.1 for an analysis of the stay-home policy using the power set of all Spanish regions. However, in order to ease the exposition, we focus here on two regions (or groups of regions). To select these regional groups, we conduct the normalization in Section 2.1 by mapping the path of Covid-19 deaths of each Spanish region onto the aggregate path for Spain. This normalization uncovers that, at the time of policy implementation, Madrid is at the most advanced stage, i.e. Madrid $= \arg\max_r s_r(t_p;\boldsymbol{\psi}^*)$. For this reason, we focus on Madrid and RoSPA for our analysis.

[49] We use a Chebyshev polynomial of degree 6 and perform robustness on the choice of the smoother.

Figure 16: The Effects of the Spanish *Confinamiento* Against Covid-19

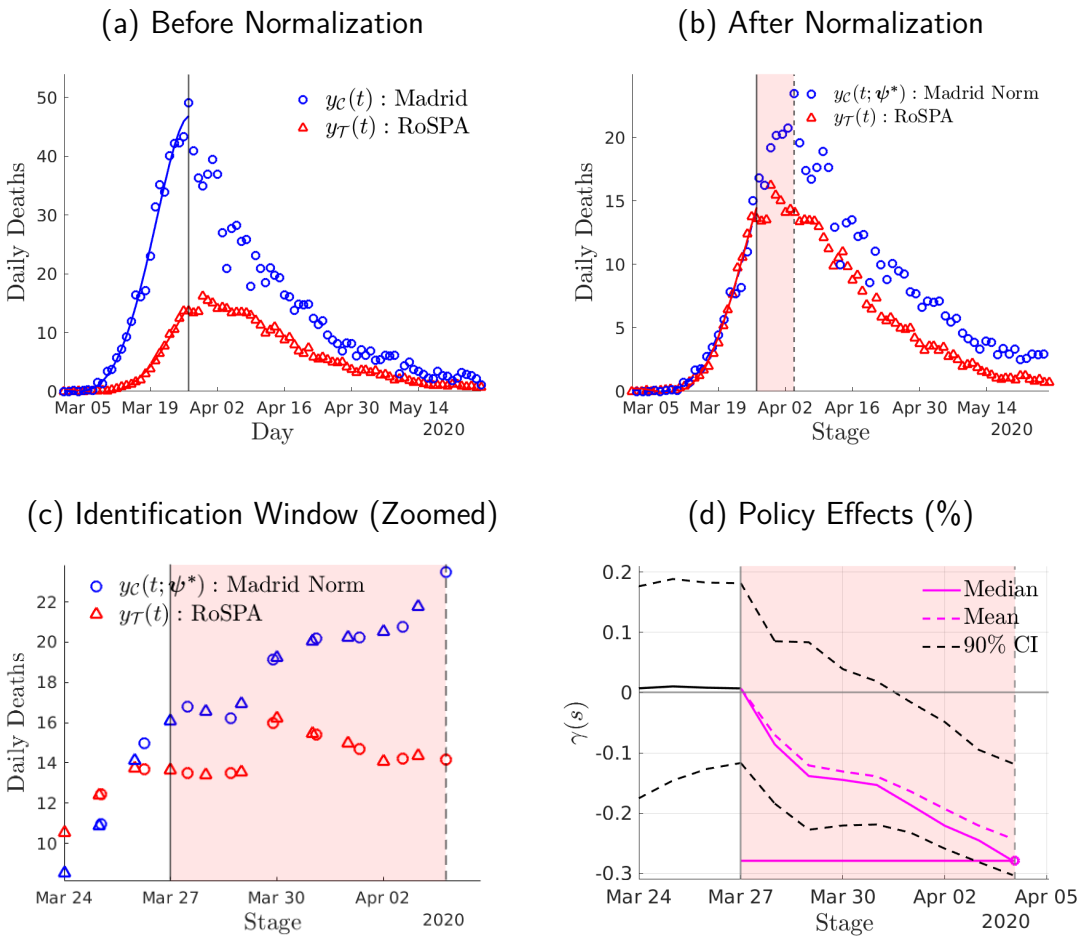


*Notes:* Panel (a) shows the daily Covid-19 deaths for Madrid, region $\mathcal{C}$, and for an artificial region $\mathcal{T}$ that aggregates the rest of Spain (RoSPA). We use a Chebyshev smoother (solid lines) of degree 6. Panel (b) shows the results of our normalization using region $\mathcal{T}$ as reference and mapping the pre-policy outcome paths of region $\mathcal{C}$ onto region $\mathcal{T}$. Panel (c) zooms the identification window. Panel (d) shows the policy effect where $\gamma$ is defined in equation (8). We show the mean, median and 90% confidence interval bands from bootstrapped simulations constructed as described in Section 3.3. We estimate a significant auto-correlation coefficient for the residuals ($\rho_{\mathcal{C}} = 0.48$ $\rho_{\mathcal{T}} = 0.55$, respectively) and thus perform block-bootstrap with a block window of 5 days.

whereas RoSPA is.[50] Therefore, under our identification assumption, the normalized path of the Madrid serves as no-policy counterfactual for RoSPA inside $\mathbb{W}(s;\boldsymbol{\psi}^*)$.

**Policy Effect.** The implied policy effects are in panel (d), where we restrict the attention to the ($B = 656$) bootstrap simulations within the neighborhood of the median window size (plus/minus 10%). Across these bootstrap draws the (mean) identified total number of lives saved (per million

[50] Precisely, the window $\mathbb{W}(s;\boldsymbol{\psi}^*)$ runs from the effective policy date in RoSPA ($t_p$ = March 27) to the effective policy date in the stage domain for Madrid, $s_{\mathcal{C}}(t_p;\boldsymbol{\psi}^*) = t_p + 7.7$ days—exactly, at 6.18pm on April 03.

inhabitants) is $\int_{\mathbb{W}(s;\psi^*)} (\widetilde{y}_{\mathcal{C}}(s;\phi^*) - y_{\mathcal{T}}(s))\, ds = 36.92$ within approximately one week after policy implementation, which corresponds to a total amount of lives saved by the policy in RoSPA of 1,734 during that week. That is, the stay-home policy prevented $\gamma = -24.71\%$ of the total deaths that would have occurred in the RoSPA had the policy not been implemented. These effects are significant with a 90% confidence interval of [-29.71,-19.30]. The median effect is similar, -26.45%. Further, considering the policy effect across all bootstrap draws (i.e., without restricting the window size) we find similar significant policy effects with mean -22.11% and median -22.95%. Last, redoing our assessment without the smoothing step implies that the policy prevented 25.61% of the deaths in RoSPA during approximately the first week. Last, we conduct a placebo diagnosis—implementing the policy days earlier than when it was actually implemented—to find that the identified policy effects that emerge from our method are not significantly different from zero; see Appendix G.[51]

### 4.2 The 1960 FDA Approval of Oral Contraceptives in the U.S.

In 1960, the first hormonal birth control pill (oral contraceptive) was approved in the U.S. by the Food and Drug Administration (FDA). The use of pill was approved for use by women above the age of majority. In a seminal paper, Goldin and Katz (2002) use state-level variation in the age of majority in order to assess how women in that threshold change schooling and career choices.[52] Since SBI does not require non-nationwide policy for identification (e.g. state-time variation of the policy that determines the age of majority), we assess the effects of the nationwide (federal) approval of the pill on the entire population of adult women. We focus on two outcome variables. First, we study the effects of the pill on women's fertility choices—crude birth rates, using as regions the state of West Virginia (ext.) and the rest of the United States (RoUSA), where we label West Virginia (ext.) as region $\mathcal{C}$ and RoUSA as region $\mathcal{T}$.[53] Second, we study the effects of the pill on women's college choices—the share of women with completed college by age 25,

[51] We further conduct a robustness exercise regarding the trend-extraction step in Appendix H. We do not find significant differences in the identified policy effects when we remove the trend-extraction step.

[52] Further, Bailey (2006) uses state-level variation in the age of majority to assess the effects of the pill on the timing of first births and women's labor force participation. Greenwood and Guner (2010) use an equilibrium matching model to assess the effects of oral contraceptives on premarital sex and how it is perceived in society.

[53] Analogously to what we did in Section 4.1, we normalize the each U.S. state's time path of crude birth rates to the aggregate path of the United States. This normalization uncovers that West Virginia leads the rest of the United States (RoUSA) in that it shows the largest cross-regional stage at the time of policy implementation. In order to increase the sample size, we further add the next three leading states (Idaho, Nevada and Arkansas) to construct an artificial region as the population weighted average of these four regions, which we label West Virginia (ext.). Then, we also construct an artificial region that consists of the RoUSA. For the case of the share of women that at age 25 have completed college, the leading state is Washington D.C. Since this state has a relatively small population size, we construct an artificial region as the population weighted average that additionally includes the next three leading states in terms of women college completion (Massachusetts, Colorado and Connecticut). We name this artificial region as Washington D.C. (ext.).

using as regions the state of Washington D.C (ext.) and RoUSA, where we label Washington D.C. (ext.) as region $\mathcal{C}$ and RoUSA as region $\mathcal{T}$.

Figure 17: The Effects of the 1960 FDA Approval of Oral Contraceptives: Crude Birth Rate

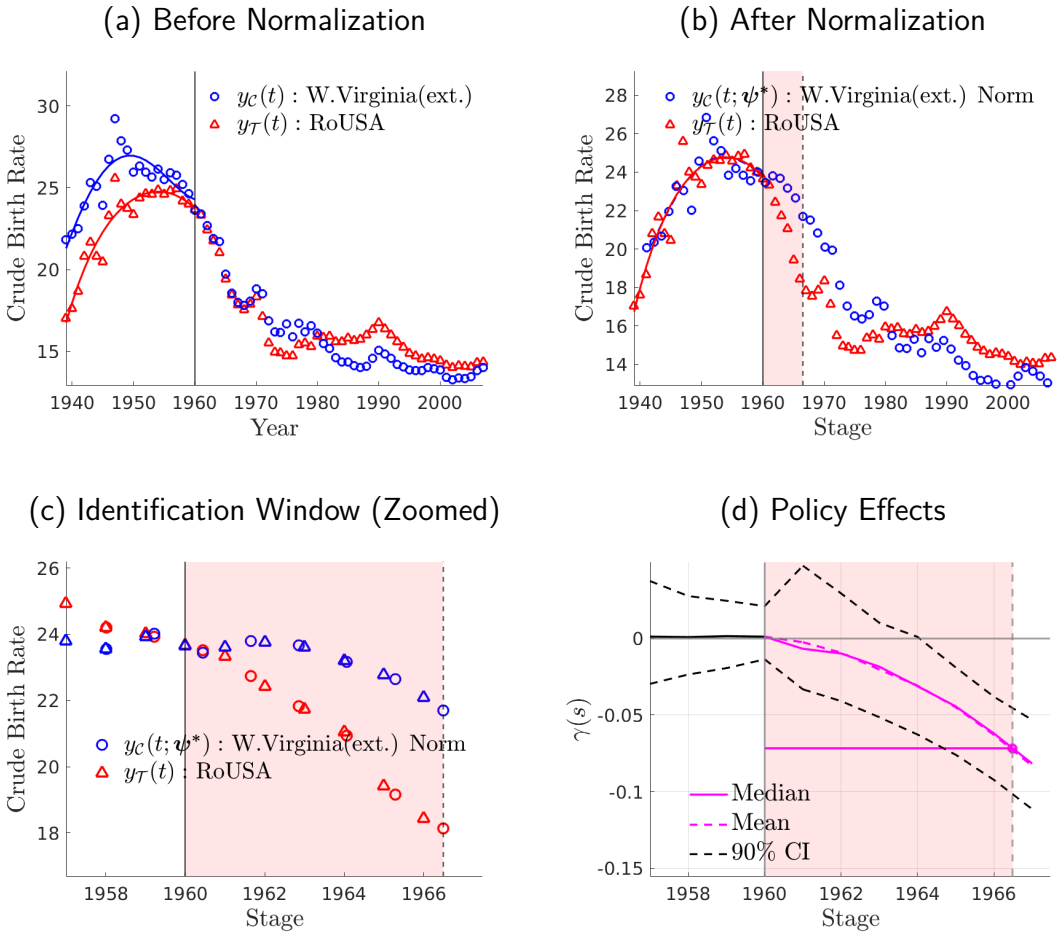


*Notes:* Panel (a) shows the crude birth rate for a region $\mathcal{C}$ which consists of a set of states leading the fertility bust (West Virginia, Idaho, Nevada and Arkansas) and a region $\mathcal{T}$ that aggregates the rest of the United States. We use a Chebyshev smoother (solid lines) of degree 5. Panel (b) shows the results of our normalization using region $\mathcal{T}$ as reference and mapping the pre-policy outcome paths of region $\mathcal{C}$ onto region $\mathcal{T}$. Panel (c) zooms the identification window. Panel (d) shows the policy effect $\gamma(s)$ as defined in equation (8). We show the mean, median and 90% confidence interval bands from bootstrapped simulations constructed as described in Section 3.3. We find a non-significant auto-correlation coefficient for the residuals, $\rho_{\mathcal{C}} = 0.31$ $\rho_{\mathcal{T}} = 0.18$, respectively.

The crude birth rates shows a inverted-U shape pattern typically labeled as the baby boom and baby bust; see panel (a) in Figure 17. We find differential patterns across states. In particular, the birth rate in the region of West Virginia (ext.) peaks in the second half of the 1940s and in 1960 is already busting and close the 1940 levels. Instead, the birth rate in the RoUSA peaks in the second half of the 1950s at somewhat lower level and, on average, has barely started to decline by year 1960. In terms of women's college completion, the proportion of women of age

25 with completed college attainment has more than tripled over a span of twenty years raising from 8% in 1950 to 26% in 1970 in the leading states; see panel (a) of Figure 18. In the RoUSA, the proportion of women of age 25 with completed college attainment shows a larger relative increase from 2% in 1950 to 15% in 1970.

Figure 18: The Effects of the 1960 FDA Approval of Oral Contraceptives: Women College

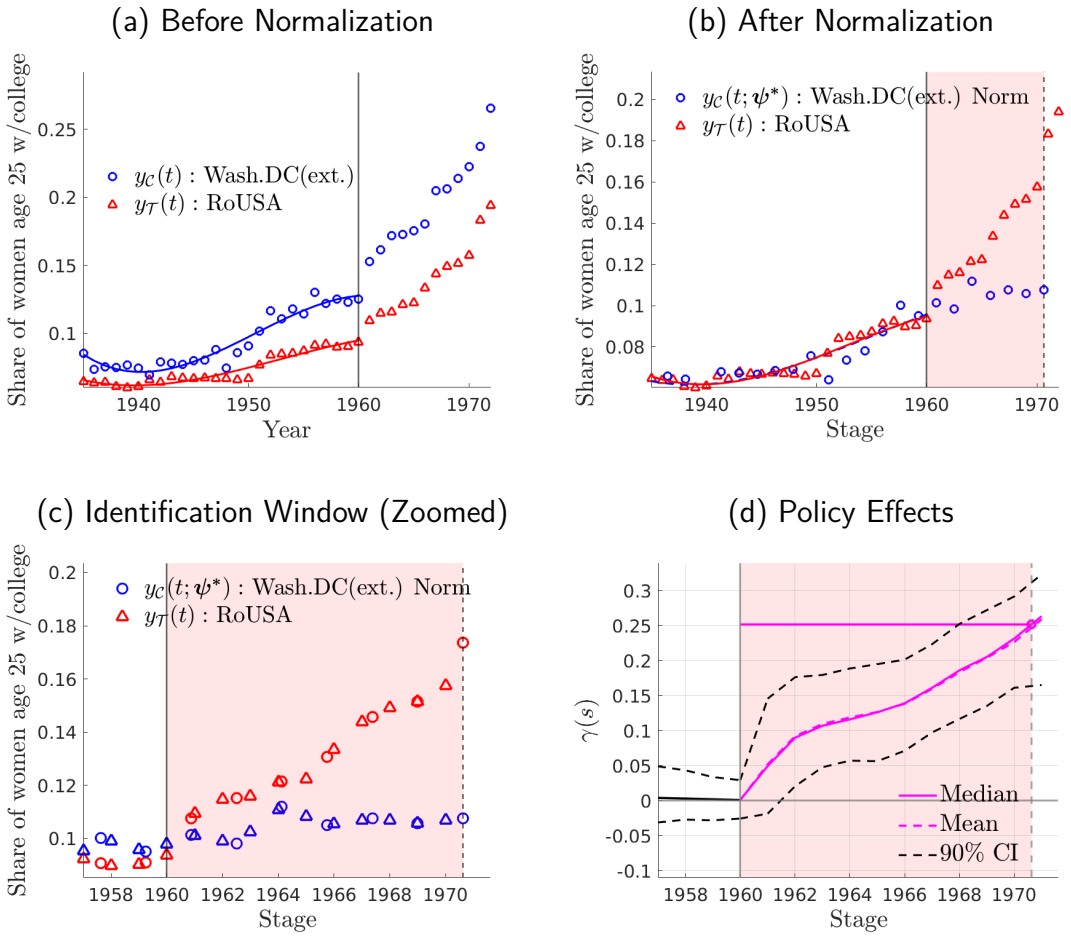


*Notes:* Panel (a) shows the proportion of women of age 25 that completed college for a region $\mathcal{C}$ which consists of a set of states leading women's college completion (Washington D.C., Massachusetts, Colorado and Connecticut) and a region $\mathcal{T}$ that aggregates the rest of the United States. We use a Chebyshev smoother (solid lines) of degree 4. Panel (b) shows the results of our normalization using region $\mathcal{T}$ as reference and mapping the pre-policy outcome paths of region $\mathcal{C}$ onto region $\mathcal{T}$. Panel (c) zooms the identification window. Panel (d) shows the policy effect $\gamma(s)$ as defined in equation (8). We show the mean, median and 90% confidence interval bands from bootstrapped simulations constructed as described in Section 3.3. We find a non-significant auto-correlation coefficient for the residuals, $\rho_{\mathcal{C}} = 0.21$ and $\rho_{\mathcal{T}} = 0.64$, respectively.

**Normalization.** In terms of crude birth rates, picking RoUSA as reference region $\mathcal{T}$, we apply our normalization by mapping the pre-policy birth rates of West Virginia (ext.) ($y_{\mathcal{C}}(t)$, solid blue circles) onto the pre-policy crude births rates of the RoUSA ($y_{\mathcal{T}}(t)$, solid red circles). This

results in a normalized path for West Virginia (ext.) $\widetilde{y}_{\mathcal{C}}(s;\boldsymbol{\phi}^*)$; see panel (b), Figure 17. The estimates are $\psi_0$ =1.85 [-0.53,9.96], $\psi_1$ =1.21 [0.41,1.58] and $\omega_1$ =0.91 [0.89,0.94] which, respectively, delays the start, slows down the growth, and lowers the peak of the baby boom for the leading region in stages.[54] A result of the normalization, West Virginia (ext.) leads the crude births rate path in that it is in a more advanced stage than RoUSA at the time of policy implementation, i.e. $s_{\mathcal{T}}(t_p;\boldsymbol{\psi}^*) = t_p < s_{\mathcal{C}}(t_p;\boldsymbol{\psi}^*)$. Hence, the normalization unveils a window of stages $\mathbb{W}(s;\boldsymbol{\psi}^*) = [t_p, s_{\mathcal{C}}(t_p;\boldsymbol{\psi}^*)]$ (shaded pink area) in which West Virginia (ext.) is not subject to policy whereas RoUSA is. For the case of women's college completion, we choose RoUSA as reference region $\mathcal{T}$ and map the pre-policy path of Washington DC (ext.) ($y_{\mathcal{C}}(t)$, solid blue circles) onto that of RoUSA ($y_{\mathcal{T}}(t)$, solid red circles), which generates a normalized path for Washington DC (ext.) $y_{\mathcal{C}}(s;\boldsymbol{\phi}^*)$; see panel (b), Figure 18. The normalizing parameters are $\psi_0$ =-5.65 [-11.17,1.84], $\psi_1$ =1.62 [1.07,1.73] and $\omega_1$ =0.85 [0.76,0.92] which results in Washington D.C. (ext.) as stage-leading region at $t_p$.

**Policy Effect.** Following our identification assumption, the stage-leading region in birth rates at the time policy implementation, West Virginia (ext.), serves as no-policy counterfactual for RoUSA inside $\mathbb{W}(s;\boldsymbol{\psi}^*)$; see the outcome paths $y_{\mathcal{C}}(s;\boldsymbol{\phi}^*)$ (normalized West Virginia (ext.)) and $y_{\mathcal{T}}(t)$ (RoUSA) inside the identification window in panel (c), Figure 17. The policy significantly reduced by $\gamma$ = -8.36% the number of births (per 10,000 inhabitants) that would have otherwise occurred without the pill; panel (d), Figure 17. The median effects are similar: a -6.94% reduction. In the previous effects, the window size is restricted to be in the neighborhood of the median window size (plus/minus 10%). Not restricting the window size, we also find significant effects, $\gamma$ = -7.53%. Analogously, for the the share of women that completed college education at age 25, the stage-leading region at the time policy implementation, Washington D.C. (ext.), serves as no-policy counterfactual for RoUSA. The FDA approval of oral contraceptives significantly increased the share of women with completed college at age 25 by $\gamma$ = 24.69% during the decade that followed the policy compared to what would have occurred without the pill; panel (c) and (d), Figure 18. The median effects are almost identical, $\gamma$ = 24.00%. Not restricting the window size also yields significant effects of $\gamma$ = 19.19%.[55,56]

[54] The fact that the policy happens after peak of the crude birth rate can provide a role for an asymmetry parameter in the stage-to-time transformation, i.e. adding the monomial basis $\psi_2 s^2$. However, at the time of policy implementation the decline in the crude birth rate for the non-leading region has barely started and when we introduce an asymmetry parameter $\psi_2$ we find that is not significantly different from zero.

[55] We provide an additional Placebo diagnosis for these policy effects in Appendix G.

[56] Without the smoothing step, the FDA approval of oral contraceptives implies a reduction of -14.81% in the number of births and an increase in the share of women of age 25 that complete college education by 18.25%. These effects are not significantly different from the mean bootstrapped effects; see Appendix H.

### 4.3 The German Reunification

In 1990, after the fall of the Berlin wall in 1989, the German Democratic Republic was abolished and integrated fully into the Federal Republic of Germany. Given large differences between the West German states and the East German states, the political and economic integration came at some cost—the size of which is subject to debate. Abadie et al. (2014) study the consequences of the German reunification for West Germany and forming a counterfactual path for GDP per capita using a Synthetic Control Group (SCG) approach. Here, we apply SBI to the same context, and construct a counterfactual for the evolution of GDP per capita in West Germany had it not been for the reunification. In contrast with Abadie et al. (2014), our counterfactual is constructed using the GDP per capita paths of West German regions only.[57] To conduct our analysis, we focus Hessen and an artificially created region for Rest of West Germany (RoGER) which is composed of all West Germany regions excluding Hessen.[58] We label Hessen as region $\mathcal{C}$ and RoGER as region $\mathcal{T}$; see panel (a) of Figure 19.

**Normalization.** Picking RoGER as reference region, we apply our normalization by mapping the pre-policy GDP per capita of Hessen ($y_{\mathcal{C}}(t)$, solid blue circles) onto that of RoGER ($y_{\mathcal{T}}(t)$, solid red circles). This results in a normalized path for Hessen $\widetilde{y}_{\mathcal{C}}(s;\boldsymbol{\phi}^*)$; see panel (b) of Figure 17. The normalizing parameters are $\psi_0$ =1.98 [1.51,6.69], $\psi_1$ =1.24 [1.13,1.48] and $\omega_1$ =1.00 [1.00,1.01]. A result of the normalization is that Hessen leads RoGER in stages at the time of policy implementation. Precisely, our normalization opens a window in stages, $\mathbb{W}(s;\boldsymbol{\psi}^*) = [t_p, s_{\mathcal{C}}(t_p;\boldsymbol{\psi}^*)]$ (shaded pink area), running from approximately seven years in which Hessen is not subject to the German reunification but RoGER is. Therefore, under our identification assumption, the normalized path for Hessen provices a no-policy counterfactual for RoGER inside that window.

**Policy Effect.** We zoom in on the identification window for the GDP per capita in panel (c) and the associated policy effects in panel (d) of Figure 17. We find that the German Reunification significantly reduced the GDP per capita of RoGER by $\gamma = 3.39\%$ compared to the GDP that it would have otherwise attained without the Reunification. The median policy effects are similar, $\gamma = 2.82\%$. In the previous effects, the window size is restricted to be in the neighborhood of the median window size (plus/minus 10%, comprising a total of 541 bootstrap samples). Again, not restricting the window size, we also find significant effects of similar size $\gamma = 3.27\%$. Further,

[57] In Section **??**, we compare the two approaches SBI and SCG in more detail.

[58] Analogously to Section 4.1, we normalize the path of GDP per capita of West Germany states to the aggregate GDP per capita path of West Germany. This normalization uncovers that the stage at which Hessen is at the time of the German reuinification is the most advanced across regions. That is, Hessen leads the rest of Germany (RoGER) at the time of policy implementation. For this reason, we focus on Hessen and RoGER for our analysis.

Figure 19: The Effects of the German Reunification on GDP per capita

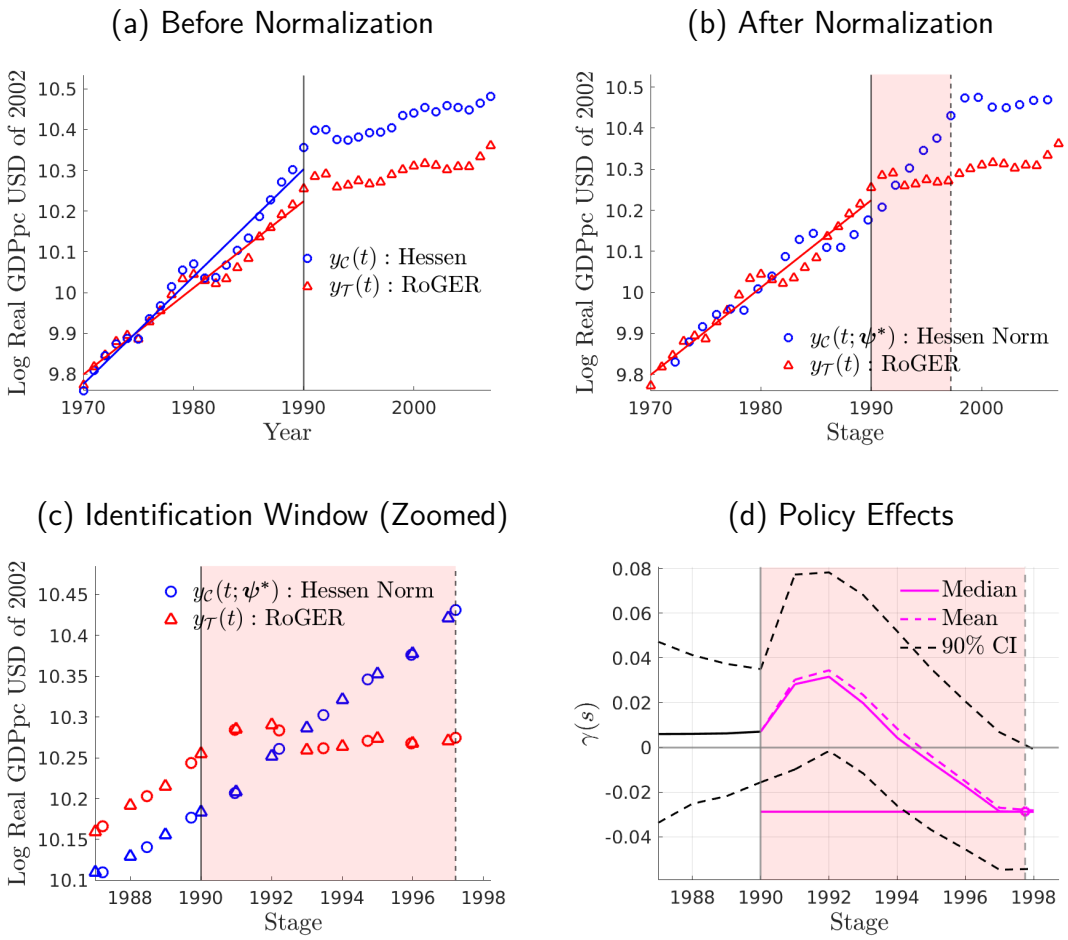


*Notes:* Panel (a) shows the GDP per capita of region $\mathcal{C}$, Hessen, that leads West Germany and a region $\mathcal{T}$ that aggregates the rest of West Germany. We use a Chebyshev smoother (solid lines) of degree 3. Panel (b) shows the results of our normalization using region $\mathcal{T}$ as reference and mapping the pre-policy outcome paths of region $\mathcal{C}$ onto region $\mathcal{T}$. Panel (c) zooms the identification window. Panel (d) shows the policy effect $\gamma(s)$ as defined in equation (8). We show the mean, median and 90% confidence interval bands from bootstrapped simulations constructed as described in Section 3.3. We find a significant auto-correlation coefficient for the residuals ($\rho_{\mathcal{C}} = 0.78$ and $\rho_{\mathcal{T}} = 0.74$, respectively) and thus perform block-bootstrap. We use a block window of 3 years.

without the smoothing step, the German reunification generates a reduction of 4.82% in the GDP per capita of RoGER, which is not significantly different from our mean bootstrapped effects.[59]

[59]We provide an additional Placebo diagnosis for these policy effects in Appendix G and assess the robustness of the trend-extraction step for this application in Appendix H.

# 5 Further Discussion

We first discuss the heterogeneity of policy effects across stages in Section 5.1. Second, we discuss the identification of the aggregate effects of policy in Section 5.2. Third, we show how our method can be applied to non-nationwide policy in section 5.3.

## 5.1 Heterogeneous Policy Effects

To conduct this analysis, we focus on the stay-home nationwide policy implemented in the first wave of Covid-19 in Spain across all regions at the same time; see Section 4.1. The idea is to use the available paths of Covid-19 deaths of multiple regions—which might differ by stage at the time of policy implementation—in order to measure policy effects by stage. Since Madrid leads all other regions we pick Madrid as reference and apply SBI to the each of the other regions—which we separately map onto Madrid. Hence, the stage domain is the same or all regions; i.e. the calendar time for Madrid. The result of this mapping is in panel (a) of Figure 20. For example, for the region of Murcia (MUR) policy implementation occurs at a stage corresponding to approximately twelve days earlier than the stage at which Madrid received the policy. The closest to Madrid is the Basque Country (PVC) that lags Madrid for approximately two days.

Our main result is that there are heterogeneous effects by region that we plot (yellow markers) in panel (b) of Figure 20. Clearly, the policy effects are larger for regions that are at less advanced stages at the time of policy implementation. For example, in the region of Murcia, the policy prevented 65% of the deaths that would have otherwise occurred in Murcia in a scenario without policy. In contrast, in the Basque Country, which is closest to Madrid in terms of stages at the time of policy implementation, the policy prevented 12% of the deaths that would have otherwise occurred in the Basque Country in a scenario without policy. To further complete our exploration, we construct hybrid regions from the power set of the treated regions, i.e. a total of $2^{16} - 1 = 131,072$ hybrid regions, that we separately map using SBI to Madrid.[60] We report the policy effects (tiny purple markers) associated with each of these hybrid regions (with 90% confidence intervals) in panel (b) of Figure 20. We reach similar insights as the policy effects are largest in instances where the the stage at the time of policy implementation is farthest away from the stage at which Madrid implemented the policy.

What drives the differences in policy effects by stage? An obvious candidate to determine these differences is the size of the identification window—i.e. the closest a region is to Madrid in terms of stages at the time of policy implementation, the smaller is the identification window.

[60] Precisely, a hybrid path between region $A$ and region $B$ is constructed as the weighted sum of the flow of deaths per capita in each region.

Figure 20: Heterogeneous Policy Effects by Stage, Spanish *Confinamiento* against Covid-19

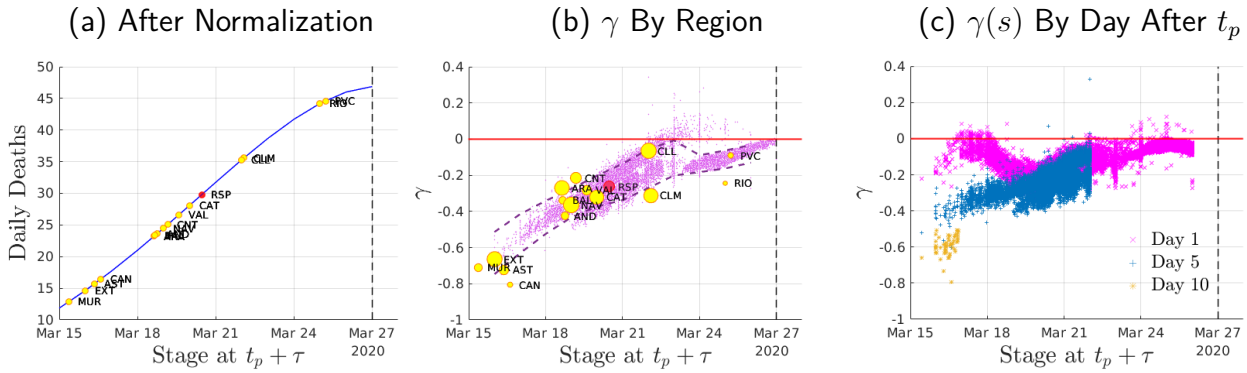


*Notes:* We have a total of 17 region (comunidad autonoma) names: Andalucia (AND), Aragon (ARA), Asturias (AST), Baleares (BAL),Canarias (CAN), Cantabria (CNT), Castilla-La Mancha (CLM), Castilla y Leon (CLL), Catalunya (CAT), Ceuta(CEU), Valencia (VAL), Extremadura (EXT), Galicia (GAL), Madrid (MAD), Melilla (MEL), Murcia (MUR),Navarra (NAV), Pais Vasco (PVC), La Rioja (RIO). We exclude GAL from the analysis due to the fact that we find positive (yet, non-significant) effects of the policy on the flow of deaths. The size of the yellow is the stock of deaths per thousand inhabitants accumulated during the identification window. In panel (b), we report the policy effects $\gamma$ (see Section 2.2) by region where the (yellow) marker size is the flow of deaths at the time of policy implementation. In addition to the policy effects by region, we also report the policy effects for each hybrid region constructed for each element in the the power set $2^{16} - 1$ of regions (tiny markers) in panel (b). In panel (b), the 90% CI's exclude the top 5% and bottom 5% of policy effects by stage in rolling windows of 2 stages/days. In panel (c) we show the interim effect $\gamma(s)$ (see Section 2.2) by stage for day 1, day 5 and day 10 after policy implementation.

At the same time, differences in policy effects can emerge within the same horizon into the policy within the identification window. To assess this question, we isolate the effects of policy by the number of stages within the identification window. Here, note that since we picked Madrid as reference, the stage for Madrid is the actual calendar time (i.e. days). In those terms, we find substantial heterogeneity across identification windows by stage. For example, one day into the policy (i.e inside the identification window) at a stage of approximately 10 days before Madrid enters policy (e.g. March 18) the policy effect is below 10%, whereas one day into the policy at a stage of approximately 7 days before Madrid enters policy (e.g. March 12) the policy effect is above 10%, and one day into the policy at a stage of approximately 3 days before Madrid enters policy (e.g. March 24) is again below 10%; see the magenta markers in panel (c) of Figure 20. We also show differences across stages in the policy effects for the cases of five days (blue markers) and ten days (yellow markers) into the policy. That is, not only the size of the identification window matters (i.e. how close in stages a given region is to Madrid at the time of policy implementation) but there are also differences in policy effects driven by the differential within-window policy effects across identification windows.

Figure 21: Aggregate Policy Effects, Spanish *Confinamiento* against Covid-19

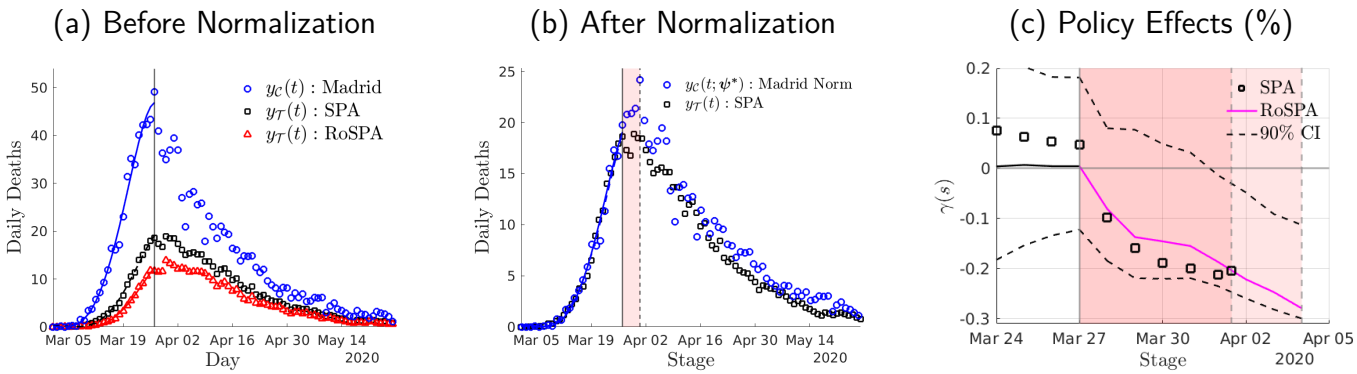


*Notes:* Panel (a) shows the daily Covid-19 deaths for Madrid, region $\mathcal{C}$, and for two artificial regions $\mathcal{T} = \{\text{SPA, RoSPA}\}$ where SPA is aggregate Spain (i.e. the complete set of all regions in Spain) and RoSPA is an alternative aggregate that excludes Madrid (as constructed in Section 4.1). We use a Chebyshev smoother (solid lines) of degree 6. Panel (b) shows the results of mapping the pre-policy outcome paths of region $\mathcal{C}$ (Madrid) onto the reference region $\mathcal{T}$: SPA. Panel (c) shows the median effects of the policy on aggregate Spain (black square makerts) and, for comparison, on RoSPA (magenta solid line, as computed in Section 4.1) with 90% confidence interval bands from bootstrapped simulations constructed as described in Section 3.3. We estimate a significant auto-correlation coefficient for the residuals ($\rho_{\mathcal{C}} = 0.48$ $\rho_{\mathcal{T}} = 0.54$, respectively) and thus perform block-bootstrap with a block window of 5 days.

## 5.2 Aggregate Policy Effects

Standard empirical strategies that rely on heterogeneity in the time of policy implementation for identification are typically silent about the aggregate effects of policy. The reason is that, under those strategies, the region that serves as control (for all other treated regions) needs to be contemporaneously untreated in the time domain which is never the case with nationwide policy; see panel (a) in Figure 21.[61] In contrast, our methodology uses heterogeneity across stages at the time of policy implementation for identification; that is, SBI does not need a contemporaneously untreated region in the time domain. For this reason, SBI allows for the aggregate (i.e. a unit consisting of the complete set of all regions) to be treated and, therefore, the assessment of aggregate policy effects is potentially feasible with our method. In particular, as long as the regions display heterogeneity in terms of the outcome paths, it will typically be the case that the aggregate path lags the path of the stage-leading region, and thus is at an earlier stage at the time of policy implementation. Again, this stage-variation can be used for the identification of aggregate policy effects. Note that the chance of a successful normalization will tend to increase relative to the implementation that uses an aggregate path without the stage-leading region (as

[61] In staggered rollouts, untreated regions can serve as controls in time-bounded windows. See the recent analysis in Goodman-Bacon (2021) for a careful assessment of difference-in-differences strategies that can be used under different timings and scenarios of staggered rollout policies.

in our benchmark applications): the outcome paths are closer when the aggregate includes the stage-leading region. By the same token, the identification window will tend to be smaller.

We focus on our application about the *confinamiento* against Covid-19 in Spain. Using aggregate Spain as reference region, we normalize Madrid to aggregate Spain in order to assess the aggregate effects of policy. After normalization, we find that Spain lags the stage-leading region of Madrid opening an identification window of 5.5 days; see panel (b) in Figure 21.[62] The stay-home policy significantly reduced the amount of deaths for aggregate Spain by $\gamma =$ -20.37% [-24.28,-14.81] inside the identification window; see panel (c) in Figure 21. Interestingly the aggregate policy effects for Spain are not significantly different from the policy effects of an alternative aggregate (RoSPA) that excludes the stage-leading region of Madrid—as computed in Section 4.1. In particular, the interim policy effects of both aggregate Spain and RoSPA are similar for the periods in which the identification windows of aggregate Spain and RoSPA overlap,[63] which indicates that the effects of the stay-home policy on Madrid are not significant.[64]

### 5.3 Non-Nationwide Policy

Here, we show that SBI works in scenarios where there are regions that never receive the policy intervention. Consider a scenario with two regions where one region, e.g. $\mathcal{T}$, receives the policy intervention at period $t_p$ and the other region, e.g. $\mathcal{C}$, is never treated. To illustrate this scenario we use our benchmark model with endogenous pandemics as described in Section 3.1.1. In that context, we introduce the stay-home policy that puts an upper bound on hours worked in region $\mathcal{T}$, but not in region $\mathcal{C}$; see panel (a) of Figure 22. The implications for the outcome of interest, the flow of deaths, is displayed in panel (b) of Figure 22. The policy has an impact on region $\mathcal{T}$, but not on region $\mathcal{C}$.

In order to identify the policy effects, we need to modify the set on which the normalization is conducted. In particular, picking region $\mathcal{T}$ as reference, the normalization parameters are the

[62] Precisely, the window $\mathbb{W}(s;\boldsymbol{\psi}^*)$ runs from the effective policy date in SPA ($t_p =$ March 27) to the effective policy date in the stage domain for Madrid, $s_{\mathcal{C}}(t_p;\boldsymbol{\psi}^*) = t_p + 5.5$ days—exactly, at 11.38am on March 31.

[63] The area in which the identification windows of aggregate Spain and RoSPA overlap is the identification window of aggregate Spain which, by incorporating the stage-leading region, is closer in stages to Madrid at the time of policy implementation—i.e. aggregate Spain has a shorter identification window. Note that since both aggregate Spain and RoSPA are chosen as reference in their respective applications of SBI (we map the stage-leading region, Madrid, separately onto each of the reference regions, aggregate Spain and RoSPA), the identification windows are defined in the same domain—i.e. time, because the stage is time in both cases.

[64] As alternative strategy to measure the aggregate effects, one may be tempted to extrapolate the heterogeneous policy effects documented in Section 5.1 in order to find the policy effects of the control region and, hence, the aggregate effects. In Appendix I, we show that these extrapolations are not a good idea in that the extrapolated effects can fall far from the true (model-generated) effects.

Figure 22: Stage-Based Identification of Non-Nationwide Policy Effects

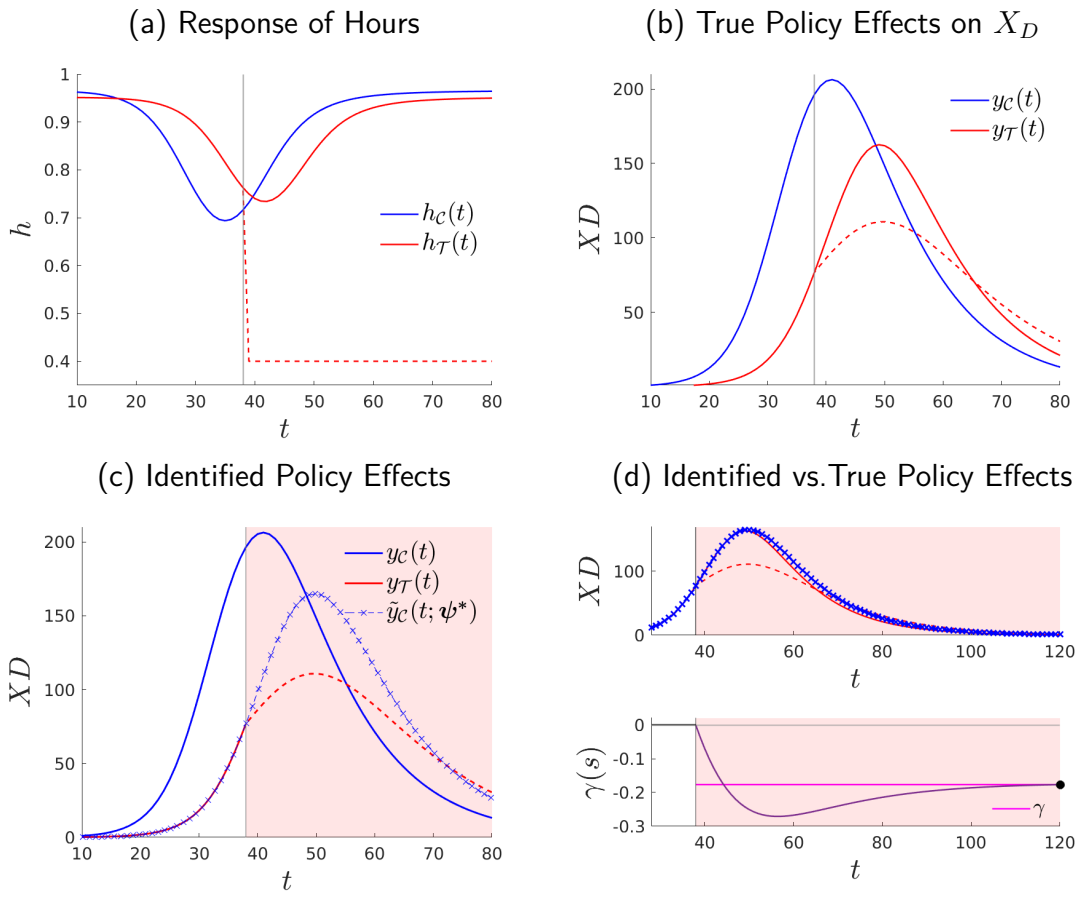


*Notes:* Where $\bar{h} = 0.4, t_p = 38, t_f = 250$, $\gamma = 17.66\%$ and $\epsilon(\gamma) = 58.19\%$

solution to the minimization of (5) subject to (3) and

$$\mathbb{C}(s) = \begin{cases} [t_0, t_p] & \text{if } \; r = \mathcal{T} \\ [s_{\mathcal{C}}(t_0;\boldsymbol{\psi}^*), s_{\mathcal{C}}(t_f;\boldsymbol{\psi}^*)] & \text{if } \; r = \mathcal{C} \end{cases} \tag{29}$$

for $r = \{\mathcal{C}, \mathcal{T}\}$ where $t_0$ denotes the first period of observed data and $t_f$ the last.

The results of the normalization are shown in panel (c) of Figure 22. Note that since only region $\mathcal{T}$ is treated, the identification window is,

$$\mathbb{W}(s;\boldsymbol{\psi}^*) = \begin{cases} [t_p, s_{\mathcal{C}}(t_f;\boldsymbol{\psi}^*)] & \text{if } \; s_{\mathcal{C}}(t_f;\boldsymbol{\psi}^*) > t_p \\ \varnothing & \text{if } \; s_{\mathcal{C}}(t_f;\boldsymbol{\psi}^*) < t_p \end{cases} \tag{30}$$

Figure 23: The Effects of the German Reunification: Stage-Based Identification (SBI) and Synthetic Control Methods (SCM)

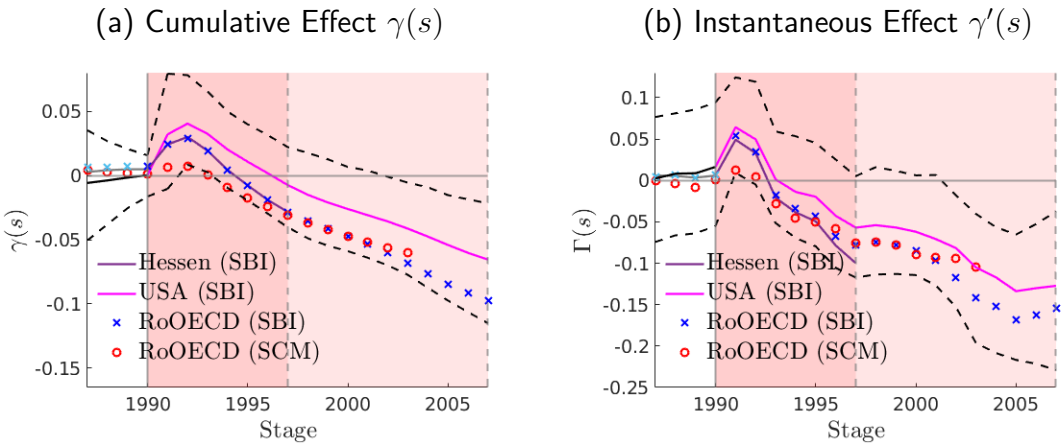


*Notes:* The outcome variable is real GDP per capita in USD of 2002. The plotted 90% confidence intervals correspond to the United States.

Hence, there is a policy effect if and only if the stage of normalized series evaluated at the last period of observed data $y_{\mathcal{C}}(s;\boldsymbol{\phi}^*)$ with $s = s_{\mathcal{C}}(t_f;\boldsymbol{\psi}^*)$ falls beyond the period of policy implementation $t_p$. Otherwise, the identification window is the empty set because the treated region leads throughout the entire sample. In our model-generated example, the normalization shows that region $\mathcal{C}$ covers stages beyond that of region $\mathcal{T}$ at the time of policy implementation which implies that $\mathbb{W}(s;\boldsymbol{\psi}^*) = [t_p, s_{\mathcal{C}}(t_f;\boldsymbol{\psi}^*)]$ and we can assess policy effects. We show the identified policy effects in panel (d) of Figure 22, for which we find that overlap with the true (model-generated) policy effects.

We further exemplify how to use stage-based identification in cases in which not all regions are treated by re-conducting our assessment of the German Reunification. Here, we take West Germany as the treated region and use as potential controls the United States and an aggregate consisting of the same sample of OECD countries (that excludes Germany) studied in Abadie et al. (2014). Hence, this exercise also serves as means for comparison between SBI and SCM (Abadie and Gardeazabal, 2003). In order to apply SBI, we pick West Germany as reference region. Then we conduct the normalization by mapping the GDP per capita path of the U.S. and the OECD aggregate onto the GDP per capita path of West Germany. We show the policy effects that emerge from SBI in panel (a) of Figure 23. To ease the comparison with Abadie et al. (2014), we also show in panel (b) of Figure 23 the instantaneous policy effects by stage defined as (abusing some notation), $\gamma'(s) = \frac{y_{\mathcal{T}}(s) - \widetilde{y}_{\mathcal{C}}(s)}{\widetilde{y}_{\mathcal{C}}(s)}$. That is, $\gamma'(s)$ measures the change in GDP per capita of region $\mathcal{T}$ (West Germany) relative to the counterfactual region $\mathcal{C}$ (e.g. the

U.S. or the rest of the OECD) at any given stage $s$ due to policy. We further show the results from using Hessen as leading region in the context of nationwide policy within Western Germany reported in Section 4.3. For inference, we show the 90% confidence intervals associated to the USA constructed as described in Section 3.3.

Our main finding is that the policy effects that emerge from using SBI either for the U.S.—or the OECD aggregate that excludes Germany—are not significantly different from those obtained using SCM in Abadie et al. (2014). In particular, the instantaneous policy effects imply a loss of income per capita for West Germany due to the Reunification of 12.73% when compared to the United States and of 15.44% when compared to the rest of the OECD in 2007. These figures are, respectively, 10.51% and 14.13% in 2003 which are not significantly different from the effects of reunification of 10.04% obtained in Abadie et al. (2014). Further, we also find that within the shorter window that emerges when the counterfactual from the SBI strategy is Hessen as in Section 4.3, the results under the alternative counterfactuals are not significantly different from the results obtained with Hessen.[65]

## 6 Conclusion

We provide a new method for policy analysis, SBI. By uncovering heterogeneity in the stage at which policy is implemented across regions, our method allows for the analysis of nationwide policy, which expands the range of policies that can be empirically evaluated. We show the ability of our method to accurately identify policy effects in various model simulations where the true effect is known, while also acknowledging limitations to our method's performance. Furthermore, we show that our method can not only recover the heterogeneous effects of policy across stages but also the aggregate effects of policy—something that is an enduring challenge for other empirical strategies that rely on heterogeneity in the time of policy implementation. In addition, we discuss how our method can be applied to non-nationwide policy with untreated regions.

## References

Abadie, A. (2005). Semiparametric Difference-in-Differences Estimators. *Review of Economic Studies*, 72(1):1–19.

[65] In Appendix J, we further discuss the identified effects that arise from one treated region that is potentially facing many potential control regions in the context of the stay-home policy against Covid-19 in Spain. An interesting outcome, analogous to that of the German Reunification application, is that the policy effects are similar independently of which control we use. Since the stage at which the treated region enters policy is the same across controls (picking the treated region as the reference region) and so are the policy effects across controls.

Abadie, A., Diamond, A., and Hainmueller, J. (2010). Synthetic Control Methods for Comparative Case Studies: Estimating the Effect of California's Tobacco Control Program. *Journal of the American Statistical Association*, 105(490):493–505.

Abadie, A., Diamond, A., and Hainmueller, J. (2014). Comparative Politics and the Synthetic Control Method. *American Journal of Political Science*, 59(2):495–510.

Abadie, A. and Gardeazabal, J. (2003). The Economic Costs of Conflict: A Case Study of the Basque Country. *American Economic Review*, 93(1):113–132.

Adam, K., Marcet, A., and Beutel, J. (2017). Stock price booms and expected capital gains. *American Economic Review*, 107(8):2352–2408.

Aleman, C., Iorio, D., and Santaeulalia, R. (2022). A quantitative theory of the hiv epidemic: Education, risky sex and asymmetric learning. Working paper, Barcelona School of Economics.

Altonji, J. and Blank, R. (1999). Race and gender in the labor market. In Ashenfelter, O. and Card, D., editors, *Handbook of Labor Economics*, volume 3, Part C, chapter 48, pages 3143–3259. Elsevier, 1 edition.

Angrist, J. D. and Krueger, A. B. (1999). Empirical strategies in labor economics. In Ashenfelter, O. and Card, D., editors, *Handbook of Labor Economics*, volume 3 of *Handbook of Labor Economics*, chapter 23, pages 1277–1366. Elsevier.

Athey, S. and Imbens, G. W. (2006). Identification and inference in nonlinear difference-in-differences models. *Econometrica*, 74(2):431–497.

Athey, S. and Imbens, G. W. (2017). The state of applied econometrics: Causality and policy evaluation. *Journal of Economic Perspectives*, 31(2):3–32.

Athey, S. and Imbens, G. W. (2021). Design-based analysis in difference-in-differences settings with staggered adoption. *Journal of Econometrics*.

Atkeson, A. (2020). What will be the economic impact of covid-19 in the us? rough estimates of disease scenarios. Working Paper 26867, National Bureau of Economic Research.

Bailey, M. J. (2006). More Power to the Pill: The Impact of Contraceptive Freedom on Women's Life Cycle Labor Supply*. *The Quarterly Journal of Economics*, 121(1):289–320.

Bertrand, M., Duflo, E., and Mullainathan, S. (2004). How Much Should We Trust Differences-In-Differences Estimates? *The Quarterly Journal of Economics*, 119(1):249–275.

Blundell, R. and Macurdy, T. (1999). Labor supply: A review of alternative approaches. In Ashenfelter, O. and Card, D., editors, *Handbook of Labor Economics*, volume 3 of *Handbook of Labor Economics*, chapter 27, pages 1559–1695. Elsevier.

Borusyak, K., Jaravel, X., and Spiess, J. (2021). Revisiting Event Study Designs: Robust and Efficient Estimation. Working papers, University College London.

Callaway, B. and Sant'Anna, P. H. (2021). Difference-in-Differences with multiple time periods. *Journal of Econometrics*, 225(2):200–230.

Card, D. (1990). The impact of the mariel boatlift on the miami labor market. *ILR Review*, 43(2):245–257.

Card, D. (2022). Design-based research in empirical microeconomics. *American Economic Review*, 112(6):1773–81.

Card, D. and Krueger, A. B. (2000). Minimum wages and employment: A case study of the fast-food industry in new jersey and pennsylvania: Reply. *The American Economic Review*, 90(5):1397–1420.

Carlstein, E. (1986). The use of subseries values for estimating the variance of a general statistic from a stationary sequence. *The Annals of Statistics*, 14(3):1171–1179.

Cervellati, M. and Sunde, U. (2015). The economic and demographic transition, mortality, and comparative development. *American Economic Journal: Macroeconomics*, 7(3):189–225.

Doudchenko, N. and Imbens, G. W. (2017). Balancing, regression, difference-in-differences and synthetic control methods: A synthesis.

Fang, H., Wang, L., and Yang, Y. (2020). Human mobility restrictions and the spread of the novel coronavirus (2019-ncov) in china. *Journal of Public Economics*, 191:104272.

Fernández-Villaverde, J., Greenwood, J., and Guner, N. (2014). From Shame To Game In One Hundred Years: An Economic Model Of The Rise In Premarital Sex And Its De-Stigmatization. *Journal of the European Economic Association*, 12(1):25–61.

Galor, O. and Weil, D. N. (2000). Population, technology, and growth: From malthusian stagnation to the demographic transition and beyond. *American Economic Review*, 90(4):806–828.

Glogowsky, U., Hansen, E., and Schächtele, S. (2021). How effective are social distancing policies? evidence on the fight against covid-19. *PLOS ONE*, 16(9):1–12.

Goldin, C. and Katz, L. F. (2002). The Power of the Pill: Oral Contraceptives and Women's Career and Marriage Decisions. *Journal of Political Economy*, 110(4):730–770.

Gollin, D., Parente, S., and Rogerson, R. (2002). The role of agriculture in development. *American Economic Review*, 92(2):160–164.

Goodman-Bacon, A. (2021). Difference-in-differences with variation in treatment timing. *Journal of Econometrics*, 225(2):254–277.

Greenwood, J. and Guner, N. (2010). Social change: The sexual revolution. *International Economic Review*, 51(4):893–923.

Greenwood, J., Seshadri, A., and Vandenbroucke, G. (2005). The Baby Boom and Baby Bust. *American Economic Review*, 95(1):183–207.

Hansen, G. D. and Prescott, E. C. (2002). Malthus to solow. *American Economic Review*, 92(4):1205–1217.

Heckman, J. J., Ichimura, H., and Todd, P. (1998). Matching As An Econometric Evaluation Estimator. *Review of Economic Studies*, 65(2):261–294.

Herrendorf, B., Rogerson, R., and Valentinyi, A. (2014). Growth and structural transformation. In *Handbook of Economic Growth*, volume 2, chapter 06, pages 855–941. Elsevier, 1 edition.

Imbens, G. W. and Rubin, D. B. (2015). *Causal Inference for Statistics, Social, and Biomedical Sciences: An Introduction*. Cambridge University Press.

Iorio, D. and Santaeulàlia-Llopis, R. (2010). Education, HIV Status, and Risky Sexual Behavior: How Much Does the Stage of the HIV Epidemic Matter? Working papers, washington university in st. louis.

Iorio, D. and Santaeulàlia-Llopis, R. (2016). Education, HIV Status, and Risky Sexual Behavior: How Much Does the Stage of the HIV Epidemic Matter? Working papers, Barcelona Graduate School of Economics.

Liu, L., Moon, H. R., and Schorfheide, F. (2021). Panel forecasts of country-level Covid-19 infections. *Journal of Econometrics*, 220(1):2–22.

Rambachan, A. and Roth, J. (2021). A More Credible Approach to Parallel Trends. Technical report.

# Appendix

## A Further Illustrations: Policy After the Peak

Here, within the context of our benchmark illustration in Section 2, we assess additional examples in which the policy is implemented when regional outcome paths have surpassed their peak in one region in Section A.1 and in two regions in Section A.1.

### A.1 Policy after the peak: One region

Consider a scenario in which the nationwide policy is implemented nationwide at the same time in two regions $r = \{\mathcal{C}, \mathcal{T}\}$. Assume the policy arrives before the outcome path of region $\mathcal{T}$ reaches its peak and, at the same time, after the outcome path of region $\mathcal{C}$ as surpassed its peak; see panel (a) of Figure 24. Since the policy is implemented at the same time across regions, standard empirical strategies that rely on time variation at the time of policy implementation are unworkable in this scenario. We pick region $\mathcal{T}$ as reference and apply SBI. That is, we map region $\mathcal{C}$ onto region $\mathcal{T}$ using pre-policy data only. This mapping generates the normalized outcome path $\widetilde{y}_{\mathcal{C}}(s; \boldsymbol{\phi}^*)$; see panel (b) in Figure 24. Our normalization opens a window in stages between $t_p$ and $s_{\mathcal{C}}(t_p; \boldsymbol{\psi}^*)$ in which we identify the effects of policy. Since region $\mathcal{C}$ is at a more advanced stage at the time of policy implementation, i.e. $t_p < s_{\mathcal{C}}(t_p; \boldsymbol{\psi}^*)$, it serves as no-policy counterfactual for region $\mathcal{T}$ inside the identification window. We zoom the identification window in panel (c) of Figure 24 and the associated policy effects in panel (d) of Figure 24.

Figure 24: Stage-Based Identification of Policy Effects: Further Illustrations: One Region After the Peak

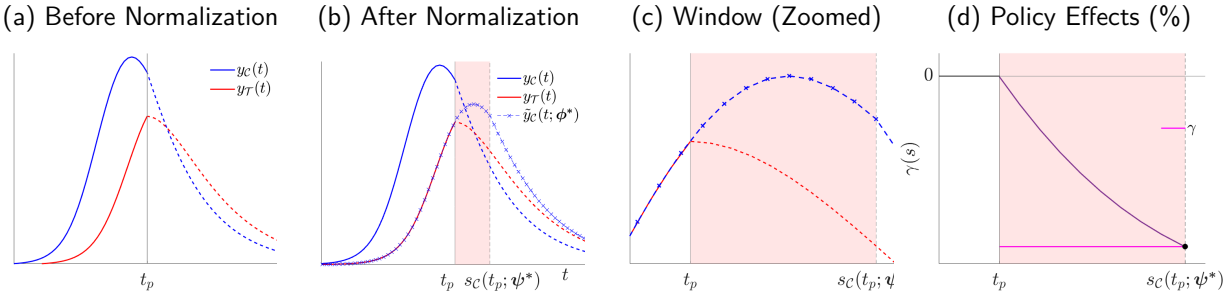


*Notes:* See the notes in Figure 3.

### A.2 Policy after the peak: Two regions

Here we discuss a scenario analogous to that of the previous Section with the variant that the nationwide policy arrives to both regions after their outcome paths has surpassed their respective peaks; see panel (a) of Figure 32. Picking again region $\mathcal{T}$ as reference, we map region $\mathcal{C}$ onto region $\mathcal{T}$ using pre-policy data only, which generates the normalized outcome path $\widetilde{y}_{\mathcal{C}}(t; \boldsymbol{\phi}^*)$; see panel (b) in Figure 32. Hence, SBI opens a window in stages between $t_p$ and $s_{\mathcal{C}}(t; \boldsymbol{\psi}^*)$ in which the effects of policy are identified. We zoom the identification window in panel (c) of Figure 32 and the associated policy effects in panel (d) of Figure 32. In Figure 26, we further

Figure 25: Stage-Based Identification of Policy Effects: Further Illustrations: Two Regions After the Peak

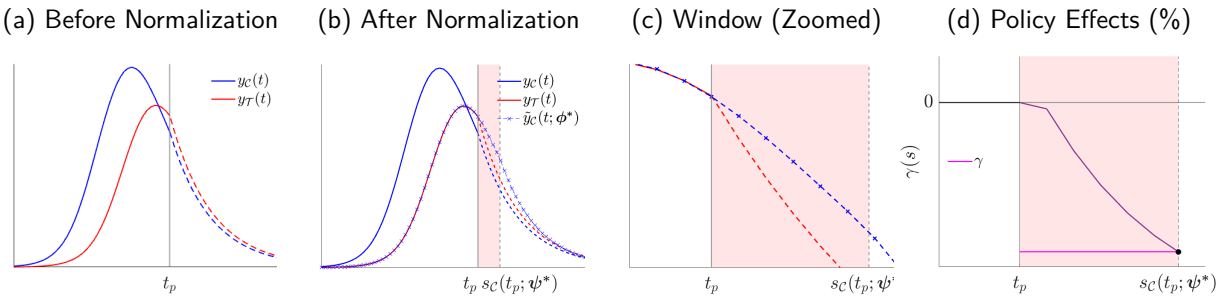


*Notes:* See the notes in Figure 3.

Figure 26: Decomposing by Normalization Coefficient: Further Illustrations: Two Regions After the Peak

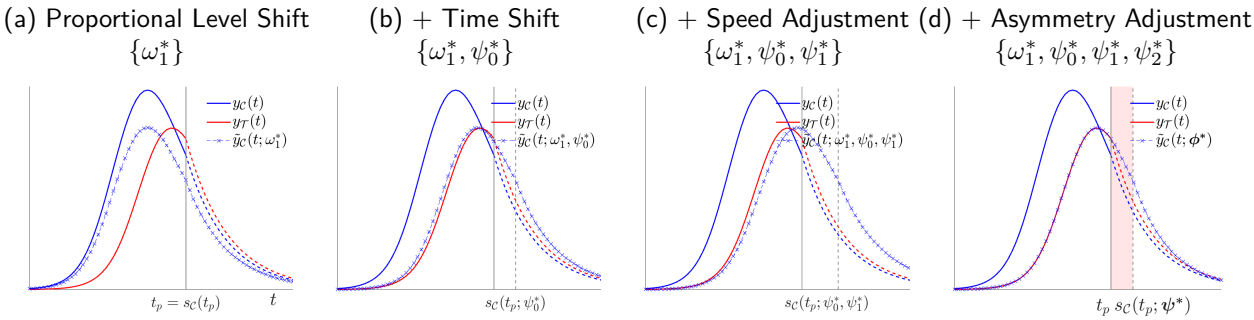


*Notes:* See the notes in Figure 4.

unpack the contribution of each normalization coefficient in generating the normalized path. Note that in this scenario, since the outcome paths of the two regions is already affected by the potential asymmetry in which the outcome paths increase before their respective peaks and decrease after the peaks, the additional parameter $\psi_2$ that asymmetrically shapes stages into time, i.e. $t_{\mathcal{C}} = \psi_0 + \psi s + \psi_2 s^2$ plays a role.

# B Some Analytical Derivations

Here, we follow our discussion in Section 2.3 and provide analytical derivations for some cases in which we can explicitly express the normalization coefficients as functions of the structural parameters of a known data generating process. As emphasized in our main text, note, again, that this exercise merely serves to illustrate our method and provide an interpretation of the normalization coefficients as those that aim to reshape the structural parameters of the non-reference regions into those of the reference region. Indeed, if the data generating process were actually known, there would be no need to apply SBI; or any other identification method for that matter.

Our method works under the proposition that if there exists a composite function (1) such that (10) holds with equality, then our normalization procedure—the minimization of (5) subject to (2) and (6)—recovers the coefficients $\boldsymbol{\phi} = \{\boldsymbol{\psi}, \boldsymbol{\omega}\}$ up to a minimization error by approximating the functions $t_{\mathcal{C}}(.) \approx t_{\mathcal{C}}(.;\boldsymbol{\psi})$, $f_{\mathcal{C}}(.) \approx f_{\mathcal{C}}(.;\boldsymbol{\omega})$ and, hence, $\widetilde{y}_{\mathcal{C}}(.) \approx \widetilde{y}_{\mathcal{C}}(.;\boldsymbol{\phi})$ for all $s \in \mathbb{C}(s)$. Thus, under our identification assumption, we can identify

the policy effects for all $s \in \mathbb{W}(s;\boldsymbol{\psi}^*)$. Here, we are interested in cases where (10) and (2) hold with equality and, hence, analytical solutions for the normalization coefficients $\boldsymbol{\phi}$ potentially exist for all $s \in \mathbb{C}(s)$. For this discussion, we focus on cases in which $t_{\mathcal{C}}$ and $f_{\mathcal{C}}$ are linear—$t_{\mathcal{C}} = \psi_0 + \psi_1 s$ and $f_{\mathcal{C}} = \omega_0 + \omega_1 y_{\mathcal{C}}(t)$, and study time paths, $y_r(t)$, that are described by trigonometric functions (Section B.1), polynomial functions (Section B.2) and generalized logistic functions (Section B.3) under the assumption that we know these data generating processes.

As in Section 2.3, the outcome time paths throughout this Appendix B follow:

$$y_r(t) = \left(1 - \gamma_{r,t}\mathbf{1}_{t \geq t_p}\right) g(t;\Theta_r)$$

for regions $r = \{\mathcal{C}, \mathcal{T}\}$ and periods $t \in \{0, \ldots, t_p, \ldots, T\}$. The region-specific policy effects for periods after $t_p$ are captured by $\gamma_{r,t}$ whereas $g(t;\Theta_r)$ captures the outcome time path of region $r$ (determined by region-specific structural parameters $\Theta_r$) occurring absent policy—that is, $g(t;\Theta_r)$ is the true region-specific no-policy counterfactual for $t \geq t_p$.

## B.1 Trigonometric functions

Here, we study a case with trigonometric time paths (see panel (b) of Figure 6). Precisely, we define

$$g(t;\Theta_r) = \theta_{1,r} \sin\left(\theta_{3,r} t + \theta_{2,r}\right) + \theta_{0,r},$$

for regions $r = \{\mathcal{C}, \mathcal{T}\}$ and periods $t \in \{0, \ldots, t_p, \ldots, T\}$. Then, picking a region (here: $\mathcal{T}$) as reference, we apply our normalization procedure. That is, we map the outcome path of the non-reference region $\mathcal{C}$ onto that of the reference region $\mathcal{T}$ using pre-policy data only. To do so, we postulate a normalized path for the non-reference region, $\widetilde{y}_{\mathcal{C}}(s;\boldsymbol{\phi}) = \left(f_{\mathcal{C}}(.;\boldsymbol{\omega}) \circ y_{\mathcal{C}} \circ t_{\mathcal{C}}(.;\boldsymbol{\psi})\right)(s)$ with outer composite $f_{\mathcal{C}} = \omega_0 + \omega_1 y_{\mathcal{C}}(t)$ and inner composite $t_{\mathcal{C}} = \psi_0 + \psi_1 s$. That is,

$$\begin{aligned}
\widetilde{y}_{\mathcal{C}}(s;\boldsymbol{\phi}) &= \omega_1 y_{\mathcal{C}}(\psi_0 + \psi_1 s) + \omega_0 \\
&= \omega_1 \left(\theta_{1,\mathcal{C}} \sin\left(\theta_{3,\mathcal{C}}(\psi_0 + \psi_1 s) + \theta_{2,\mathcal{C}}\right) + \theta_{0,\mathcal{C}}\right) + \omega_0 \\
&= \underbrace{\omega_1 \theta_{1,\mathcal{C}}}_{=\theta_{1,\mathcal{T}}} \sin\left(\underbrace{\theta_{3,\mathcal{C}}\psi_1}_{=\theta_{3,\mathcal{T}}} s + \underbrace{\left(\theta_{3,\mathcal{C}}\psi_0 + \theta_{2,\mathcal{C}}\right)}_{=\theta_{2,\mathcal{T}}}\right) + \underbrace{\omega_1 \theta_{0,\mathcal{C}} + \omega_0}_{=\theta_{0,\mathcal{T}}} = y_{\mathcal{T}}(s),
\end{aligned}$$

where the last equality emerges from holding equation (10) with equality, i.e. $\widetilde{y}_{\mathcal{C}}(s;\boldsymbol{\psi}) = y_{\mathcal{T}}(s)$ (note that $s = t$ for the reference region $\mathcal{T}$). Then, we find the undetermined normalization coefficients as,

$$\begin{aligned}
\omega_0 &= \theta_{0,\mathcal{T}} - \frac{\theta_{1,\mathcal{T}}}{\theta_{1,\mathcal{C}}}\theta_{0,\mathcal{C}}, \qquad & \omega_1 &= \frac{\theta_{1,\mathcal{T}}}{\theta_{1,\mathcal{C}}}, \\
\psi_0 &= \frac{\theta_{2,\mathcal{T}} - \theta_{2,\mathcal{C}}}{\theta_{3,\mathcal{C}}}, & \psi_1 &= \frac{\theta_{3,\mathcal{T}}}{\theta_{3,\mathcal{C}}}.
\end{aligned}$$

That is, the normalization coefficients have an exact and unique solution. For our illustration in panel (b) of Figure 6, we set $\Theta_{\mathcal{C}} = \{1.0, 5.0, 4.1, 1.00\}$ and $\Theta_{\mathcal{T}} = \{1.5, 3.0, 1.1, 1.05\}$, which implies the following unique solution for $\boldsymbol{\phi}^* = \{\psi_0^*, \psi_1^*, \omega_0^*, \omega_1^*\} = \{-3.0, 1.05, -4.5, 1.5\}$. We show the role of each of these normalizaiton coefficients in the non-orthogonal decomposition in Figure 27.

Figure 27: Decomposition by Normalization Coefficient: Trigonometric Time Paths

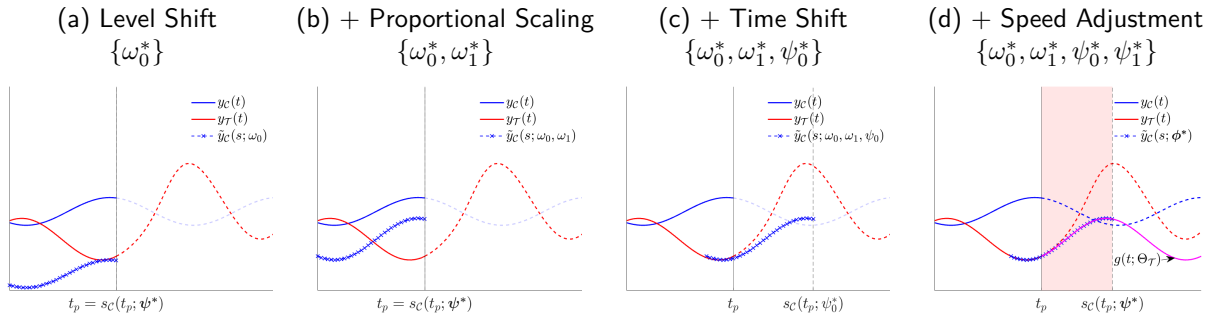


*Notes:* See the notes in Figure 4.

## B.2 Polynomial functions

Here we use a set of polynomial functions to generate outcome time paths. We discuss a case with unique solutions for $\boldsymbol{\phi}^*$ that emerges from cubic time paths and a case with multiple solutions for $\boldsymbol{\phi}^*$ that emerges from quadratic time paths.

### B.2.1 Cubic time paths

Here, we assume cubic time paths (see panel (c) of Figure 6):

$$g(t;\Theta_r) = \theta_{0,r} + \theta_{1,r}t + \theta_{2,r}t^2 + \theta_{3,r}t^3$$

for regions $r = \{\mathcal{C}, \mathcal{T}\}$ and periods $t \in \{0, \ldots, t_p, \ldots, T\}$. Then, picking a region (here: $\mathcal{T}$) as reference, we apply our normalization procedure. That is, we map the outcome path of the non-reference region $\mathcal{C}$ onto that of the reference region $\mathcal{T}$ using pre-policy data only. To do so, we postulate a normalized path for the non-reference region, $\widetilde{y}_{\mathcal{C}}(s;\boldsymbol{\phi}) = (f_{\mathcal{C}}(.;\boldsymbol{\omega}) \circ y_{\mathcal{C}} \circ t_{\mathcal{C}}(.;\boldsymbol{\psi}))(s)$ with outer composite $f_{\mathcal{C}} = \omega_0 + \omega_1 y_{\mathcal{C}}(t)$ and inner composite $t_{\mathcal{C}} = \psi_0 + \psi_1 s$. That is,

$$\begin{aligned}
\widetilde{y}_{\mathcal{C}}(s;\boldsymbol{\phi}) &= \omega_1 y_{\mathcal{C}}(\psi_0 + \psi_1 s) + \omega_0 \\
&= \omega_1 \left(\theta_{0,\mathcal{C}} + \theta_{1,\mathcal{C}}(\psi_0 + \psi_1 s) + \theta_{2,\mathcal{C}}(\psi_0 + \psi_1 s)^2 + \theta_{3,\mathcal{C}}(\psi_0 + \psi_1 s)^3\right) + \omega_0 \\
&= \omega_0 + \omega_1 \left(\theta_{0,\mathcal{C}} + \theta_{1,\mathcal{C}}\psi_0 + \theta_{2,\mathcal{C}}\psi_0^2 + \theta_{3,\mathcal{C}}\psi_0^3\right) \\
&\quad + \omega_1 \left(\theta_{1,\mathcal{C}}\psi_1 + 2\theta_{2,\mathcal{C}}\psi_0\psi_1 + 3\theta_{3,\mathcal{C}}\psi_0^2\psi_1\right) s \\
&\quad + \omega_1 \left(\theta_{2,\mathcal{C}}\psi_1^2 + 3\theta_{3,\mathcal{C}}\psi_0\psi_1^2\right) s^2 \\
&\quad + \omega_1 \theta_{3,\mathcal{C}}\psi_1^3 s^3 = y_{\mathcal{T}}(s)
\end{aligned}$$

where the last equality emerges from holding equation (10) with equality, i.e. $\widetilde{y}_{\mathcal{C}}(s;\boldsymbol{\psi}) = y_{\mathcal{T}}(s)$ (note that $s = t$ for the reference region $\mathcal{T}$). This implies the following system with four equations and four unknowns,

$\boldsymbol{\phi} = \{\boldsymbol{\psi}, \boldsymbol{\omega}\} = \{\psi_0, \psi_1, \omega_0, \omega_1\}$:

$$\theta_{0,\mathcal{T}} = \theta_{0,\mathcal{T}}(\omega_0, \omega_1, \psi_0) = \omega_0 + \omega_1 \left(\theta_{0,\mathcal{C}} + \theta_{1,\mathcal{C}}\psi_0 + \theta_{2,\mathcal{C}}\psi_0^2 + \theta_{3,\mathcal{C}}\psi_0^3\right) \tag{31}$$

$$\theta_{1,\mathcal{T}} = \theta_{1,\mathcal{T}}(\omega_1, \psi_0, \psi_1) = \omega_1 \left(\theta_{1,\mathcal{C}}\psi_1 + 2\theta_{2,\mathcal{C}}\psi_0\psi_1 + 3\theta_{3,\mathcal{C}}\psi_0^2\psi_1\right) \tag{32}$$

$$\theta_{2,\mathcal{T}} = \theta_{2,\mathcal{T}}(\omega_1, \psi_0, \psi_1) = \omega_1 \left(\theta_{2,\mathcal{C}}\psi_1^2 + 3\theta_{3,\mathcal{C}}\psi_0\psi_1^2\right) \tag{33}$$

$$\theta_{3,\mathcal{T}} = \theta_{3,\mathcal{T}}(\omega_1, \psi_1) = \omega_1\theta_{3,\mathcal{C}}\psi_1^3 \tag{34}$$

Then, we find the undetermined normalization coefficients ($\boldsymbol{\phi}$) that solve the system (31)-(34) using the following steps:

STEP 1. Isolate $\omega_1$ in $\theta_{3,\mathcal{T}}(\omega_1, \psi_1)$,

$$\omega_1 = \omega_1(\psi_1) = \frac{\theta_{3,\mathcal{T}}}{\theta_{3,\mathcal{C}}\psi_1^3}$$

STEP 2. Plug $\omega_1(\psi_1)$ in $\theta_{3,\mathcal{T}}(\omega_1, \psi_0, \psi_1)$ and isolate $\psi_0$:

$$\begin{aligned}
\theta_{2,\mathcal{T}} &= \omega_1 \left(\theta_{2,\mathcal{C}}\psi_1^2 + 3\theta_{3,\mathcal{C}}\psi_0\psi_1^2\right) \\
&= \frac{\theta_{3,\mathcal{T}}}{\theta_{3,\mathcal{C}}\psi_1^3} \left(\theta_{2,\mathcal{C}}\psi_1^2 + 3\theta_{3,\mathcal{C}}\psi_0\psi_1^2\right) \\
&= \frac{\theta_{3,\mathcal{T}}}{\theta_{3,\mathcal{C}}\psi_1} \left(\theta_{2,\mathcal{C}} + 3\theta_{3,\mathcal{C}}\psi_0\right)
\end{aligned}$$

hence,

$$\psi_0(\psi_1) = \frac{1}{3}\frac{\theta_{2,\mathcal{T}}}{\theta_{3,\mathcal{T}}}\psi_1 - \frac{1}{3}\frac{\theta_{2,\mathcal{C}}}{\theta_{3,\mathcal{C}}}$$

STEP 3. Plug $\omega_1(\psi_1)$ and $\psi_0(\psi_1)$ in $\theta_{1,\mathcal{T}}(\omega_1, \psi_0, \psi_1)$ and isolate $\psi_1$:

$$\begin{aligned}
\theta_{1,\mathcal{T}} &= \omega_1 \left(\theta_{1,\mathcal{C}}\psi_1 + 2\theta_{2,\mathcal{C}}\psi_0\psi_1 + 3\theta_{3,\mathcal{C}}\psi_0^2\psi_1\right) \\
&= \frac{\theta_{3,\mathcal{T}}}{\theta_{3,\mathcal{C}}\psi_1^3} \left(\theta_{1,\mathcal{C}}\psi_1 + 2\theta_{2,\mathcal{C}}\psi_0\psi_1 + 3\theta_{3,\mathcal{C}}\psi_0^2\psi_1\right) \\
&= \frac{\theta_{3,\mathcal{T}}}{\theta_{3,\mathcal{C}}\psi_1^2} \left(\theta_{1,\mathcal{C}} + 2\theta_{2,\mathcal{C}}\psi_0 + 3\theta_{3,\mathcal{C}}\psi_0^2\right) \\
&= \frac{\theta_{3,\mathcal{T}}}{\theta_{3,\mathcal{C}}\psi_1^2} \left(\theta_{2,\mathcal{C}} + 2\theta_{3,\mathcal{C}} \left(\underbrace{\frac{1}{3}\frac{\theta_{3,\mathcal{T}}}{\theta_{3,\mathcal{T}}}\psi_1 - \frac{1}{3}\frac{\theta_{3,\mathcal{C}}}{\theta_{3,\mathcal{C}}}}_{\psi_0(\psi_1)}\right) + 3\theta_{3,\mathcal{C}} \left(\underbrace{\frac{1}{3}\frac{\theta_{3,\mathcal{T}}}{\theta_{3,\mathcal{T}}}\psi_1 - \frac{1}{3}\frac{\theta_{3,\mathcal{C}}}{\theta_{3,\mathcal{C}}}}_{\psi_0(\psi_1)}\right)^2\right) \\
&= \frac{\theta_{3,\mathcal{T}}}{\theta_{3,\mathcal{C}}\psi_1^2} \left(\theta_{1,\mathcal{C}} + 2\theta_{2,\mathcal{C}} \left(\frac{1}{3}\frac{\theta_{2,\mathcal{T}}}{\theta_{3,\mathcal{T}}}\psi_1 - \frac{1}{3}\frac{\theta_{2,\mathcal{C}}}{\theta_{3,\mathcal{C}}}\right) + 3\theta_{3,\mathcal{C}} \left(\frac{1}{9}\left(\frac{\theta_{2,\mathcal{T}}}{\theta_{3,\mathcal{T}}}\right)^2\psi_1^2 + \frac{1}{9}\left(\frac{\theta_{2,\mathcal{C}}}{\theta_{3,\mathcal{C}}}\right)^2 - 2\frac{1}{9}\frac{\theta_{2,\mathcal{T}}}{\theta_{3,\mathcal{T}}}\frac{\theta_{2,\mathcal{C}}}{\theta_{3,\mathcal{C}}}\psi_1\right)\right) \\
&= \frac{1}{3}\frac{\theta_{2,\mathcal{T}}^2}{\theta_{3,\mathcal{T}}} + \frac{2}{3}\left(\frac{\theta_{2,\mathcal{C}}}{\theta_{3,\mathcal{T}}}\theta_{2,\mathcal{T}} - \frac{\theta_{2,\mathcal{T}}}{\theta_{3,\mathcal{T}}}\theta_{2,\mathcal{C}}\right)\frac{1}{\psi_1} + \frac{\theta_{3,\mathcal{T}}}{\theta_{3,\mathcal{C}}}\left(\theta_{1,\mathcal{C}} - \frac{1}{3}\frac{\theta_{2,\mathcal{C}}^2}{\theta_{3,\mathcal{C}}}\right)\frac{1}{\psi_1^2}
\end{aligned}$$

Figure 28: Decomposition by Normalization Coefficient: Cubic Time Paths

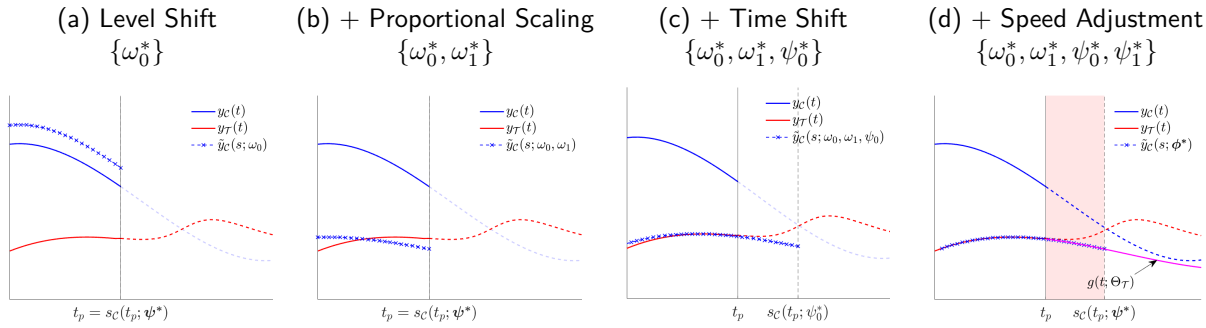


*Notes:* See the notes in Figure 4.

That is,

$$\underbrace{\frac{\theta_{3,\mathcal{T}}}{\theta_{3,\mathcal{C}}}\left(\theta_{1,\mathcal{C}} - \frac{1}{3}\frac{\theta_{2,\mathcal{C}}^2}{\theta_{3,\mathcal{C}}}\right)}_{a}\frac{1}{\psi_1^2} + \underbrace{\frac{2}{3}\left(\frac{\theta_{2,\mathcal{C}}}{\theta_{3,\mathcal{T}}}\theta_{2,\mathcal{T}} - \frac{\theta_{2,\mathcal{T}}}{\theta_{3,\mathcal{T}}}\theta_{2,\mathcal{C}}\right)}_{b=0}\frac{1}{\psi_1} + \underbrace{\frac{1}{3}\frac{\theta_{2,\mathcal{T}}^2}{\theta_{3,\mathcal{T}}} - \theta_{1,\mathcal{T}}}_{c} = 0$$

where note that $b = 0$. Thus, we can isolate $\psi_1 = \sqrt{\frac{a}{-c}}$ which delivers a unique solution for $\psi_1$ if $\frac{a}{-c} > 0$ (and no solution otherwise).[66]

STEP 4. Plug $\psi_1$ into $\omega_1(\psi_1)$ and $\psi_0(\psi_1)$ in order to recover $\omega_1$ and $\psi_0$.

STEP 5. Plug $\omega_1$, $\psi_0$ and $\psi_1$ into $\theta_{0,\mathcal{T}}(\omega_0, \omega_1, \psi_0)$ and isolate (recover) $\omega_0$.

That is, the normalization coefficients have an exact and unique solution. For our illustration in panel (c) of Figure 6, we set $\Theta_{\mathcal{C}} = \{12, -4.5, 0.3, 0.2\}$ and $\Theta_{\mathcal{T}} = \{7.84, -1.28, -0.17, 0.07\}$, which implies the following unique solution for $\boldsymbol{\phi}^* = \{\psi_0^*, \psi_1^*, \omega_0^*, \omega_1^*\} = \{-1.350, 1.093, 2.788, 0.278\}$. We show the role of each of these normalizaiton coefficients in the non-orthogonal decomposition in Figure 28.

### B.2.2 Quadratic time paths

Here, we assume quadratic time paths:

$$g(t;\Theta_r) = \theta_{0,r} + \theta_{1,r}t + \theta_{2,r}t^2$$

for regions $r = \{\mathcal{C}, \mathcal{T}\}$ and periods $t \in \{0, \ldots, t_p, \ldots, T\}$. Then, picking a region (here: $\mathcal{T}$) as reference, we apply our normalization procedure. That is, we map the outcome path of the non-reference region $\mathcal{C}$ onto that of the reference region $\mathcal{T}$ using pre-policy data only. To do so, we postulate a normalized path for the non-reference region, $\widetilde{y}_{\mathcal{C}}(s;\boldsymbol{\phi}) = (f_{\mathcal{C}}(.;\boldsymbol{\omega}) \circ y_{\mathcal{C}} \circ t_{\mathcal{C}}(.;\boldsymbol{\psi}))(s)$ with outer composite $f_{\mathcal{C}} = \omega_0 + \omega_1 y_{\mathcal{C}}(t)$ and inner composite

[66] One can further elaborate this to show that $\frac{a}{-c} = \frac{(3\theta_{1,\mathcal{C}}\theta_{3,\mathcal{C}} - \theta_{2,\mathcal{C}}^2)/\theta_{3,\mathcal{C}}^2}{(3\theta_{1,\mathcal{T}}\theta_{3,\mathcal{T}} - \theta_{2,\mathcal{T}}^2)/\theta_{3,\mathcal{T}}^2}$ and hence the solution to the system (31)-(34) emerging from the cubic time paths exists as long as the term in the numerator $(3\theta_{1,\mathcal{C}}\theta_{3,\mathcal{C}} - \theta_{2,\mathcal{C}}^2)$ and the term in the denominator $(3\theta_{1,\mathcal{T}}\theta_{3,\mathcal{T}} - \theta_{2,\mathcal{T}}^2)$ have the same sign.

Figure 29: Quadratic Time Paths

(a) After Normalization

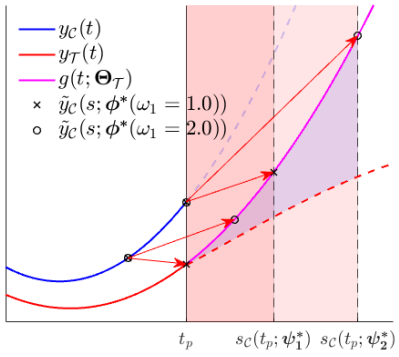


(b) Identified Policy Effects(%)

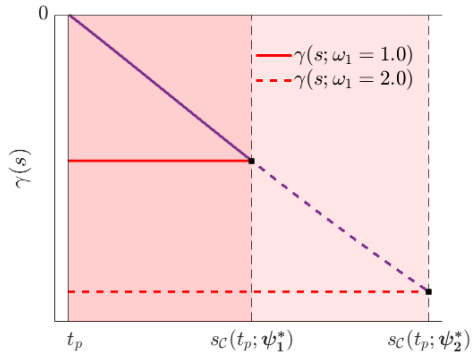


*Notes:* This is an example with multiple solutions for $\boldsymbol{\phi}^*$ (as described in Appendix B.2.2). In panel (a), as an illustration, we show two mappings of $\mathcal{C}$ onto $\mathcal{T}$ (reference region) that depend on two alternative solutions $\boldsymbol{\phi}^*(\omega_1)$ which are a function of a choice for $\omega_1$. In panel (b), we show the (interim) policy effects $\gamma(s)$ which are identical across solutions. We also show the (cumulative) policy effects $\gamma$ which depend not only on the interim effects, but also on the size of the window and, hence, on the solution $\boldsymbol{\phi}^*(\omega_1)$.

$t_{\mathcal{C}} = \psi_0 + \psi_1 s$. That is,

$$\begin{aligned}
\widetilde{y}_{\mathcal{C}}(s;\boldsymbol{\psi}) &= \omega_1 y_{\mathcal{C}}(\psi_0+\psi_1 s)+\omega_0 \\
&= \omega_1\left(\theta_{0,\mathcal{C}}+\theta_{1,\mathcal{C}}(\psi_0+\psi_1 s)+\theta_{2,\mathcal{C}}(\psi_0+\psi_1 s)^2\right)+\omega_0 \\
&= \omega_1\theta_{0,\mathcal{C}}+\omega_1\left(\theta_{1,\mathcal{C}}\psi_0+\theta_{1,\mathcal{C}}\psi_1 s\right)+\omega_1\left(\theta_{2,\mathcal{C}}\psi_0^2+\theta_{2,\mathcal{C}}2\psi_0\psi_1 s+\theta_{2,\mathcal{C}}\psi_1^2 s^2\right)+\omega_0 \\
&= \omega_1\theta_{0,\mathcal{C}}+\omega_1\theta_{1,\mathcal{C}}\psi_0+\omega_1\theta_{2,\mathcal{C}}\psi_0^2+\omega_0+\left(\omega_1\theta_{1,\mathcal{C}}\psi_1+\omega_1\theta_{2,\mathcal{C}}2\psi_0\psi_1\right)s+\omega_1\theta_{2,\mathcal{C}}\psi_1^2 s^2 = y_{\mathcal{T}}(s)
\end{aligned}$$

where the last equality emerges from holding equation (10) with equality, i.e. $\widetilde{y}_{\mathcal{C}}(s;\boldsymbol{\psi}) = y_{\mathcal{T}}(s)$ (note that $s=t$ for the reference region $\mathcal{T}$). This implies the following system with three equations and four unknowns, $\boldsymbol{\phi}=\{\boldsymbol{\psi},\boldsymbol{\omega}\}=\{\psi_0,\psi_1,\omega_0,\omega_1\}$:

$$\theta_{0,\mathcal{T}} = \theta_{0,\mathcal{T}}(\omega_0,\omega_1,\psi_0) = \omega_0+\omega_1\left(\theta_{0,\mathcal{C}}+\theta_{1,\mathcal{C}}\psi_0+\theta_{2,\mathcal{C}}\psi_0^2\right) \tag{35}$$

$$\theta_{1,\mathcal{T}} = \theta_{1,\mathcal{T}}(\omega_1,\psi_0,\psi_1) = \omega_1\left(\theta_{1,\mathcal{C}}\psi_1+\theta_{2,\mathcal{C}}2\psi_0\psi_1\right) \tag{36}$$

$$\theta_{2,\mathcal{T}} = \theta_{2,\mathcal{T}}(\omega_1,\psi_1) = \omega_1\theta_{2,\mathcal{C}}\psi_1^2 \tag{37}$$

This is an underidentified system with multiple exact solutions. For example, for any value of $\omega_1$ (or $\psi_2$) we obtain a different exact solution of $\boldsymbol{\phi}^*$.

As an illustration, let $\Theta_{\mathcal{C}}=\{8,-5,3\}$ and $\Theta_{\mathcal{T}}=\{4,-4,-2\}$. Then, initiating the system at $\omega_1=1.0$, we obtain the solution $\boldsymbol{\phi}^*=\{\psi_0^*,\psi_1^*,\omega_0^*,\omega_1^*\}=\{0.016,0.816,-3.916,1.0\}$. Alternatively, initiating the system at $\omega_1=2.0$, we obtain the alternative solution $\boldsymbol{\phi}^*=\{\psi_0^*,\psi_1^*,\omega_0^*,\omega_1^*\}=\{0.256,0.577,-9.833,2.0\}$; see panel (a) of Figure 29 Then, as our Remark 1 in Section 2.3 states, note that these two (and all for that matter) solutions ($\boldsymbol{\phi}^*$) to the system (35)-(37) deliver a counterfactual path that is exactly identical to the true counterfactual path without policy, $y_{\mathcal{T}}(s)=g(s;\Theta_{\mathcal{T}})$. In panel (a) of Figure 29, we graphically show the identified counterfactual

path, $\widetilde{y}_{\mathcal{C}}(s;\boldsymbol{\phi})$, of two (of the many possible) solutions assuming either $\omega_1 = 1.0$ (crossed markers) or $\omega_1 = 2.0$ (circle markers). This implies that the (interim) policy effects $\gamma(s)$ are identical across both (all for that matter) solutions of the normalization coefficients ($\boldsymbol{\phi}^*$); see panel (b) of Figure 29. At the same time, note that the overall policy effect $\gamma$ is determined by the behavior of the interim policy effects and the size of the window, $\mathbb{W}(s,\boldsymbol{\psi}^*) = [t_p, s_{\mathcal{C}}(t_p;\boldsymbol{\psi}^*(\omega_1)]$, which differs by the solution. Further, note that if policy is applied non-nationwide (e.g. assume that the policy is never implemented in region $\mathcal{C}$), then the overall policy effect $\gamma$ is also identical across potential multiple solutions of $\boldsymbol{\phi}^*$ because the identification window is open, i.e. $\mathbb{W}(s;\boldsymbol{\psi}^*) = [t_p, \infty)$.

## B.3 Generalized logistic functions

Here, we assume the outcome time paths follow the log of a generalized logistic function,

$$g(t;\Theta_r) = \ln\left(\frac{\theta_{1,r}}{\left(1+\exp\left(-\theta_{3,r}t+\theta_{2,r}\right)\right)^{\frac{1}{\theta_{4,r}}}}\right) \tag{38}$$

for regions $r = \{\mathcal{C},\mathcal{T}\}$ and periods $t \in \{0,\ldots,t_p,\ldots,T\}$. Note that the outcome time path in equation (38) generalizes the logistic function discussed in Section 2.3. In particular, we introduce an asymmetry parameter, $\theta_{4,r}$.[67] In this case, as we show next, exact solutions for $\boldsymbol{\phi}^*$ are achieved taking the log of the generalized logistic function—as stated in equation (38).

Then, picking a region (here: $\mathcal{T}$) as reference, we apply our normalization procedure. That is, we map the outcome path of the non-reference region $\mathcal{C}$ onto that of the reference region $\mathcal{T}$ using pre-policy data only. To do so, we postulate a normalized path for the non-reference region, $\widetilde{y}_{\mathcal{C}}(s;\boldsymbol{\phi}) = \left(f_{\mathcal{C}}(.;\boldsymbol{\omega}) \circ y_{\mathcal{C}} \circ t_{\mathcal{C}}(.;\boldsymbol{\psi})\right)(s)$ with outer composite $f_{\mathcal{C}} = \omega_0 + \omega_1 y_{\mathcal{C}}(t)$ and inner composite $t_{\mathcal{C}} = \psi_0 + \psi_1 s$. That is,

$$\begin{aligned}\widetilde{y}_{C} &= \omega_0 + \omega_1 y_C\left(\psi_0+\psi_1 s\right) \\ &= \underbrace{\omega_0 + \omega_1 \ln\left(\theta_{1,\mathcal{C}}\right)}_{=\ln(\theta_{1,\mathcal{T}})} - \underbrace{\omega_1 \frac{1}{\theta_{4,\mathcal{C}}}}_{=\frac{1}{\theta_{4,\mathcal{T}}}} \ln\left(1+\exp\left(\underbrace{-\theta_{3,\mathcal{C}}\psi_1}_{=\theta_{3,\mathcal{T}}} s + \underbrace{\theta_{2,\mathcal{C}} - \psi_0\theta_{3,\mathcal{C}}}_{=\theta_{2,\mathcal{T}}}\right)\right) = y_{\mathcal{T}}(s)\end{aligned}$$

where the last equality emerges from holding equation (10) with equality, i.e. $\widetilde{y}_{\mathcal{C}}(s;\boldsymbol{\phi}) = y_{\mathcal{T}}(s)$ (note that $s = t$ for the reference region $\mathcal{T}$). This implies a system with four equations and four unknowns, $\boldsymbol{\phi} = \{\boldsymbol{\psi},\boldsymbol{\omega}\} = \{\psi_0,\psi_1,\omega_0,\omega_1\}$:

$$\theta_{1,\mathcal{T}} = \theta_{1,\mathcal{T}}(\omega_0,\omega_1) = \exp\left(\omega_0 + \omega_1 \ln\theta_{1,\mathcal{C}}\right) \tag{39}$$

$$\theta_{4,\mathcal{T}} = \theta_{4,\mathcal{T}}(\omega_1) = \frac{1}{\omega_1}\theta_{4,\mathcal{C}} \tag{40}$$

$$\theta_{3,\mathcal{T}} = \theta_{3,\mathcal{T}}(\psi_1) = \psi_1\theta_{3,\mathcal{C}} \tag{41}$$

$$\theta_{2,\mathcal{T}} = \theta_{2,\mathcal{T}}(\psi_0) = \theta_{2,\mathcal{C}} - \psi_0\theta_{3,\mathcal{C}} \tag{42}$$

[67] In addition, we drop the level parameter $\theta_{0,r}$ present in the logistic function in Section 2.3.

Figure 30: Decomposition by Normalization Coefficient: Generalized Logistic Paths

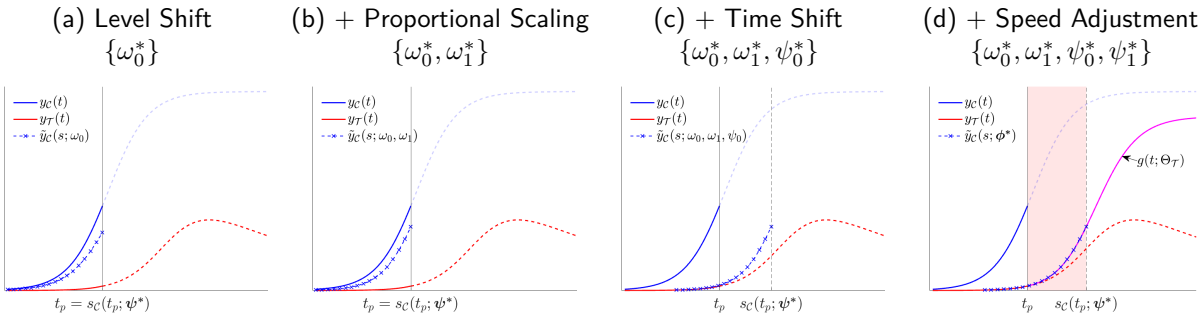


*Notes:* See the notes in Figure 4.

Then, the undetermined normalization coefficients are:

$$\omega_1^* = \frac{\theta_{4,\mathcal{C}}}{\theta_{4,\mathcal{T}}}, \qquad \omega_0^* = \ln\theta_{1,\mathcal{T}} - \frac{\theta_{4,\mathcal{C}}}{\theta_{4,\mathcal{T}}}\ln\theta_{1,\mathcal{C}},$$
$$\psi_1^* = \frac{\theta_{3,\mathcal{T}}}{\theta_{3,\mathcal{C}}}, \qquad \psi_0^* = \frac{\theta_{2,\mathcal{C}} - \theta_{2,\mathcal{T}}}{\theta_{3,\mathcal{C}}}.$$

That is, the normalization coefficients have an exact and unique solution. For example, let's set the structural parameters $\Theta_{\mathcal{C}} = \{4.00, 5.25, 0.15, 1.00\}$ and $\Theta_{\mathcal{T}} = \{3.50, 7.70, 0.14, 0.85\}$. This implies $\boldsymbol{\phi}^* = \{\psi_0^*, \psi_1^*, \omega_0^*, \omega_1^*\} = \{-16.33, 0.93, -0.37, 1.17\}$. We show the role of each of these normalization coefficients in the non-orthogonal decomposition in Figure 30.

# C Solution Algorithms for the Theoretical Frameworks

Here, we provide additional details on the solution algorithms for the three theoretical models that we pose in Section 3.

## C.1 Public health policy against a pandemic

Here we discuss the solution of the model posed in Section 3.1.1. We separately solve for the pre-pandemic equilibrium at $t = 0$ (actually, for any $t \leq 0$) before the unexpected arrival of the pandemic at $t = 1$. In this pre-pandemic era there are no infections and, hence, $\phi_i(h_0) = 1$. That is, the equilibrium labor supply sets the right-hand side of the Euler equation (16) to zero in which case $h_0$ simply solves an intra-temporal trade-off. The same equilibrium emerges after the pandemic at some large $t = T$ which delivers a terminal condition $h_T = h_0$.

Step 1. Solve for hours worked in the pre-pandemic steady state ($\bar{h}$).

Step 2. Select the number of periods to simulate $\mathfrak{T}$. Pick a large number $T$. Set $h_0 = h_T = \bar{h}$.

Step 3. Given parameters $\Theta$, guess a sequence $\{h_t\}_{t=0}^T$.

Step 4. With $\{h_t\}_{t=0}^T$, compute sequences for $S_t, I_t, R_t, D_t, N_t$.

Step 5. Use the above sequences to back out a new sequence for $\{h_t\}_{t=0}^T$ using (16). Solve backwards.

Step 6. If the new sequence $\{h_t\}_{t=0}^{T}$ is different than the guess in Step 3, update the guess and go back to Step 4.

Step 7. Store the second value of the sequence, namely $h_1$, and set $h_0 = h_1$. Go back to Step 3. Repeat this step $\mathfrak{T}$ times. Construct a solution sequence $\{h_{sol,t}\}_{t=1}^{\mathfrak{T}}$ using all values stored. Simulate the underlying epidemic dynamics associated to the solution sequence.

Step 8. To obtain the series with the effect of policy: set all values of the solution sequence after $t_p$ equal to $h_{pol}$, and simulate the epidemic dynamics.

**Further details on the extended model with endogenous policy** (in Section 3.2.2): In this case, the policy hits when the cumulative number of deaths reaches a certain number $\overline{D}$. In Step 5 solve backwards only from the date in which policy is implemented, continue with the rest of the steps as described above. Further, to obtain the series without policy, use as initial values those immediately before the policy hits, go to Step 3 and solve for a new sequence of $h$ assuming the policy constrain is never binding.

### C.2 Growth policy and structural transformation

Here we discuss the solution of the model posed in Section 3.1.3. We solve the economy by guessing the sequences of factor prices $\{w, r\}_{t=0}^{\infty}$ with $w_t = w_{at} = w_{mt}$. Given these prices, we find the allocations $c_{at}, k_{t+1}$ and $n_{at}$ that solve the set of first order conditions (25)-(27) with $p_{at} = \frac{w_t}{\phi z_{at}} \left(\frac{n_{at}}{\ell}\right)^{1-\phi}$.[68] There is market clearing in labor and capital, and aggregate consistency. Note that the interemporal Euler condition (26) is a second order different equation in $\{k_t, k_{t+1}, k_{t+2}\}$ at every period $t$. We use as initial and terminal conditions the corresponding stationarized economies at $t = 0$ and at a large $T$ with negligible agricultural share of labor.

## D Further Details on the Analysis of Confounding Factors

In Section 3.2.2, we discuss how SBI performs in the presence of confounding factors. Here, in Appendix D.1, we show the path of time-varying latent heterogeneity that we assumed for our analysis in the main text. In Appendix D.2, we further assess the implications of confounding policy for the performance of SBI.

### D.1 Time-varying latent heterogeneity

Here, we show the assumed path for the beliefs on the probability of infection conditional on hours work, $\xi_{\mathcal{P}}$, in region $\mathcal{T}$ that generates the time-varying latent heterogeneity studied in Section 3.2.2. Precisely, for our analysis of the performance of SBI in the context where there is time-varying latent heterogeneity, we assume that beliefs on the probability of infection conditional on hours work $\xi_{\mathcal{P}}$ are our source of time-varying latent heterogeneity. In Figure 31, we showed the assume time path for $\xi_{\mathcal{P}}$ (magenta dashed line) converging from below (from $t = 0 \leq t_p$)

[68] Note that without the distortion $\tau$, if $\phi = \alpha$ and if we had the same factor inputs in the production of both goods, then the equality of the ratio of factor input prices across sectors would imply that the ratio of factor inputs must be identical across sectors. In turn, this would imply a standard result for the pricing of agricultural goods, $p_{at} = \frac{z_{mt}}{z_{at}}$, which renders the price of agricultural good as exogenous. The fact that we allow for $\phi$ to differ from $\alpha$ and that we have different factor inputs differ across sectors both prevents the standard result. Indeed, in our case, the price of agricultural goods depends endogenously on $n_{at}$.

to the true probability $\xi$ (dashed gray line). Hence, a structural parameter, $\xi_{\mathcal{P}}$, that is unobserved to the policy evaluator evolves over time before and after policy implementation.

Figure 31: Time-Varying Latent Heterogeneity: Assumed Path of Beliefs $\xi_{\mathcal{P}}$ for region $\mathcal{T}$

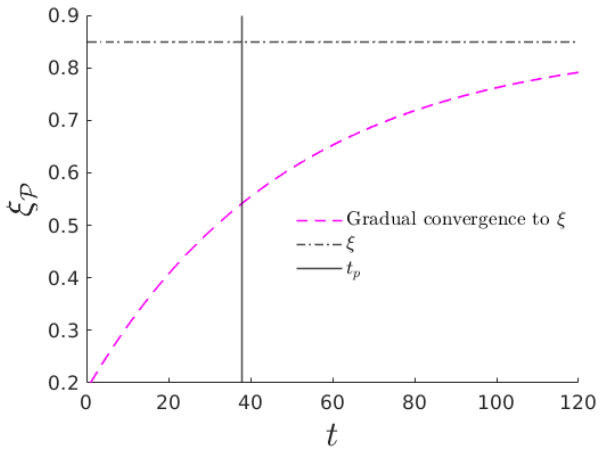


## D.2 Additional confounding policy

In Section 3.2.2, we show how SBI performs when confounding policy—happening before the stay-home policy under study is implemented—occurs in region $\mathcal{T}$ (and not in region $\mathcal{C}$). Here, we discuss the opposite scenario in which confounding policy is implemented in region $\mathcal{C}$ (and not in region $\mathcal{T}$) before the stay-home policy under study takes place. In this case, we find that the policy effect is recovered with an error of 2.34%. Again, we can make this error larger if the confounding policy drives the outcome path of region $\mathcal{C}$ further away from the outcome path of region $\mathcal{T}$.

Figure 32: Stage-Based Identification of Policy Effects: With Confounding Policy in $\mathcal{C}$

(a) Response of Hours (b) True Effects (c) Identified Effects (d) Identified vs. True Effects

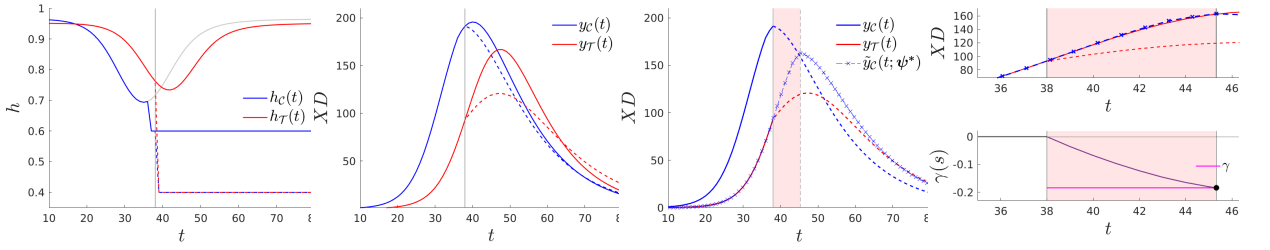


*Notes:* Where $\bar{h}_1 = 0.6$ at $t = 37$ in $\mathcal{C}$, his policy is unobserved, $\bar{h}_2 = 0.4$ (lockdown) at $t_p = 38, t_f = 250$, $\gamma = -18.34\%, \epsilon(\gamma) = 2.34\%$.

# E Alternative Inference Procedure

In Section 3.3.2, we discuss how we conduct inference in our applications throughout our applications. In this Appendix, we discuss an altogether alternative way to conduct inference. This alternative way proceeds by using the recovered estimates for the error terms $u_r(t)$ in order to estimate the sample variance of the errors, i.e. $\widehat{\sigma}_r$. Then, under a normality assumption on the error term in (28), we simulate $Q = 1,000$ paths of errors and, hence, the same number of pre-policy outcome paths onto which we apply the smoothing step in order to recover a simulation-specific estimand $\widehat{\widehat{y}}_{r,q}(t)$. Since the estimand $\widehat{\widehat{y}}_{r,q}(t)$ differs by simulation $q \in Q$, each simulation delivers an stage-based identified policy effect, $\gamma_q$. We show the results of this different inference in Figure 33. Overall, we find similar insights with an identified mean policy effect of 21.12% [14.41,28.23] and 19.61% [12.32,29.35] with, respectively, classical measurement error and with auto-correlated measurement error. The recovered policy effect is not significantly different from the true (model-generated) policy effect. In Figure 34, we show the policy effects from directly using the $Q = 1,000$ simulations of data $\widehat{y}_{r,q}(t)$, that is, without applying the smoothing step. The identified mean policy effect obtained without the smoothing step is 20.92% [7.88,30.32] and 21.55% [7.51,30.81] with, respectively, classical measurement error and with auto-correlated measurement error.

Figure 33: Stage-Based Identification of Model-Generated Policy Effects: Alternative Inference

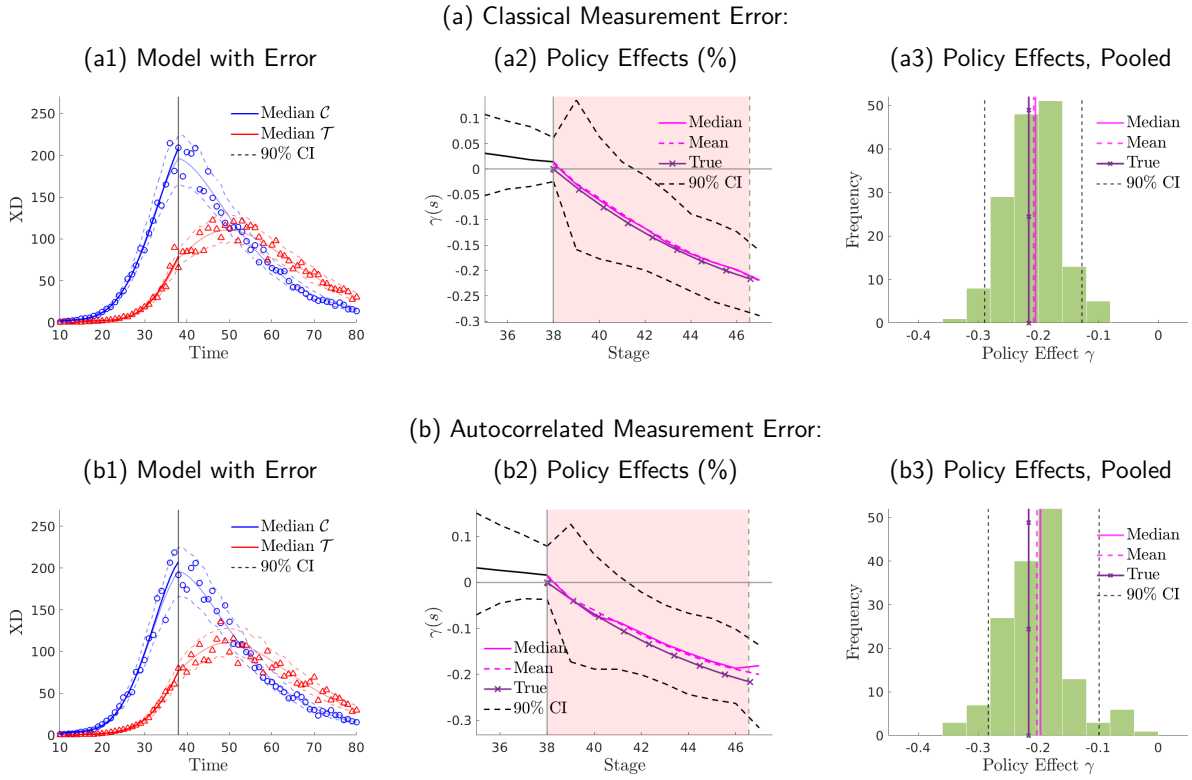


*Notes:* We use the benchmark calibration in Section 3.1.1. the top panels (a), we introduce classical measurement error in our model with $\{\sigma^2_{\mathcal{C}}, \sigma^2_{\mathcal{T}}\} = \{0.01, 0.01\}$. In the bottom panels (b), we introduce non-classical measurement error with $\{\rho_{\mathcal{C}}, \rho_{\mathcal{T}}\} = \{0.13, 0.13\}$ and $\{\sigma^2_{\mathcal{C}}, \sigma^2_{\mathcal{T}}\} = \{0.01, 0.01\}$.

Figure 34: Stage-Based Identification of Model-Generated Policy Effects: Alternative Inference, No Smoother

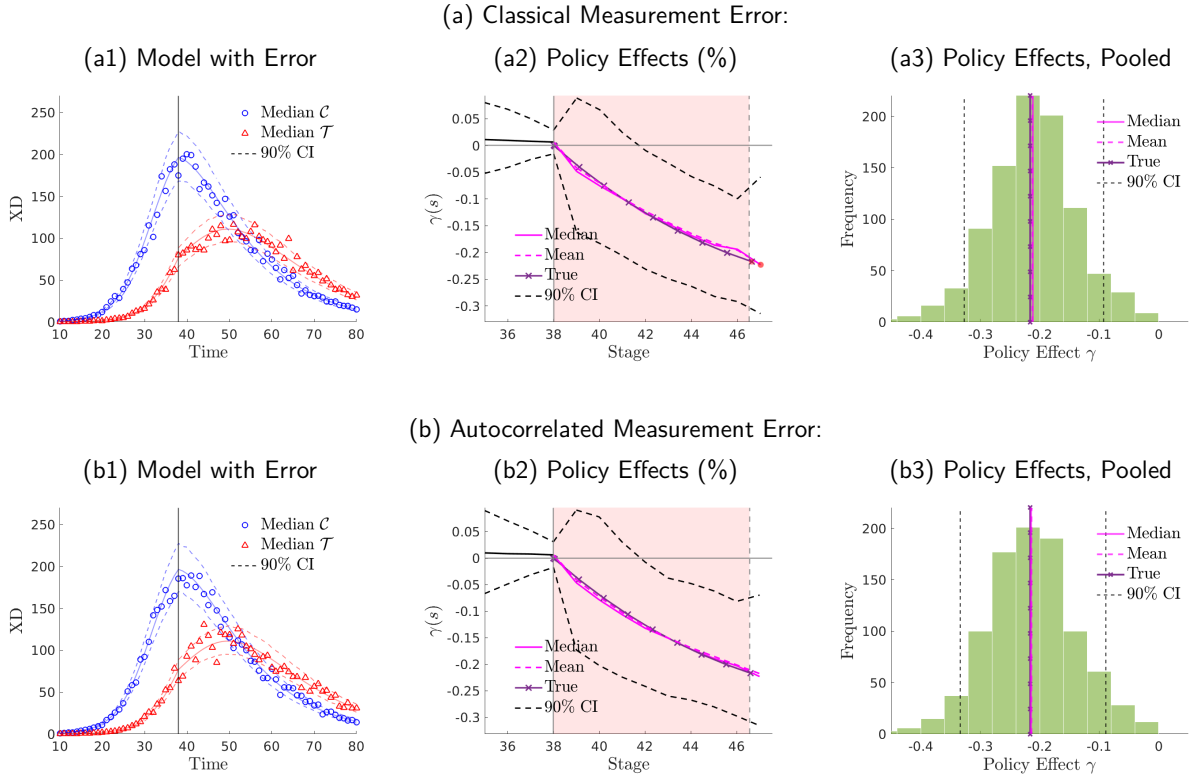


*Notes:* We use the benchmark calibration in Section 3.1.1. the top panels (a), we introduce classical measurement error in our model with $\{\sigma^2_{\mathcal{C}}, \sigma^2_{\mathcal{T}}\} = \{0.008, 0.008\}$. In the bottom panels (b), we introduce non-classical measurement error with $\{\rho_{\mathcal{C}}, \rho_{\mathcal{T}}\} = \{0.13, 0.13\}$ and $\{\sigma^2_{\mathcal{C}}, \sigma^2_{\mathcal{T}}\} = \{0.008, 0.008\}$.

# F Data

In Section 4, we apply SBI to three applications. Here, we discuss the data construction and sources used in each of our applications. Note that only data needed for our identify policy effects through SBI is that of the time path of the outcomes of interest.

## F.1 Covid-19 Application

For the assessment of the national lockdown against the first wave of Covid-19 in Spain in Section 4.1, we use Covid-19 deaths regional series provided by the Ministerio de Sanidad. Data from the Ministerio de Sanidad can be found under the following link: www.mscbs.gob.es. All values in figure 16 are expressed per million inhabitants of each region, with Spain having 47 million inhabitants and Madrid 6.6 million.

## F.2 Oral Contraceptives Application

For our assessment of the effects of the 1960 FDA approval of oral contraceptives on fertility and women college education in Section 4.2, we use state-level data on crude brith rates and the share of women with completed college of age 25:

- To construct the crude birth rate (by state), we divide total number of births in a given year and diving it by the respective population. Birth counts by state from 1939 to 2007 are provided by IPUMS NHGIS, Vital Statistics: Natality and Mortality Data. We use population data provided by the U.S. Census Bureau annual estimates.
- To measure the share of women of a certain age with college attainment we use decennial CENSUS data from IPUMS starting in 1940 up to 1980. In the absence of information on the year of graduation, we construct the historical series by using cohort information by CENSUS year. For example when using CENSUS data for 1960, the share of college women of age 25 in 1959 will be the share of a woman age 26 who reported (already) having attained college by 1960.[69] After computing the historical series per CENSUS year we compute the average across CENSUS series.

## F.3 German Reunification Application

To assess the effects of the German reunification on the income per capita of West Germany in Section 4.3, we retrieve 1970-2007 GDP data for West Germany from the Statistisches Bundesamt. Likewise, the respective price index from the Destatis postal. Our current GDP measure of West Germany does not include West Berlin, our results do not change significantly when including West Berlin.

Finally, GDP data, inflation, PPP deflators and population for the USA and the rest of OECD countries for 1970-2007 is taken from the OECD data portal OECD.STAT. The list of countries that comprises our hybrid Rest of OECD (RoOECD) is the same as the one chosen in Abadie et al. (2014), namely Australia, Austria, Belgium,

[69] Later completion and death could hinder the precision of our measure, however after comparing the historical series from various census years, the measure doesn't seem to be suffering from these problems

Denmark, France, Greece, Italy, Japan, Netherlands, New Zealand, Norway, Portugal, Spain, Switzerland, United Kingdom and United States.

# G Placebo Diagnosis for our Applications

Here, we conduct further inference using a placebo diagnosis in each of our applications in Section 4. That is, we show the policy effects that emerge from our method if we conduct our normalization at a some period before the actual policy takes place. Precisely, for our placebo, we assume that the stay-home policy was imposed on March 10 2020, i.e. about two weeks earlier than its actual implementation; the pill was introduced 5 year before its actual market release; and that German Reunification occurred 5 years before the actual reunification date. Our method will survive this test if it identify policy effects that are not significantly different from zero. We find that this is the case for each and all our applications; see Figure 35.

Figure 35: Stage-Based Identification of Policy Effects: Placebo Diagnosis

(a) Effects of the Spanish *Confinamiento* on Daily Deaths

(a1) Identification Window (Zoomed) (a2) Policy Effects (%)

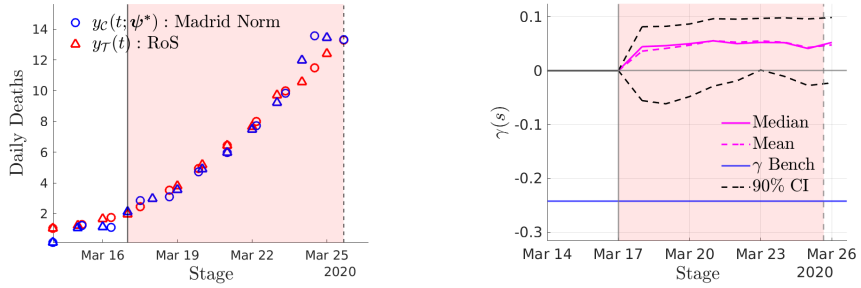


(b) Effects of Oral Contraceptives on Crude Birth Rate

(b1) Identification Window (Zoomed) (b2) Policy Effects

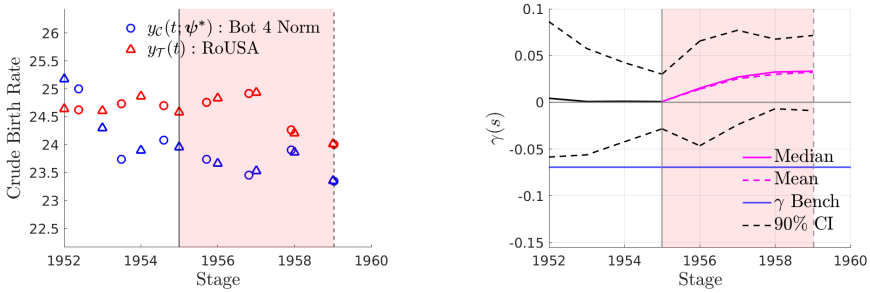


(c) Effects of Oral Contraceptives on Share of Women with College

(c1) Identification Window (Zoomed) (c2) Policy Effects

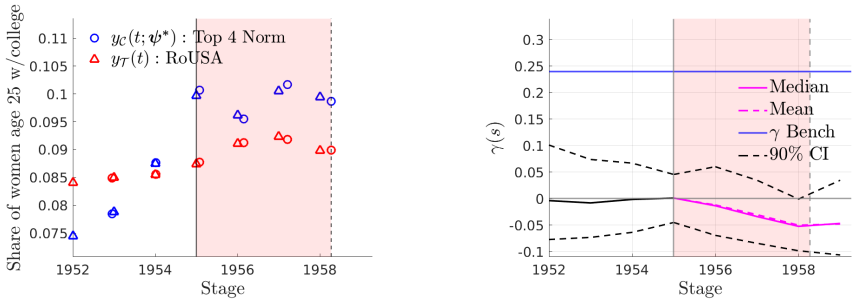


(d) Effects of the German Reunification on GDP

(d1) Identification Window (Zoomed) (d2) Policy Effects

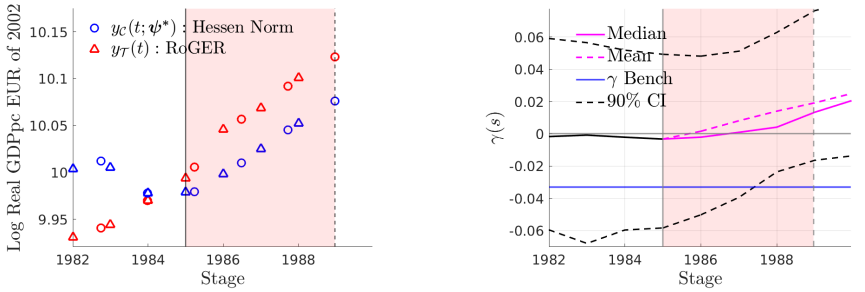


*Notes:* In our placebo, we assume that the stay-home policy was imposed on March 10 2020; the pill was introduced 5 year before its actual market release; and that German Reunification occured 5 years before the actual reunification date.

Figure 36: Identified Policy Effects Without the Trend-Extraction Step

(a) Spanish *Confinamiento* (b) Crude Birth Rate (c) Women College Attainment (d) German Reunification

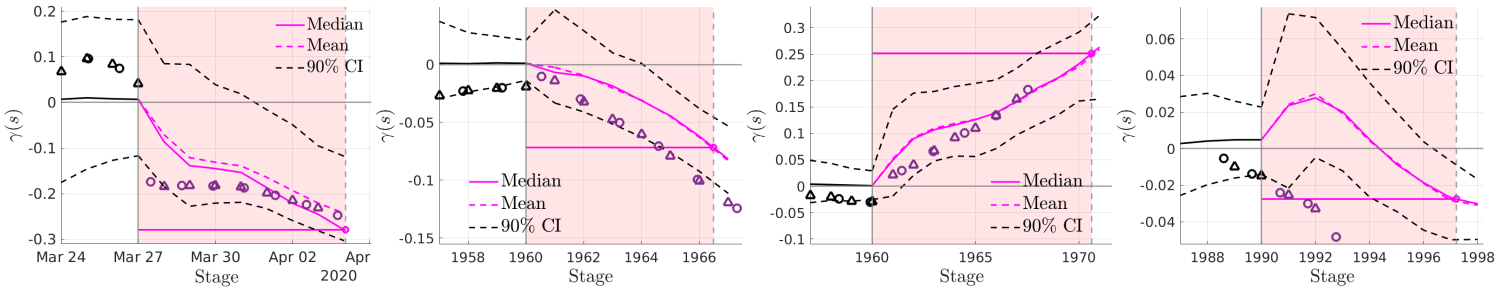


*Notes:* We show the policy effects identified without the implementation of the smoothing step and around the neighborhood of the point estimate, as described in Section 4.

# H Robustness to the Trend-Extraction

We mainly use the trend-extraction step described in Section 4 in order to conduct inference using as stochastic component the data deviations from trend. Here, in Figure 36, we compare the policy effects of all our empirical applications in which we used a trend-extraction step in order to conduct inference described in Section 4 with a counterpart where we skip the trend-extraction step and minimize the original data points. Our exercise shows that the trend extraction does not affect the identified effects of the Spanish Confinamiento on daily deaths (see panel (a) of Figure 36) and the effects of the 1960 FDA approval of oral contraceptives on the crude birth rate (see panel (b) of Figure 36) and women college attainment (see panel (c) of Figure 36).

However, we find that the identified policy effects without the trend-extraction step differ from those with the trend-extraction in the context of the German Reunification; see panel (d) in Figure 36. The reason for this differential result is that in the case of the German Reunification the outcome variable (GDP per capita) shows fluctuations at a larger frequency (business cycles) than the frequency in which we are ultimately interested in for the evaluation of the German Reunification. Since all regions share the same aggregate fluctuations, if we do not purge GDP per capita from the business cycle fluctuations our algorithm that aims to minimizes the distance between the GDP per capita across regions (to some reference region) will be drawn to map the business cycle fluctuations of all regions to that of the reference region. For this reason, and since our interest is not the business cycle but the longer run, we extract the trend from the GDP in order to remove the higher frequency fluctuations of GDP. Therefore, in addition to be useful to conduct inference, the trend-extraction step can also serve the purpose of removing fluctuations that are of higher frequency than the ones in which the policy evaluator is interested in.

Figure 37: The Effects of the German Reunification on GDP per capita

(a) Before Normalization

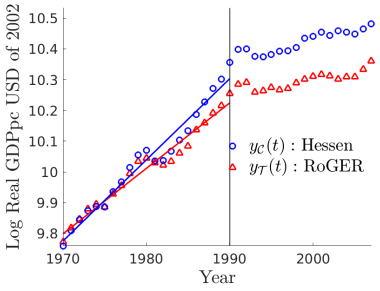


(b) After Normalization (smoothing)

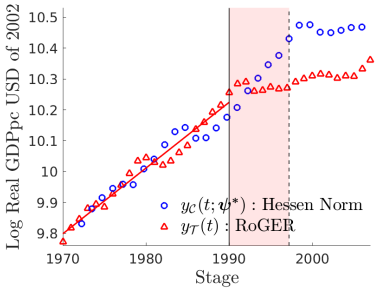


(c) After Normalization (not smoothing)

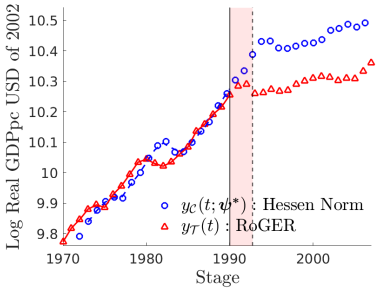


# I Extrapolating to Find Policy Effects on the Control Region: Not a Good Idea

In Section 5.2, we discuss the identificiation of aggregate policy effects. Alternatively, one may be tempted to extrapolate the heterogeneous policy effects in Section 5.1 in order to find the policy effects of the control region and, hence, the aggregate. In particular, given that the policy effects depend on the size of the identification window one could extrapolate the per-period policy effects forward. That is, one could fit a curve to the well-identified per-period policy effects (within the identification window) across stages and use the fitted curves to find the effects for the control region via extrapolation. We do this using a log-linear fit and a quadratic fit using our benchmark econ-epi model in Section 3.1.1; see, respectively, panel (a1) and panel (b1) of Figure 38. The policy effect of the control region is constructed using the value of the extrapolated per-period policy effect (after policy implementation). Precisely, we find where the extrapolated per-period policy effect hits the period when the policy effectively enters the control region.

Overall, we find that conducting extrapolations in order to pin down the policy effects on the control region is not a good idea. In this specific example, a extrapolations from a log linear fit recovers the true per-period policy effect on the control region; see panel (a2) of Figure 38. However, this is not the case with a quadratic fit; see panel (a2) of Figure 38. One can imagine situations in which the extrapolation works are those in which the per-period policy effects are well approximated by the fitted curve, at least, locally around the last stages where the policy effects are available (hence, closer to when the control enters policy). However, there is no reason to think that is generally the case. In Figure 39, we show the extrapolated policy effects in the control region, Madrid, emerging from extrapolating the heterogenous effects by stage in our empirical application of the stay-home policy implemented in Spain during Covid-19.

Figure 38: Extrapolated Policy Effects of the Control Region: Model

(a) Log-Linear Fit: (b) Quadratic Fit:

(a1) Per-Period Policy Effect | (a2) Extrapolated Policy Effect (Control Region) | (b1) Per-Period Policy Effect | (b2) Extrapolated Policy Effect (Control Region)

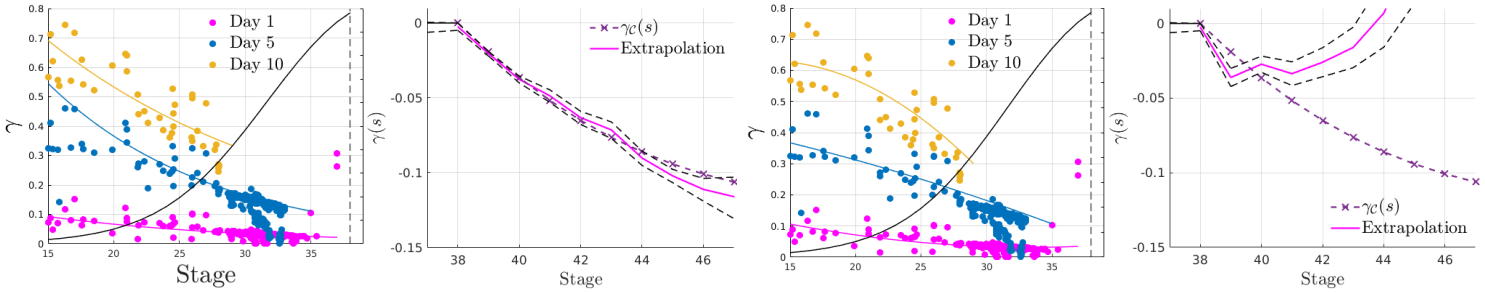


Figure 39: Extrapolated Policy Effects of the Control Region: Data (Madrid, Covid-19 Application)

(a) Log-Linear Fit: (b) Quadratic Fit:

(a1) Per-Period Policy Effect | (a2) Extrapolated Policy Effect (Control Region) | (b1) Per-Period Policy Effect | (b2) Extrapolated Policy Effect (Control Region)

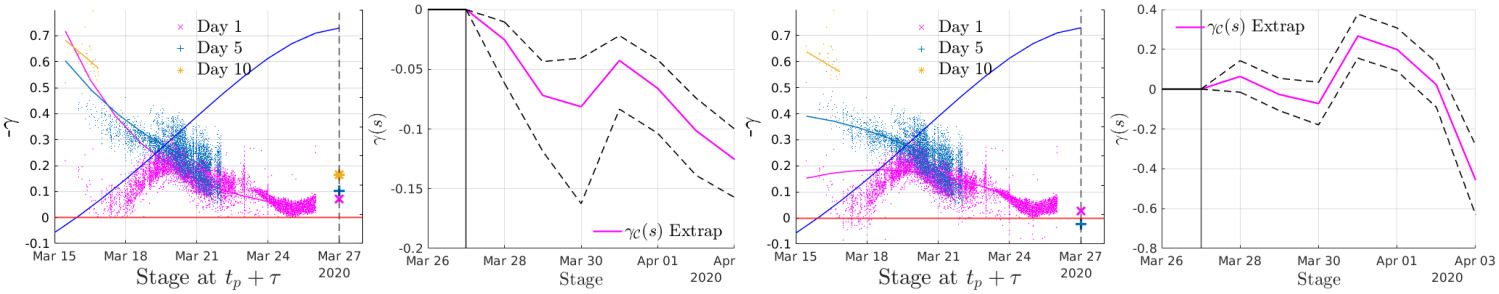


# J Many Control Regions for One Treated Region

In Section 5.3, we show that applying SBI with alternative controls (Hessen, United States, and OECD) on West Germany income per capita we identify similar policy effects of the German Reunification. This is perhaps not surprising because by mapping all potential controls onto West Germany, the outcome path of each control is normalized to be at the same stage when West Germany enters policy.

In this Appendix, we show the stage-based identified policy effects of applying alternative controls for one of the regions in which the national lockdown in Spain catches at earlier stages of the first Covid-19 wave, the Canary Islands. We conduct SBI choosing the Canary Islands as reference path and map a set of alternative non-reference regions (potential controls) onto the outcome path of the Canary Islands. These set of non-reference regions are, namely: Andalucia, Castilla y Leon, Catalunya, Valencia, Castilla la Mancha, Islas Baleares and Madrid. In Figure 40, we show that the identified policy effects are independently of the associated control region.

Figure 40: The Effects of the Spanish *Confinamiento* in the Canary Islands, with Different Controls

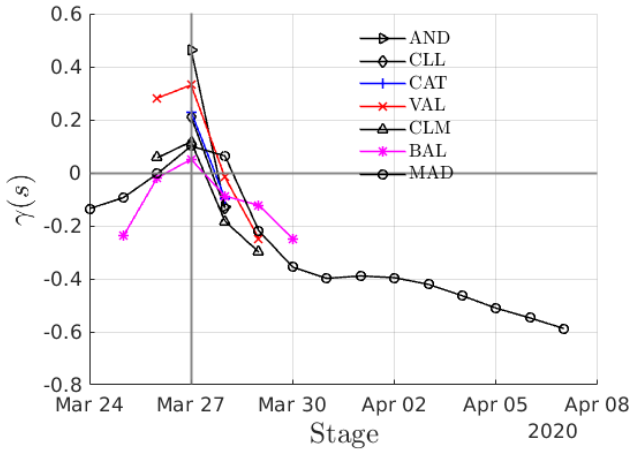


*Notes:* Reference region: Canary Islands. The rest of regions are non-reference: Andalucia (AND), Castilla y Leon (CLL), Catalunya (CAT), Valencia (VAL), Castilla La Mancha (CLM), Balearic Islands (BAL) and Madrid (MAD). Note that all these regions lead the reference region and, hence, serve as control for the reference region.